5-2012

Nanoparticles in Solution-Derived Chalcogenide Glass Films

Spencer Novak
Clemson University, spencen@g.clemson.edu

NANOPARTICLES IN SOLUTION-DERIVED CHALCOGENIDE GLASS FILMS

A Thesis
Presented to
the Graduate School of
Clemson University

In Partial Fulfillment
of the Requirements for the Degree
Master of Science
Materials Science and Engineering

---

by
Spencer Novak
May 2012

Accepted by:
Dr. Kathleen Richardson, Committee Chair
Dr. Konstantin Kornev
Dr. Igor Luzinov
Dr. Nathan McClenaghan
Dr. Marc Dussauze

ABSTRACT

The results in this thesis are from our efforts to modify the optical properties of solution-derived chalcogenide glass films by the incorporation of nanomaterials. First, the composition $Ge_{23}Sb_7S_{70}$ was selected as the appropriate glass matrix for testing because solution-derived films of this composition have been well-studied in our group. Additionally, this composition was found to be less sensitive to certain processing parameters than As_2S_3, another well-studied, candidate chalcogenide glass composition, making $Ge_{23}Sb_7S_{70}$ more suitable for the addition of nanomaterials. Optimization of film process parameters was performed to obtain high-quality films appropriate for doping with nanomaterials. This consisted of determining the maximum solubility of glass in propylamine solvent to obtain films of adequate thickness, as well as optimizing the water content in the propylamine to minimize surface roughness and cracking. Two classes of nanomaterials were used to investigate the principles of doped films, spherical metallic nanoparticles (MNPs), and spherical semiconductor nanoparticles, also known as quantum dots (QDs). Gold was the particular type of MNP used, and is characterized by its surface plasmon resonance (SPR) absorption band, which is tunable and environment sensitive, and leads to interesting properties such as magneto-optic effects. Two types of QDs were used, CdSe and PbS. QDs are widely known for their high photostability and luminescence, which is tunable by varying the size of the QD. CdSe exhibits luminescence in the visible spectral region, while PbS emits in the near-infrared (NIR).

With Au nanoparticles, experiments were performed to determine the maximum nanoparticle concentration in the glass solution by utilizing UV-vis-NIR spectroscopy.

Films were then deposited and characterized by their absorption spectra. In the case of QDs, solutions were not stable for long enough periods of time, so only the films deposited from the solutions could be analyzed. UV-vis-NIR spectroscopy and photoluminescence measurements were used to observe the intensity and location of the characteristic absorption and luminescence bands of the QDs. Quantum yield and luminescence lifetime were used to quantitatively characterize the behavior of the QDs in different environments when possible. Different organic ligands on the surface of the QDs were tested and compared to evaluate their effect on the behavior of the QD. The results show that small amounts of Au MNPs can be dispersed in a chalcogenide glass solution with minimal aggregation, as quantified by the absorption spectra. Comparison of the optical behavior of the films to that of the solutions showed that the concentration of Au MNPs was too low to observe the characteristic SPR band. The results of the QD testing show that luminescence can be observed from a deposited film, and that the behavior of the QDs, characterized by quantum yield and lifetime, varies greatly in different environments. Furthermore, it was found that different capping agents led to different behavior of the QDs in the glass solution, affecting the properties of the deposited film.

ACKNOWLEDGMENTS

Many people have contributed to the work done in this thesis. Of course, none of this research would be possible without my advisor at Clemson University, Dr. Kathleen Richardson. Thanks to her, I have had to opportunity to work with many great collaborators, such as Dr. Alex Martucci and Dr. Yaw Obeng, and to study at Université Bordeaux 1 through the Atlantis-MILMI program. In France, Dr. Jean-Louis Bobet and Dr. Evelyne Fargin have helped me greatly to be successful in a foreign country.

This research has also been made possible thanks to my advisor in Bordeaux, Dr. Nathan McClenaghan, who has furthered this project immensely thanks to his knowledge of chemistry and luminescence. Through the expertise of both advisors, I was able to plan good experiments, learn the most that I could from the data, and present the results in a clear manner. I also thank my committee members, Dr. Igor Luzinov and Dr. Konstantin Kornev from Clemson, and Dr. Marc Dussauze from Bordeaux for their support.

The students and post-docs in both groups, especially Dr. Dave Musgraves and Dr. Luca Scarpantonio, have given me much assistance in my day-to-day lab work. Thanks to these great, helpful people, I was able to take good measurements, and learn the laboratory techniques necessary for successful experiments. They also helped to provide an enjoyable work environment.

Additionally, the administration at both Clemson University and Université Bordeaux 1 were essential to this project thanks to all that they do “behind-the-scenes” to help everything run smoothly.

Finally, I thank my wife, Jackie, and my family for all of their love and support.

TABLE OF CONTENTS

Page

LIST OF TABLES

LIST OF FIGURES

CHAPTER ONE

MOTIVATION AND RESEARCH OBJECTIVES

1.1 Motivation

Over the past few decades, an explosion of research has been conducted on materials of dimension less than 100 nm due to their extraordinary optical and electronic properties. These materials, defined as nanomaterials, sometimes possess interesting phenomenon that differs from their analogous macroscopic bulk material. Dispersing nanomaterials into an appropriate host matrix therefore allows the potential to fabricate new materials with properties unattainable by any single material. Metallic nanoparticles (MNPs) exhibit a characteristic surface plasmon resonance (SPR) absorption band, while quantum dots (QDs) exhibit quantum confinement effects, leading to luminescence. These properties are size-dependent, so they can be tuned depending on the application. Additionally, the properties also depend on the surrounding environment.

Chalcogenide glasses are well known for their attractive optical properties, such as transparency to infrared light and high refractive index. These properties make them ideal candidates for optical systems such as chemical sensors, which requires the fabrication of films or formation into fibers. There are several ways to deposit films of chalcogenide glass (ChG), such as pulsed laser deposition (PLD), thermal evaporation (TE), and sputtering [1-2]. However, a solution-derived approach, which consists of dissolving the glass in an appropriate solvent, then film deposition by spin-coating or dip-coating, offers the potential to easily incorporate dispersed nanostructures, without some

of the drawbacks of TE, PLD, or sputtering processes. These methods can sometimes show evidence of segregation or preferential deposition due to differences in vapor pressure/laser absorption cross-section of the dopant material that leads to either dopant deficient materials or local inhomogeneities in the resulting film. In solution-based processing of doped ChG materials, nanoparticles which are dispersed in an organic solvent can be effectively dispersed into solution before film deposition, yielding nanoparticle-doped films with desirable optical properties. In the case of MNP doping, inclusion of the environment-sensitive SPR band is attractive for detecting the presence of chemicals, as well as enhancing magneto-optic effects like the Verdet coefficient, a measure of a material's ability to rotate the polarization plane of light in a magnetic field. Luminescent QDs also have many applications, as they are an efficient, compact source of light. This leads to applications in optical chemical sensors of small size, and attractive candidate technology for low-cost, compact point sensors.

1.2 Research Objectives

The goal of this thesis has been to investigate the incorporation of Au MNPs and CdSe and PbS QDs in solution-derived $Ge_{23}Sb_7S_{70}$ glass films. In doing so, there are several issues that must be addressed, as both spin-coating of ChGs and the properties and dispersion of nanoparticles can be very sensitive to a number of processing parameters. In the case of spin-coating, research in our group has found that solubility of the glass in a solvent and resulting film quality are both sensitive to the amount of water in the solvent. Furthermore, the resulting properties of the film are affected by residual solvent in the film matrix, and the addition of nanoparticles most often introduces a

second solvent into the solution besides the solvent used to dissolve the glass. It is unlikely that the chalcogenide glass would be soluble in the solvent used to disperse the nanoparticles, so this raises the question of what volume percentage of nanoparticle solution can be added before the glass begins to precipitate. Finally, film thickness also decreases as glass concentration in the solution decreases, which is an inherent effect when adding a solution of nanoparticles. These topics comprise the key goals of this thesis.

In the case of nanoparticles, their properties and ability to disperse are often strongly dependent on the environment within the host matrix. Due to the high surface area to volume ratio of a nanoparticle, it is often necessary to "cap" the surface with an organic ligand that allows it to disperse in the desired environment, as well as enhance the inherent stability. One end of the capping agent must be able to bond strongly to the surface of the nanoparticle, while the other end must have a functional group with a high affinity for the desired solvent for dispersion. Generally, it is not difficult to disperse relatively high concentrations of nanoparticles in organic solvents such as alcohols and chloroform. However, obtaining high concentrations of nanoparticles in amine solvents that are stable over long enough periods of time has been studied much less, and dissolved glass in the solvent further complicates the chemistry of the system.

Because of these issues, the addition of a nanoparticle solution to a chalcogenide glass solution therefore raises many questions regarding the optical properties and

characteristics of the resulting spin-coated film. The main questions addressed in this thesis are the following.

1. How can the surface of the nanoparticle be modified with different capping agents so that it can disperse well in the glass film?
2. What is the maximum loading level of the nanoparticles in the glass solution?
3. How, and in what concentration, does the addition of nanoparticles affect the film properties, such as absorption bands and luminescence of the film?

This thesis is formatted with the following organization. Following an introduction which discusses the state of the art in this field, the experimental details used in this thesis are described. The results of these experiments, divided by class of nanoparticle, are then presented along with a discussion of their meaning. Finally, conclusions drawn from the work done in this thesis are reported, and future work in this exciting field is suggested.

1.3 References

[1] L. Petit, N. Carlie, H. Chen, S. Gaylord, J. Massera, G. Boudebs, J. Hu, A. Agarwal, L. Kimerling, K. Richardson, "Compositional dependence of the nonlinear refractive index of new germanium-based chalcogenide glasses" *J. Solid State Chem*., **2009**, *182*, 2756-2761.

[2] V. Balan, C. Vigreux, A. Pradel, "Chalcogenide glass rib ARROW guide" *J. Optoelectron. Adv. Mater.*, **2004**, *6*, 875.

CHAPTER TWO

INTRODUCTION

A nanomaterial is a particle that is less than 100 nm in size and exhibits variation of optical and electronic properties with particle size [1], as well as environment. Such nanostructures can be classified by their dimensionality (D), for example, as 0-D dots, 1-D quantum wires, and 2-D thin films or quantum wells. Their properties often differ from their analog 3-D bulk material because as the particle becomes smaller, there is an increasing percentage of surface atoms, which have lower coordination than interior atoms. This much larger quantity of surface thereby results in the nanostructure's surface properties playing a significant role in the determination of the ultimate properties of the material [2]. The incorporation of nanomaterials into a glass matrix has generated much attention because these materials offer a wide range of unique optical properties. In particular, metal nanoparticles (MNPs) have been shown to exhibit non-linear optical properties and magneto-optic effects, while semiconductor nanoparticles, or quantum dots (QDs), are attractive due to their luminescence [1, 3-4].

One such host material that is interesting for the incorporation of nanostructure dopants, are chalcogenide glasses (ChGs). ChGs contain elements from Group VI of the periodic table, such as sulfur, selenium and tellurium, and usually other semi-metal elements such as germanium, antimony, gallium and arsenic [5]. These elements have high atomic weights and bond relatively weakly, giving ChGs their distinctive properties: high linear and non-linear refractive index, and transparency to infrared light [6]. However, a by-product of the weak bonding in ChGs is that they typically exhibit less

robust thermo-mechanical properties and chemical stability as compared to oxide glasses which benefit from higher bond energy metal-oxygen (M-O) bonds. The properties of ChGs make them good candidates for planar mid-infrared (MIR) sensing applications, requiring the fabrication of films [5]. The Ge-Sb-S system is attractive for this application due to their wide transparency window from about 0.6 – 10 μm, and tunable properties which can be modified as the Ge/Sb/S ratio is varied [7]. The composition $Ge_{23}Sb_7S_{70}$ is particularly interesting because of its oxidation resistance [7], and relatively high T_g (for sulfides) of 311°C [8], enabled by the presence of four-coordinated Ge. Other important properties are linear refractive index of 2.05, and non-linear refractive index of 1.7×10^{-18} m^2/W at 1064 nm [9]; for reference, this non-linear index is 55 times that of fused silica. Increasing Ge/Sb ratio decreases index, blue-shifts the visible cut-off, and decreases the non-linear index [8]. Typical methods of depositing thin films of Ge-Sb-S and other ChGs include thermal evaporation, sputtering, and pulsed laser deposition [9-10]. However, a solution-based approach has also been demonstrated, and has the advantages of producing thick films over large areas [11], as well as the possibility to easily incorporate dispersed nanostructures. The particular nanostructures that this thesis focuses on are Au nanoparticles, and CdSe and PbS quantum dots, and their uniform dispersion within a Ge-Sb-S host matrix. Once dispersed, the optical properties of the doped ChG material in solution and film form (upon removal of solvent) are compared.

2.1 Solution-Derived Chalcogenide Glass Films

The first step in the fabrication of solution-derived ChG films is to prepare bulk glass starting material. This is done with a standard ChG melting procedure designed to prevent oxidation [8]. In this procedure, high-purity elemental ingredients are batched into a fused silica ampoule inside of a nitrogen-purged glove box. The ampoule is then vacuumed for a few hours at around 100°C to drive off any residual moisture. The batch can then be sealed using a gas-oxygen torch and melted overnight in a rocking furnace to ensure homogeniety. $Ge_{23}Sb_7S_{70}$ glass is typically melted at around 925°C. In order to prevent crystallization, the melt is air-quenched, and stresses formed during the quench are relieved by annealing overnight at 40-50°C below the T_g.

To fabricate solution-derived films, the bulk glass is crushed into a powder, and dissolved in an amine solvent, generally propylamine, ethylenediamine, or ethanolamine. Typical loading levels of glass in the solvent are 0.1 to 0.2 M. Dissolution usually takes place in under two days, depending on the composition and loading level. Film deposition is done by dripping the glass solution on a microscope slide substrate or Si wafer, and spinning at speeds in the range of 1000 to 4000 rpm for 10 to 30 s. These parameters can be varied in order to obtain films of different thicknesses. During spin-coating, the solvent begins to evaporate, but a heat treatment in a vacuum oven with active pumping is necessary in order to drive off as much residual solvent as possible. Residual solvent often has negative effects such as infrared absorption bands and lowering the refractive index of the film, as well as affecting the environment-dependent properties of an incorporated nanomaterial. A detailed investigation of the optimization

of solution-based ChG film process parameters needed to realize high optical quality thin films is discussed in a parallel investigation [12].

To incorporate nanomaterials, which are generally dispersed in an organic solvent, the nanoparticles of interest are dispersed in the glass solution just before spin-coating. In principle, adding nanostructures to a solution-derived film is a simple process, but the challenge of aggregation is faced, which means that the particles have grouped together in order to minimize surface energy. This degrades the size-dependent properties of the nanostructure that were originally intended, and imposes a maximum possible dopant concentration of nanoparticles in the resulting glass film.

2.2 Surface Structure of Nanoparticles

For a nanostructure to disperse well in the glass solution with minimal aggregation, it must have compatible surface chemistry, which is typically achieved using an organic ligand grafted to the surface. This is shown schematically in Figure 2.1.

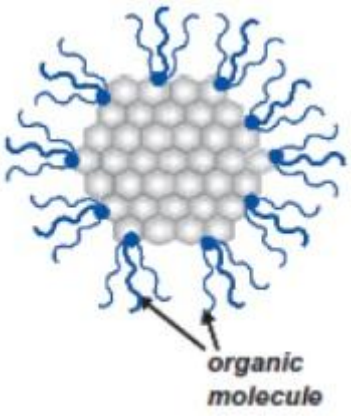

Fig. 2.1: Schematic of organically capped nanoparticle, taken from reference [13]

Through steric hindrance, and electrostatic repulsion in the case of a charged capping agent, the organic ligand prevents nanoparticles from coming into contact with each other and aggregating. The organic ligand is chosen such that it can bond to the surface of the nanoparticle on one end, and disperse in the desired solvent with the functional group on the other end. Typical organic capping agents for MNPs are cetyltrimethylammonium bromide (CTAB) and poly(N-vinylpyrolidone) (PVP); for QDs, typically mercaptans and tri-n-octyl-phosphine oxide (TOPO) are used.

2.3 Properties of Nanoparticles

To understand the properties of nanoparticles, it is useful to first estimate the percentage of surface atoms as a function of diameter for a spherical nanoparticle. Consider a PbS QD, which is assumed to have the same rock-salt crystal structure as the bulk material, shown in Figure 2.2.

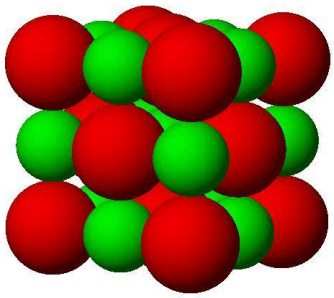

Fig. 2.2: Schematic of rock-salt crystal structure of PbS. Pb atoms are red, S atoms are green, taken from reference [14]

This structure has a packing efficiency given by Equation 2.1, where R_A/R_C is the ratio of anion to cation radius.

$$PE = \frac{2\pi}{3\left(\frac{R_A}{R_C}+1\right)^2} \qquad \text{(Eq. 2.1)}$$

The volume occupied by surface atoms is approximated by multiplying the surface area of the QD by the average diameter of one atom. Dividing this volume by the average volume occupied by one atom approximates the number of surface atoms. Incorporation of the packing efficiency improves the estimate. Equation 2.2 summarizes this calculation, where PE is the packing efficiency, $D_{avg,\ atom}$ is the average diameter of an atom, R_{QD} is the QD radius, and V_{avg} is the average volume of one atom:

$$\%Surface\ atoms = \frac{\left(\frac{PE \cdot D_{avg\ atom} \cdot 4\pi R_{QD}^2}{V_{avg}}\right)}{Total\ atoms\ in\ QD} \cdot 100\% \qquad \text{(Eq. 2.2)}$$

The atomic radius of Pb is 0.146 nm, and S is 0.105 nm, giving a packing efficiency of 0.71. Assuming that the PbS QDs have a similar packing efficiency to bulk PbS, a good estimate of the number of atoms per QD and the percentage of surface atoms can then be plotted as a function of QD diameter, shown in Figure 2.3.

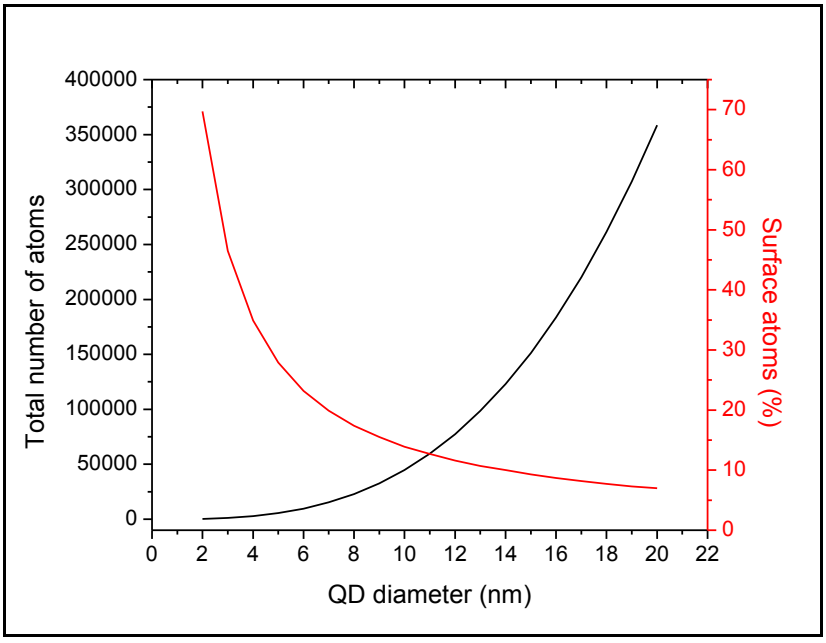

Fig. 2.3: Number of atoms and percentage of surface atoms in PbS QD as a function of QD diameter

The percentage of surface atoms varies greatly, from 70% to less than 10% over the range of diameters from 2-20 nm. Assuming that the properties of materials are determined by both the interior and surface atoms, such a variation may lead to size-dependent properties. This has been observed in many systems of nanomaterials, including PbS and Au [15-16]

2.3.1 Properties of Metal Nanoparticles

The properties of metal nanoparticles are dictated primarily by their surface plasmon resonance (SPR). SPR is defined as the collective oscillation of conduction electrons, and is shown schematically in Figure 2.4.

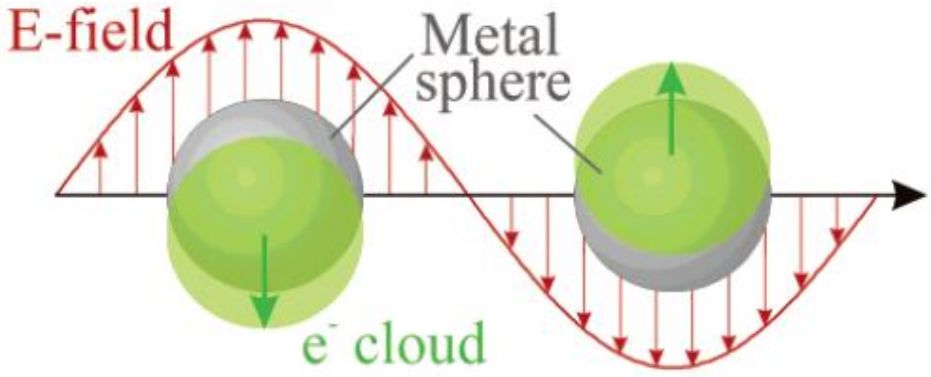

Fig. 2.4: Schematic representation of surface plasmon resonance in a metal nanoparticle, showing the displacement of the conduction electron charge cloud relative to the nuclei, taken from reference [17]

The wavelength and intensity of the SPR band is dependent on several factors including the density of electrons, the effective electron mass, and the shape and size of the charge distribution, as well as the surrounding environment [17-18]. Figure 2.5 shows how the SPR band of Au MNPs shifts with particle size.

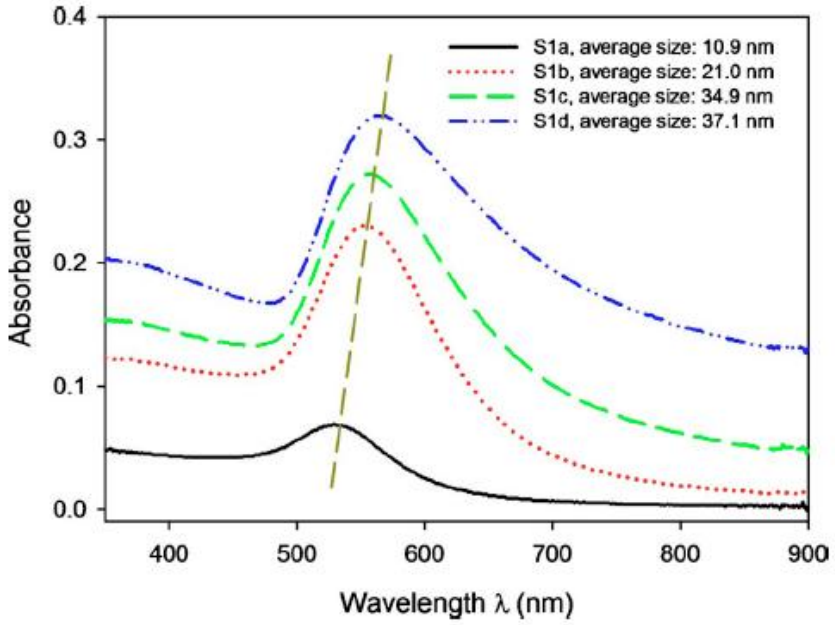

Fig. 2.5: Absorption spectra of various sizes of Au MNP films deposited on a fused silica substrate, taken from reference [15]

The SPR band of MNPs is also environment dependent. In a study on Au MNPs in sol-gel derived TiO_2 films [19], Buso et al showed that the SPR band of Au MNPs red-shifts with increasing refractive index of the environment, according to Figure 2.6.

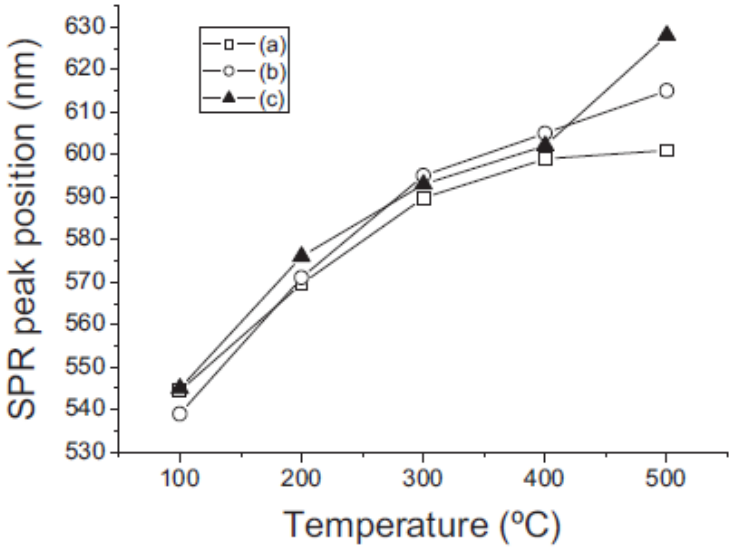

Fig. 2.6: Peak position of the SPR band of Au MNPs dispersed in a TiO_2 film matrix as a function of annealing temperature, taken from reference [19]

In this figure, the horizontal axis represents annealing temperature. Higher annealing temperatures effectively increase the refractive index of the matrix as porosity decreases. The refractive index of undoped matrices ranges from 1.75 to 2.17 for annealing temperatures ranging from 100 to 500°C. In the same study, it was shown that the refractive index of the Au MNP doped films was increased over that of the undoped films for corresponding annealing temperatures as shown in Table 2.1. Thus in the higher refractive index ChGs, we might also expect to see similar variation in MNPs incorporated within these high (n_{ChG} ~ 2-2.5) refractive index glasses.

Table 2.1: Refractive indices of doped and undoped TiO_2 films, taken from reference [19]

Annealing Temperature [°C]	Film thickness [nm]		Refractive index, *n*	
	TiO_2	TiO_2–Au	TiO_2	TiO_2–Au
100	82	99	1.75	1.80
200	48	58	2.06	2.08
300	48	48	2.09	2.14
400	42	42	2.19	2.20
500	41	42	2.17	2.18

2.3.2 Properties of Quantum Dots

Luminescence from QDs is a result of the difference in energy between the valence and conduction bands of the QD. This difference in energy is known as the band-gap, which is size-dependent, and its value determines the wavelength of luminescence. If a QD absorbs energy equal to or greater than the band gap, an electron is excited from the valence band to the conduction band. This results in an exciton, or an electron-hole pair that is bound by electrostatic attraction. The exciton is characterized by the Bohr radius, which is the distance between the hole and the electron in the exciton. The limited number of electrons causes the band structure to split into discrete levels, and the difference between the highest occupied level and lowest unoccupied level decreases with increasing particle size. This means that the positions of both absorption and photoluminescence shift to longer wavelengths as particle size increases. PbS and PbSe are important IV-VI semiconductor quantum dots because of their large exciton Bohr radii, which leads to strong quantum confinement. PbS and PbSe have exciton Bohr radii

of 18 nm and 46 nm, respectively [20]. Figure 2.7 shows the dependence of band-gap energy on particle size of PbS QDs [21].

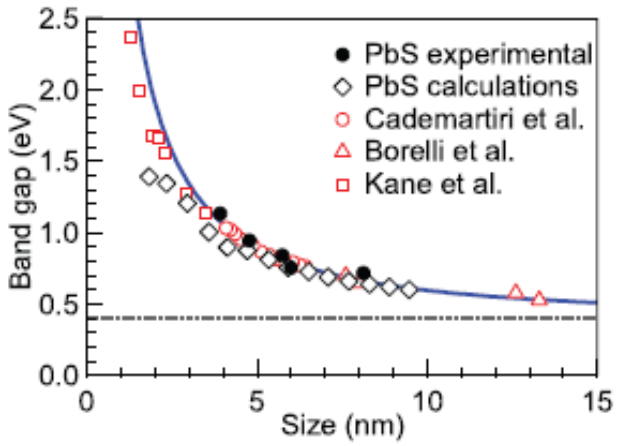

Fig. 2.7: PbS QD band-gap energy as a function of size. The dashed line at 0.4 eV is the bulk PbS band-gap, taken from reference [21]

The band-gap of a QD is size-dependent because of quantum confinement. The quantum confinement effect [22] is when the band-gap increases in energy (blue shifts) when the particle size approaches the Bohr radius. The density of states (DOS) describes the number of states that are able to be occupied by electrons per interval of energy. Quantum confinement modifies the DOS near the band-edges. This allows tuning of the band-gap with particle size, and the optical and electronic properties thus become size dependent. Figure 2.8 shows how the DOS changes with the number of atoms in a material.

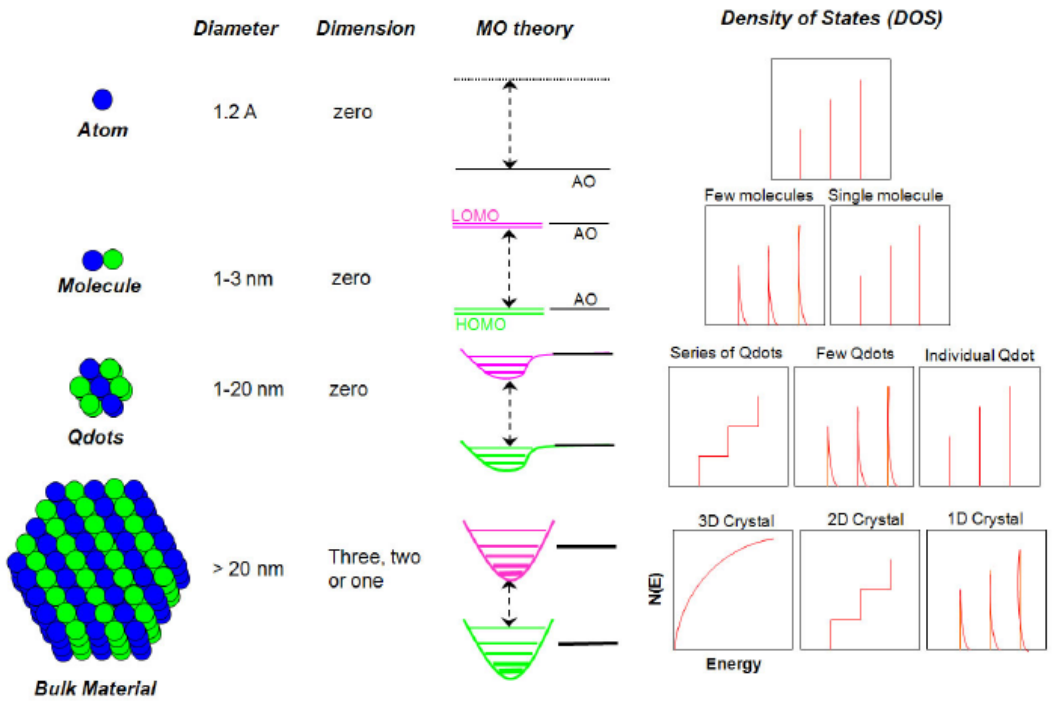

Fig. 2.8: Schematic representation of density of states as a function of particle size in a material, taken from reference [1]

Quantum dots are well known for their strong luminescence. As mentioned previously, an electron can be excited above ground state when a QD absorbs energy equal to or greater than the band gap. The excitation energy leading to luminescence can be delivered in various ways such as a photon (photoluminescence), an electric field (electroluminescence), or an electron (cathodoluminescence). The excited electron will relax to recombine with the hole through radiative transitions where the excess energy is emitted in the form of a photon, or dissipated through non-radiative processes. Two common non-radiative de-excitation pathways involve phonons, where excess energy vibrates the surrounding lattice, or Auger transitions, where a second electron fills the hole created by the first, and the excess energy ejects a third electron from the atom. The emission wavelength of a quantum dot is dependent on band-gap energy, and therefore a

function of size. Figure 2.9 shows how the luminescence spectra of PbSe quantum dots can be tuned with QD size.

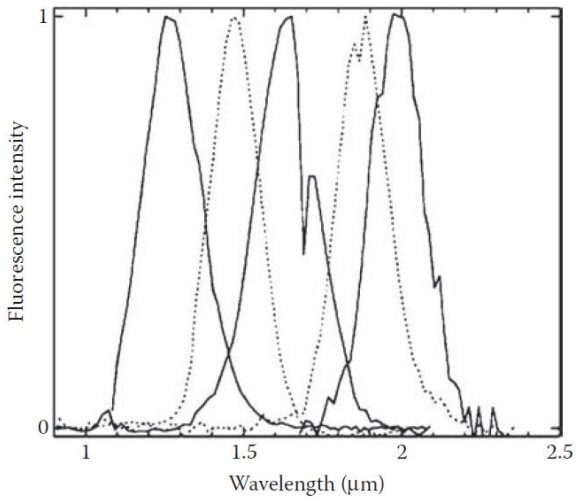

Fig. 2.9: Luminescence spectra of PbSe QDs of varying sizes using 1064 nm excitation source, taken from reference [21]

Band-edge emission is the most common radiative relaxation process, where an electron in the conduction band recombines with a hole in the valence band. Another type of radiative transition is defect emission. Defect states can be caused by impurities or other lattice defects, and lie inside the band-gap [23]. They can be classified as donors if they have excess electrons or acceptors if they have a deficit of electrons. If the defect state has energy near the conduction band or valence band, it is considered shallow. Shallow defect states often only exhibit radiative relaxation at low temperatures where thermal energy cannot excite the carriers out of the defect state. Deep levels have positions intermediate between the valence band and conduction band, and generally experience non-radiative de-excitation.

One important characterization of photoluminescence is the Stokes shift. The Stokes shift is the band edge photoluminescence red-shift with respect to the absorption edge, meaning that the emission is at a longer wavelength (lower energy) than the excitation [24]. It is caused by the excited electron experiencing some level of non-radiative relaxation before radiative recombination. Figure 2.10 shows schematically the Stokes shift of a material on an absorption and photoluminescence spectrum.

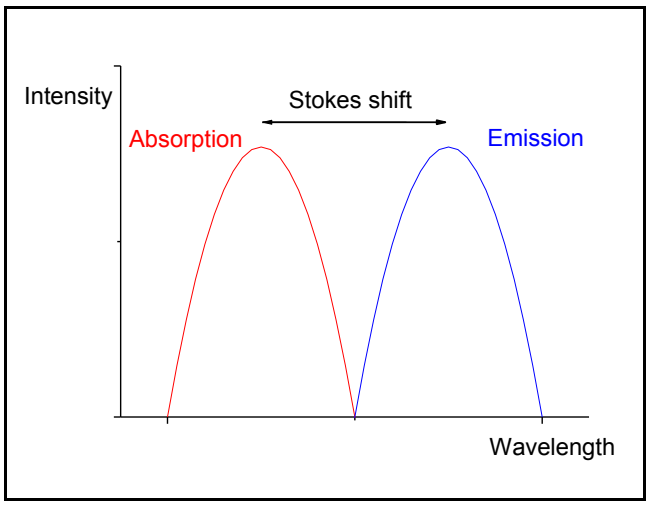

Fig. 2.10: Schematic representation of Stokes shift

Quantum yield, Φ, is another important metric of the luminescence of quantum dots, and is given by the ratio in Equation 3. This represents the internal efficiency of luminescence.

$$\Phi = \frac{number\ emitted\ photons/sec}{number\ absorbed\ photons/sec} \qquad \text{(Eq. 2.3)}$$

Shown in Figure 2.11, Semonin et al report that the quantum yield of PbS and PbSe QDs is strongly dependent on QD size. The absorption spectrum of the capping agent, oleic acid, is also shown for reference, as reabsorption of luminescence decreases calculated quantum yield [25].

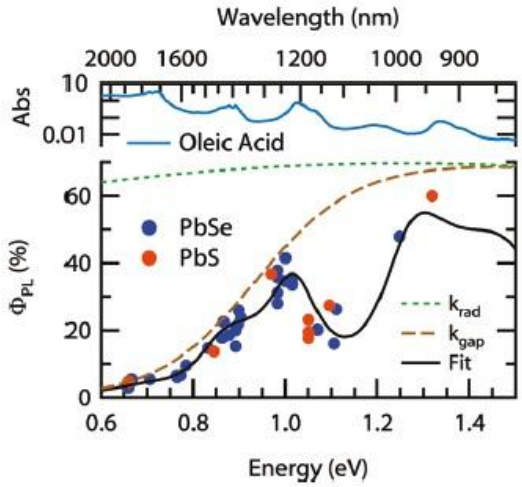

Fig. 2.11: Quantum yield of PbS and PbSe plotted as a function of band-gap energy from 0.65 eV (10 nm diameter) to 1.3 eV (2 nm diameter)., taken from reference [25]

One way to improve quantum yield is by passivating the surface of the QD [21]. As mentioned earlier, organic capping agents allow a nanostructure to disperse in a solvent with reduced/minimal aggregation as compared to its dispersion in an uncapped state. For a QD, surface passivation also plays the role of saturating dangling surface bonds. This reduces the number of surface defects, which often lie in the band-gap of the QD, reducing non-radiative de-excitation and increasing quantum yield [1]. However, the number of organic molecules that can reach the surface is limited by the molecular weight of the ligand through steric hindrance, so a large percentage of surface defects

remain. Core-shell QDs are an attractive solution because the surface of the QD is passivated by a material with the same crystal structure. This allows nearly all dangling surface bonds to be satisfied, and very high quantum yields to be obtained. A schematic of a core-shell QD is shown in Figure 2.12.

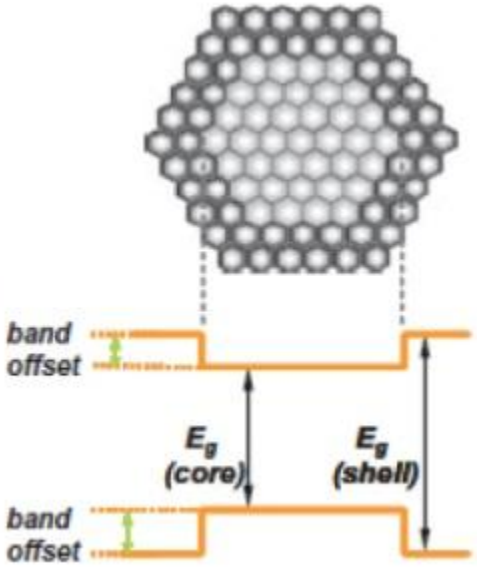

Fig. 2.12: Inorganically passivated QD and the difference in band-gap energy between core and shell in an inorganically passivated QD, taken from reference [13]

It is necessary for the shell to have a larger band-gap so that an excited electron cannot transfer from the core to the shell and experience non-radiative recombination or a shift in luminescence wavelength. The shell should also have a lattice parameter within 12% of the core to minimize strain, which red-shifts the absorption and emission spectra of the QDs [26].

Another important metric of QD luminescence is lifetime, which is defined as the length of time required for the luminescence to decay to 1/e of the original value.

Lifetime is an indication of the driving force for an excited electron to de-excitate (also called decay) through both radiative and non-radiative processes. Lifetime, expressed by τ in units of inverse time, is given by Equation 2.4, where k_r is the rate of radiative processes, and k_{nr} is the rate of all non-radiative processes.

$$\tau = \frac{1}{k_r + k_{nr}} \qquad \text{(Eq. 2.4)}$$

Experimentally, lifetime is measured using time-correlated single photon counting techniques, which involves a pulsed excitation source. Quantum yield can also be expressed in terms of lifetime, as shown in Equation 2.5.

$$\Phi = k_r \tau = \frac{k_r}{k_r + k_{nr}} \qquad \text{(Eq. 2.5)}$$

2.4 Synthesis of Nanoparticles

MNPs and QDs can be synthesized in several ways. They are classified as either top-down, where bulk material is thinned to form nanoparticles, or bottom-up, which includes self-assembly techniques, most often carried out in solution. Top-down synthesis of MNPs is done using methods such as vacuum deposition, electron beam lithography, or laser ablation [18], and techniques used for the top-down synthesis of QDs include electron beam lithography, reactive-ion etching, wet chemical etching and focused ion beam techniques [1]. Top-down techniques often suffer from disadvantages such as incorporation of impurities, structural imperfections, and inability to form small enough sizes of nanoparticles. Furthermore, bottom-up methods are more attractive for our

interests because the MNPs can be dispersed directly in an organic solvent compatible with solution-derived ChG film processing.

2.4.1Bottom-up Synthesis of Au MNPs

The classic citrate method was established by Turkevich et al in 1951 [27] and refined throughout the years by serveral authors including Frens et al [28]. This method consists of the reduction of chloroauric acid ($HAuCl_4$) by sodium citrate ($Na_3C_6H_5O_7$) in water. The reaction is generally initiated by temperature, such as at the boiling point of water, and also by ultraviolet light, as shown by Kimling et al [29]. As reduction of the $AuCl_4^-$ ions progresses, the solution color changes from black, to purple, to blue, to dark red. Particle size can be controlled by varying the ratio of initial concentrations of citrate to gold, as shown in Figure 2.13.

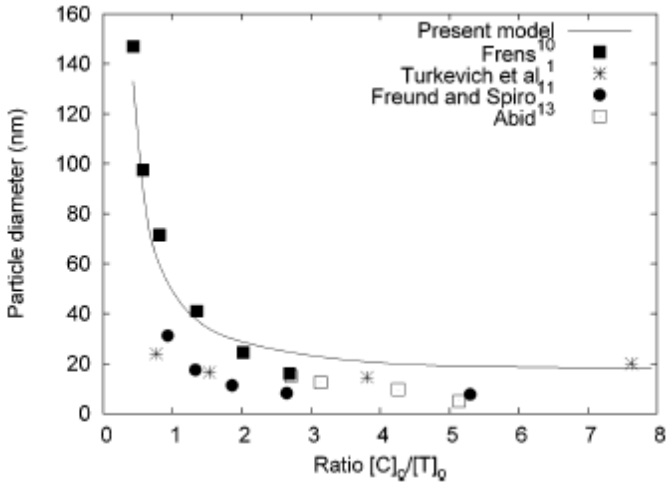

Fig. 2.13: Au nanoparticle size using the citrate synthesis method, taken from reference [30]

Another method uses ultrasonic waves to form nanoparticles by reduction of Au^{3+} ions in aqeous solution in the presence of various organic compounds such as polyethylene glycol monostearate or polyvinylpyrrolidone [31]. Okitsu et al [32] report that using a 200 kHz frequency ultrasonic generator creates bubbles with extremely high temperatures of several thousands of degrees, and pressures of hundreds of atmospheres. This forms H atoms and OH radicals, which reduce the Au ions and form nanoparticles in the presence of 2-propanol according to the following reactions.

$$H_2O \rightarrow {}^{\cdot}OH + {}^{\cdot}H \qquad \text{(Eq. 2.6)}$$

$$(CH_3)CHOH + {}^{\cdot}OH\ ({}^{\cdot}H) \rightarrow (CH_3)_2COH + H_2O\ (H_2) \qquad \text{(Eq. 2.7)}$$

$$(CH_3)_2CHOH \rightarrow \text{pyrolysis radicals} \qquad \text{(Eq. 2.8)}$$

$$Au^{3+} + \text{reducing radicals} \rightarrow\rightarrow Au^0 \qquad \text{(Eq. 2.9)}$$

The reducing radicals include the pyrolysis radicals, which are formed through the decomposition of organic molecules at high temperature, as well as H atoms, and (1-hydroxymethyl) ethyl radicals.

2.4.2 Bottom-Up Synthesis of PbS QDs

The reverse micelle technique consists of mixing cationic and anionic reverse micelles. Pellegri et al fabricated PbS QDs by mixing two sodium dioctyl sulfosucinate-heptane reverse micelles containing Na_2S and $Pb(NO_3)_2$, respectively [33]. They achieved a final PbS concentration of 4.7×10^{-3} M, and sizes ranging from 2.3-4 nm. Advantages

of the reverse micelle technique are that the size of the QDs can be controlled easily, a narrow size distribution is possible, and ease of dispersion. Disadvantages are low yield and incorporation of impurities and defects [1].

Another bottom-up method of fabricating PbS QDs is through the sol-gel method. There are three main steps in traditional sol-gel processes: hydrolysis, condensation, and growth. The ‘sol’ or solution is created (nanoparticles dispersed by Brownian motion in a solvent, typically an alcohol with water co-dispersed with a catalyst at a specific pH to stimulate network growth); the network is ‘grown’ during the condensation step, and a gel is formed during the growth step through polymerization. Following solvent removal and network consolidation to remove pores, a solid or porous material can be realized. Sashchiuk et al synthesized PbS QDs through a reaction of lead acetate trihydrate and ammonium thiocyanate in 2-methoxymethanol at its boiling point [34]. It was found that up to 50% excess of sulfur was needed to complete the reaction, and that the nanocrystals were spherical with size of about 2-4.5 nm. The QDs were successfully incorporated into sol-gel derived glass zirconia films. The sol-gel method of synthesizing QDs is very simple and cost-effective, but the QDs generally have a broad size distribution and contain defects and impurities [1].

The organometallic route, also known as hot-solution decomposition, has been used to synthesize PbS QDs [35]. PbO is first dissolved in oleic acid at 150°C under Ar. Bis-trimethylsilylsulfide in trioctylphosphine is then injected to provide a source of sulfur ions. The size of the PbS nanocrystals is controlled by reaction parameters such as temperature and concentration of reactants. The QDs are stabilized with oleate ligands

coordinated to the Pb atoms. A ligand exchange can be done to obtain shorter chain capping agents, such as octylamine, and the QDs can then be dispersed in a variety of organic solvents. This technique results in QDs with low amounts of defects, but the organometallic precursors are often toxic, and the higher processing temperatures required lead to higher costs. Furthermore, the QDs generally do not disperse in water [1].

Sono-chemical methods use ultrasonic irradiation to initiate the precipitation of nanocrystals in solution. *Sono-chemistry*, as it is called, is becoming more common to synthesize new materials, and arises from acoustic cavitation phenomenon. This phenomenon is the formation, growth, and collapse of bubbles in liquid, which generates a local hotspot with temperature up to 5000°C [36]. Li et al used 18 kHz ultrasonic irradiation to react $Pb(CH_3COO)_2 \cdot 3H_2O$ with elemental chalcogens in ethylenediamine to form QDs of PbS and PbSe [20]. The reaction took place at room temperature for 3 hours, and the nanocrystals were found to have cubic crystallinity and to be uniformly cube shaped with an edge length of about 350 nm. This method shows promise, but currently can only produce cubic nanocrystals of edge length 130 nm, while spherical QDs of diameter <5 nm are required.

2.5 Incorporation of Nanoparticles into Glass Matrices

Quantum dots have been incorporated into glass film matrices with methods such as sol-gel, precipitation, and reaction of a film containing ions with an appropriate gas [1].

The sol-gel route combines sol-gel and colloidal chemistry, and consists of three basic steps. First, a colloidal solution of quantum dots is prepared. Next, the precursor solution for the glass matrix is prepared. The colloidal solution is then added to the precursor solution to form the coating solution, which can be dip-coated to produce a quantum dot-doped film. The concentration of the quantum dots in the glass matrix is controlled by varying the amount of colloidal solution mixed with the glass matrix precursor. Pellegri et al used this method to fabricate silica gels doped with PbS QDs synthesized by the reverse micelle method [33]. As shown in Figure 2.14, they found that the absorption edge of the PbS nanocrystals in the silica gel blue shifted relative to the as-prepared PbS.

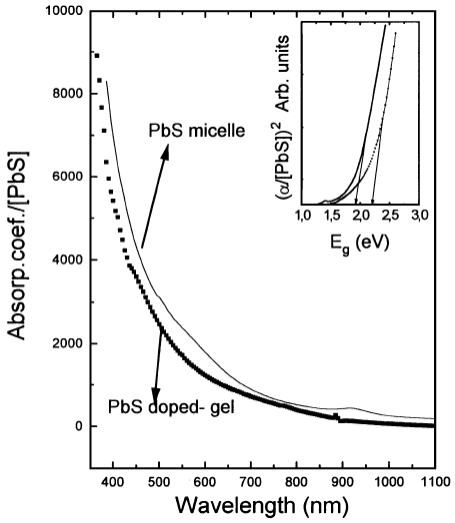

Fig. 2.14: Absorption spectra comparing as-prepared PbS micelles and PbS doped silica gel, taken from reference [33]

This shift could have been caused by either a reduction of the particle size during processing conditions, or effects from different environments. In a study done by Martucci et al [37], PbS QDs with average size of 4.8 nm were incorporated into sol-gel

derived zirconia-ormosil (organically-modified silicate) glass films. The QDs were not deteriorated by the processing conditions, and two concentrations of PbS, 5 and 10 mol%, film were deposited by dip coating. The nonlinear optical index of the films was measured at 1.064 μm, and found to be negative in the range of 10^{-15} – 10^{-16} m^2/W.

The sol-gel route has also been used to fabricate QD-doped chalcogenide films. Mashford et al [38] prepared CdSe QDs with an epitaxial layer of ZnS and ZnS nanocrystals dispersed in the same alcohol solution. The ratio of CdSe QDs to ZnS was 5 wt%. The solution was then spin-coated, and as shown in Figure 2.15, during annealing the solvent evaporates and the organic capping agent volatilizes, leaving behind a ZnS matrix containing CdSe QDs.

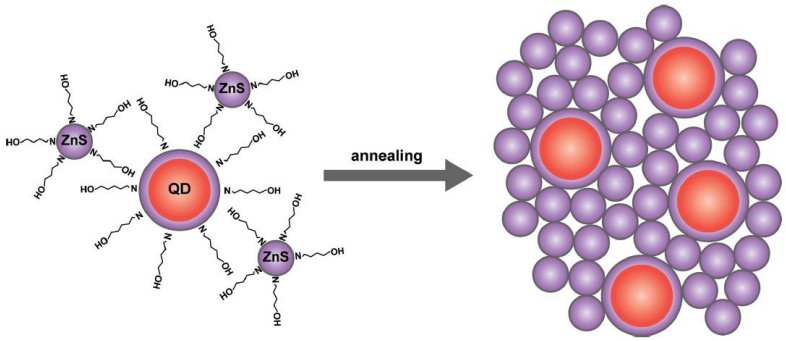

Fig. 2.15: Schematic of mechanism of CdSe doped ZnS film formation during annealing step, taken from reference [38]

Various sizes of CdSe QDs were incorporated into ZnS films using this approach, and strong photoluminescence was observed, with the emission wavelength depending on the size of the QD. The QDs were also found to be photostable, as evidenced by a constant PL intensity over 60 minutes of exposure to 3 mW/cm^2 UV irradiation of 380-390 nm.

Film porosity was estimated by comparing the measured refractive index of the film to that of bulk ZnS using an effective medium model. This is an important characterization because the index of the film must be high for certain applications, such as waveguides. Shown in Figure 2.16, porosity was found to decrease with annealing temperature.

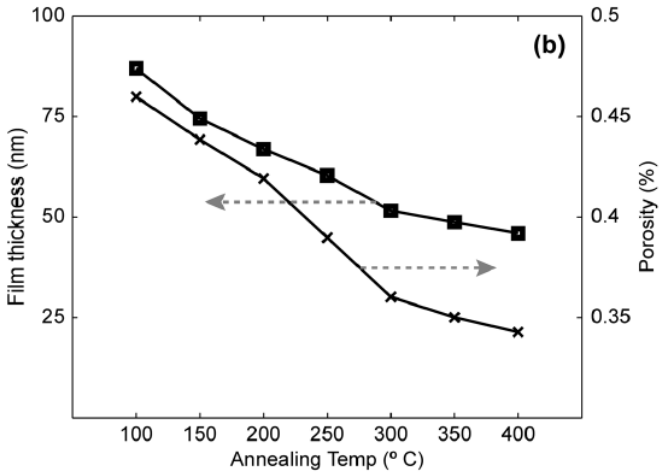

Fig. 2.16: Porosity and film thickness of CdSe QD doped ZnS film, taken from reference [38]

The method of precipitation consists of traditional glass forming techniques: batching raw ingredients, melting, and quenching. However, small amounts of PbSe salt are added during the batching step, and after quenching the glass can be heat treated to precipitate PbSe QDs [39]. One might envision using this type of strategy to precipitate PbTe QDs in a matrix such as the ChGs of interest to the present effort. As is known, the heavier, higher atomic number material would be expected to have a longer wavelength (lower energy) spectral emission than the sulfide or selenide materials. As shown in

Figure 2.17, the absorption (size) of the QDs can be controlled by varying the temperature and duration of the heat treatment.

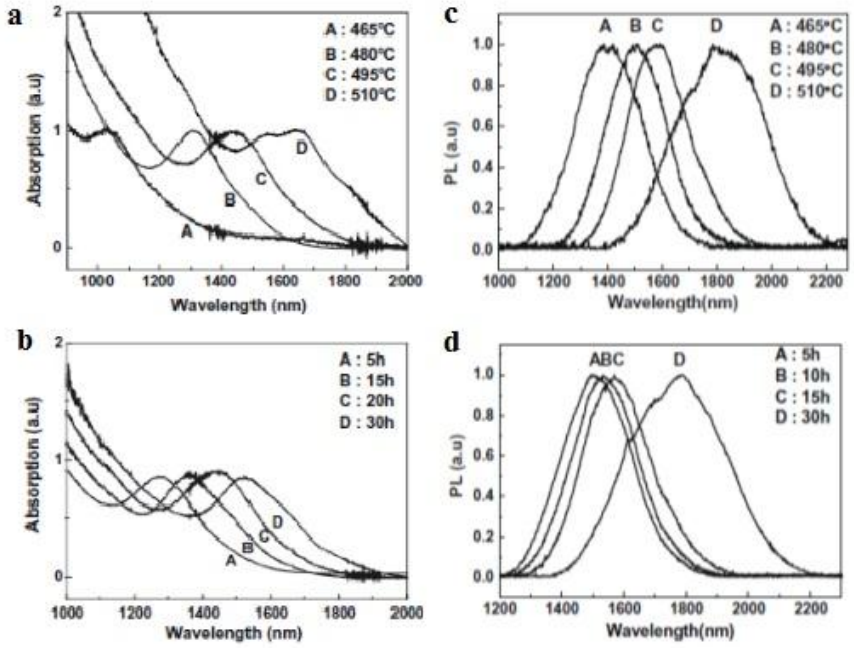

Fig. 2.17: Absorption and photoluminescence spectra of PbSe QDs precipitated in borosilicate matrix. Heat treatment temperature is varied in a) and c) at 20 hrs, and duration is varied in b) and d) at 495°C, taken from reference [39].

This shows that absorption and emission peaks can be tuned easily in the near-infrared by varying QD size in an oxide glass matrix. However, the required temperatures are well above the T_g of $Ge_{23}Sb_7S_{70}$ of interest to the present study so a precipitation method is not appropriate. However, consideration of this approach for a higher (Ge-content) T_g matrix could be considered possible.

PbS QDs can also be formed in a porous silica matrix by passing H_2S gas over silica xerogels doped with Pb^{2+} ions. Parvathy et al [40] found that a minimum

temperature of 250°C is required for the reaction between H_2S and Pb ions. Shown in Figure 2.18, they also found that QD size can be controlled by varying the initial Pb^{2+} concentration, but could not obtain larger sizes for unknown reasons. Like the precipitation method, the technique of reacting a doped film with a gas requires temperatures that are known to deteriorate the quality of $Ge_{23}Sb_7S_{70}$ films thus rendering this approach untenable for our candidate materials.

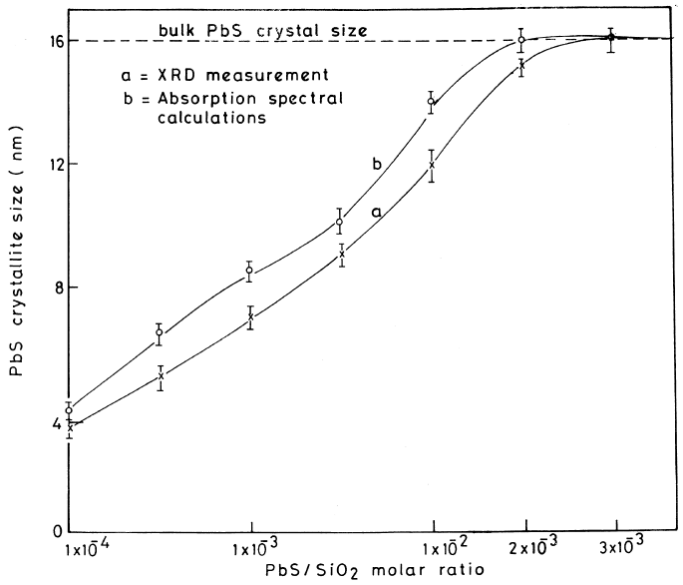

Fig. 2.18: Variation of PbS crystallite size with PbS/SiO_2 ratio. [40]

2.6 Summary

This section has summarized the state of the art in the fabrication of MNPs and QDs and subsequent doping into glass matrices using a diverse means of chemical and physical techniques. A wide variety of synthesis methods have been demonstrated, and this lends to the incorporation of these nanomaterials into several types of host matrices

with a broad range of processing conditions. Target properties of the host matrix can be successfully improved in several ways, including increased nonlinear index and Verdet coefficient in the case of MNPs, and luminescence in the case of QDs. The field of nanomaterial doped glasses is relatively young, and there are numerous exciting discoveries still to be made. Despite this, many systems have been studied, and the principles learned pave the way for the incorporation of MNPs and QDs into solution-derived chalcogenide glass films.

2.7 References

[1] D. Bera, L. Qian, T-K. Tseng, P. Holloway, "Quantum dots and their multi-modal applications: A review" *Materials* **2010**, *3*, 2260-2345.

[2] T. Trindade, P. O'Brien, N. Pickett, "Nanocrystalline semiconductors: Synthesis, properties and perspectives" *Chem. Mater*. **2001**, *13*, 3843-3858.

[3] J. A. Schuller, E. S. Barnard, W. Cal, Y. C. Jun, J. S. White, M. L. Brongersma, "Plasmonics for extreme light concentration and manipulation" *Nature Materials*, **2010**, *9*, 193-205.

[4] Y. Gu, K. Kornev, "Plasmon enhanced direct and inverse Faraday effects in non-magnetic nanocomposites" *J. Opt. Soc. Am. B*, **2010**, *11*, 2165-2173.

[5] N. Carlie, "A solution-based approach to the fabrication of novel chalcogenide glass materials and structures," **2010**, PhD thesis, Clemson University.

[6] J. Hu, V. Tarasov, A. Agarwal, L. Kimerling, N. Carlie, L. Petit, K. Richardson, "Fabrication and testing of planar chalcogenide waveguide integrated microfluidic sensor" *Optics Express*, **2007**, *15(5)*, 2307-2314.

[7] J.D. Musgraves, N. Carlie, J. Hu, L. Petit, A. Agarwal, L. Kimerling, K. Richardson, "Comparison of the optical, thermal and structural properties of Ge-Sb-S thin films deposited using thermal evaporation and pulsed laser deposition techniques" *Acta Materialia*, **2011**, *59(12)*, 5032-5039.

[8] L. Petit, N. Carlie, F. Adamietz, M. Couzi, V. Rodriguez, K. Richardson, "Correlation between physical, optical and structural properties of sulfide glasses in the system Ge–Sb–S" *Mat. Chem. and Phys*, **2006**, *97(1)*, 64-70.

[9] L. Petit, N. Carlie, H. Chen, S. Gaylord, J. Massera, G. Boudebs, J. Hu, A. Agarwal, L. Kimerling, K. Richardson, "Compositional dependence of the nonlinear refractive index of new germanium-based chalcogenide glasses" *J. Solid State Chem.*, **2009**, *182*, 2756-2761.

[10] V. Balan, C. Vigreux, A. Pradel, "Chalcogenide glass rib ARROW guide" *J. Optoelectron. Adv. Mater.*, **2004**, *6*, 875.

[11] S. Song, N. Carlie, J. Broudies, L. Petit, K. Richardson, C. Arnold, "Spin-coating of $Ge_{23}Sb_7S_{70}$ chalcogenide glass thin films" *J. Non-Cryst. Solids*, **2009**, *355*, 2272-2278.

[12] J. Wilkinson, "Characterization and optimization of solution-derived chalcogenide glass thin films" MS thesis, Clemson University **2012**.

[13] D. Bera, L. Qian, P. Holloway, "Phosphor Quantum Dots" *John Wiley & Sons, Ltd*, **2008**.

[14] http://www.seas.upenn.edu/~chem101/sschem/ionicsolids.html

[15] S. Zhu, T.P. Chen, Y.C. Liu, S.F. Yu, Y. Liu, "Tunable surface plasmon resonance of gold nanoparticles self-assembled on fused silica substrate" Electrochemical and Solid-State Letters, **2010**, *13*, K96-K99.

[16] I. Moreels, K. Lambert, D. Smeets, D. De Muynck, T. Nollet, J. C. Martins, F. Vanhaecke, A. Vantomme, C. Delerue, G. Allan, Z. Hens, "Size-dependent optical properties of colloidal PbS quantum dots" *A. C. Nano*, **2009**, *3*, 3023-3030

[17] K.L. Kelly, E. Coronado, L.L.Zhao, G.C. Schatz, *J. Phys. Chem. B.*, **2003**, *107*, 668.

[18] Hutter, E: Exploitation of localized surface plasmon resonance. Adv. Mater. **2004**.

[19] D. Buso, J. Pacifico, A. Martucci, P. Mulvaney, "Gold nanoparticle-doped TiO_2 semiconductor thin films: optical characterization" *Adv. Funct. Mater.*, **2007**, *17*,347-354.

[20] Q. Li, Y. Ding, M. Shao, J. Wu, G. Yu, Y. Qian, "Sonochemical synthesis of nanocrystalline lead chalcogenides: PbE (E = S, Se, Te)" *Materials Research Bulletin*, **2003**, *38*, 539-543.

[21] V. Klimov, "Nanocrystal quantum dots" *CRC Press*, **2010**.

[22] A.D. Yoffe, "Semiconductor quantum dots and related systems: Electronic, optical, luminescence and related properties of low dimensional systems" *Adv. Phys.* **2001**, *50*, 1–208.

[23] A. Issac, C. von Borczyskowski, F. Cichos, "Correlation between photoluminescence intermittency of CdSe quantum dots and self-trapped states in dielectric media" *Phys. Rev. B* **2005**, *71*, 161302-1-4.

[24] N. Dantas, P. de Paula, R. Silva, V. Lopez-Richard, G. Marques, "Radiative versus nonradiative optical processes in PbS nanocrystals" *J. Appl. Phys*, **2011**, *109*, 024308.

[25] O. Semonin, J. Johnson, J. Luther, A. Midgett, A. Nozik, M. Beard, "Absolute photoluminescence quantum yields of IR-26 dye, PbS, and PbSe quantum dots" *J. Phys. Chem. Lett.*, **2010**, *1*, 2445-2450.

[26] X. Peng, M. Schlamp, A. Kadavanich, A. Alivisatos, "Epitaxial growth of highly luminescent CdSe/CdS core/shell nanocrystals with photostability and electronic accessibility" *J. Am. Chem. Soc.* **1997**, *119*, 7019–7029.

[27] J. Turkevich, "A study of the nucleation and growth processes in the synthesis of colloidal gold" *Discussions of the Faraday Society*, **1951**, *11*, 55.

[28] G. Frens, "Controlled Nucleation for the Regulation of the Particle Size in Monodisperse Gold Suspensions" *Nat. Phys. Sci.*, **1973**, *20*, 241.

[29] J. Kimling, M. Maier, B. Okenve, V. Kotaidis, H. Ballot, A. Plech, "Turkevich method for gold nanoparticle synthesis revisited" *J. Phys. Chem. B*, **2006**, *110*, 15700-15707.

[30] S. Kumar, K. S. Gandhi, R. Kumar, "Modeling the formation of gold nanoparticles by citrate method" *Ind. Eng. Chem. Res.*, **2007**, *46*, 3128-3136.

[31] K. Okitsu, Y. Mizukoshi, H. Bandow, Y. Maeda, T. Yamamoto, Y. Nagata, "Formation of noble metal particles by ultrasonic irradiation" *Ultrasonics Sonochemistry*, **1996**, *3*, S259-S251.

[32] K. Okitsu, A. Yue, S. Tanabe, H. Matsumoto, Y. Yobiko, "Formation of colloidal gold nanoparticles in an ultrasonic field: control of rate of gold (III) reduction and size of formed gold particles" *Langmuir*, **2001**, *17*, 7717-7720.

[33] N. Pellegri, R. Trbojevich, O. de Sanctis, K. Kadono, "Fabrication of PbS nanoparticles embedded in silica gel by reverse micelles and sol-gel routes" *Journal of Sol-Gel Science and Technology*, **1997**, *8*, 1023-1028.

[34] A. Saschiuk, E. Lifshitz, R. Reisfeld, T. Saraidarov**,** M. Zelner, A. Willenz, "Optical and conductivity properties of PbS nanocrystals in amorphous zirconia sol-gel films" *Journal of Sol-Gel Science and Technology*, **2002**, *24*, 31-38.

[35] L. Bakueva, S. Musikhin, M. Hines, T. Chang, M. Tzolov, "Size-tunable infrared (1000–1600 nm) electroluminescence from PbS quantum-dot nanocrystals in a semiconducting polymer" *Appl. Phys. Lett.*, **2003**, *82*, 2895.

[36] S.J. Doktycz, K.S. Suslick, "Interparticle collisions driven by ultrasound" *Science*, **1990**, *247*, 1067-1069.

[37] A. Martucci, P. Innocenzi, J. Fick, J. Mackenzie, "Zirconia-ormosil films doped with PbS quantum dots" *J. Non-Cryst. Sol.*, **1999**, *244*, 55-62.

[38] B. Mashford, J. Baldauf, T. Nguyen, A. Funston, P. Mulvaney, "Synthesis of quantum dot doped chalcogenide glasses via sol-gel processing" *J. Appl. Phys*., **2011**, *109*, 094305.

[39] J. Chang, C. Liu, J. Heo, "Optical properties of PbSe quantum dots doped in borosilicate glass" *J. Non-Cryst. Sol.*, **2009**, *355*, 1897-1899.

[40] N. Parvathy, A. Rao, G. Pajonk, "Effects of temperature and sol-gel parameters on PbS crystallite sizes and their spectral and physical properties in a porous silica matrix" *J. Non-Cryst. Sol.*, **1998**, *241*, 79-90.

CHAPTER 3

EXPERIMENTAL

3.1 Fabrication of Solution-Derived Glass Films

3.1.1 Fabrication of Bulk Glass

A schematic of the steps used to fabricate bulk ChG is shown in Figure 3.1.

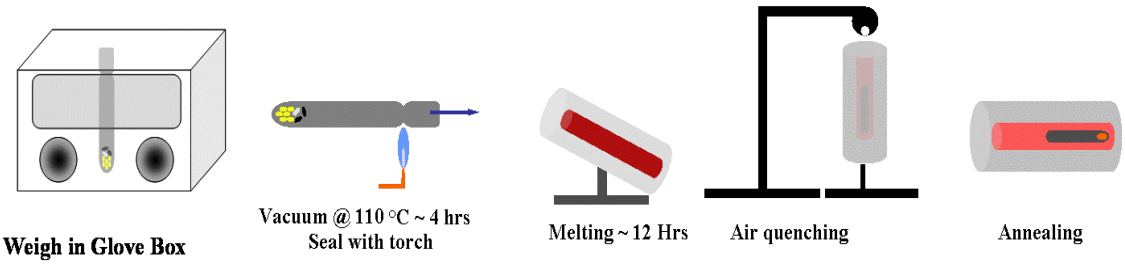

Fig. 3.1: Schematic showing the steps used to fabricate a chalcogenide glass while preventing oxidation, taken from reference [1]

Initially, both $Ge_{23}Sb_7S_{70}$ and As_2S_3 glass were envisioned as candidate host matrices for nanomaterial doping in this study. However, it was found that $Ge_{23}Sb_7S_{70}$ is much less sensitive to processing parameters, such as solvent water content, than As_2S_3. Therefore, $Ge_{23}Sb_7S_{70}$ was chosen as the sole composition for doping. The reasoning will be discussed in more detail later. Both bulk glass compositions were made by batching elemental ingredients into a fused silica ampoule inside of a nitrogen-purged glove box using techniques discussed in detail in [2] to prepare bulk materials for subsequent solution-based film formation [3, 4]. The ampoule was vacuumed using a “turbo-pump” for 4 hours at 90°C to drive off any residual moisture. The batch was then sealed using a gas-oxygen torch. It was melted for 15 hours in a rocking furnace to ensure homogeniety,

air-quenched, and annealed at 40°C below the T_g of the glass. $Ge_{23}Sb_7S_{70}$ was melted at 925°C and annealed at 271°C, while As_2S_3 was melted at 650°C and annealed at 145°C. The bulk glass was characterized using transmission UV-vis spectroscopy and ellipsometry.

3.1.2 Glass Dissolution and Film Deposition

Thin films of both glass compositions were fabricated by dissolving crushed bulk glass in propylamine, and then spin-coating the solution on a microscope slide or silicon wafer. Dissolution typically takes place in 1-2 days, depending on the loading level of the glass in the solvent. Propylamine was chosen as the solvent because of its low boiling point compared to other amine solvents such as ethanolamine, which allows it to evaporate easier during spin-coating, yielding thicker films. After spin-coating, heat treatment is necessary to drive off as much residual solvent as possible. The heat treatment typically contains two steps, a soft bake for a few minutes on a hot plate at 50°C ±10°C, and a hard bake in a vacuum oven with active pumping at 105°C ±5°C. In addition to this thesis, a detailed investigation of the effect of various heat treatment parameters on solvent removal and resulting film quality has been carried out in parallel to this work [5]. Knowledge learned from these experiments was utilized as it became available and relevant toward the end of the study on PbS doped $Ge_{23}Sb_7S_{70}$.

Film attributes required for the intended application of this material are shown in Table 3.1.

Table 3.1: Target film properties for sensing application

Film Property	Target Value	Purpose
Thickness (nm)	800-1000	Guide 3-3.5 μm light
RMS Roughness (nm)	<1	Very low loss from scattering of light
Other characteristics	Homogeneous Minimal cracking and pinholes Minimal residual solvent	Uniform refractive index, minimal mid-infrared spectral loss due to scattering and solvent absorption bands

Therefore, process optimization was necessary. It was suspected that water content in the solvent plays a role in the solubility and resulting film quality, so varying amounts of water were tested. This was done by drying the propylamine for at least 24 hours using 3 angstrom molecular sieve, and then adding deionized water with a micropippette. A loading level of 0.02 g glass / mL solvent was used, and films were deposited by spin-coating at 4000 rpm for 10 s, and analyzed with a Zygo NewView white-light interferometer to determine thickness, roughness, and homogeneity. For the purposes of experiments with the doping by nanomaterials, it is not necessary to meet the target attributes in Table 3.1. In order to test the behavior of MNPs and QDs in the films, a good signal is needed for absorption and luminescence spectra. Attributes which permit such measurements are summarized in Table 3.2.

Table 3.2: Target film properties for doping experiments

Film Property	Target Value	Purpose
Thickness (nm)	>100	Adequate signal for absorption and luminescence measurements
RMS Roughness (nm)	<5 nm	Miminal scattering sources of error during measurements
Other characteristics	Homogeneous	Measurements are not affected by location on sample

3.2 Fabrication of Doped Films

A schematic of the steps in the process used in this study to fabricate doped solution-derived films is shown in Figure 3.2.

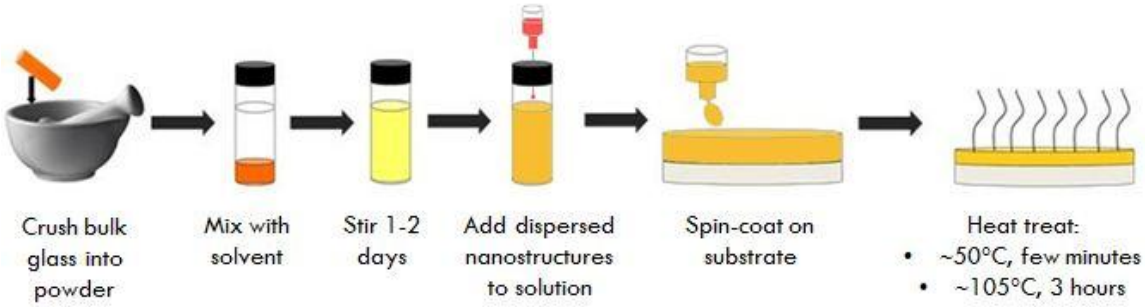

Fig. 3.2: Schematic showing the steps used to fabricate a doped solution-derived chalcogenide glass film

Several types of dispersed nanostructures were incorporated into the films. Sections 3.2 below describe specifics of process parameters used for both MNPs and QDs doped into Ge-Sb-S glasses in the present study.

3.2.1 Doping with Au MNPs

12 nm Au nanoparticles were synthesized by Dr. Alex Martucci's group in Padova, Italy according to the Turkevich method [6]. 12 mL of 1% aqueous $NaBH_4$ was used to reduce 200 mL of 0.5 mM $HAuCl_4$ in boiling water. The solution turned red, and was stirred for 15 min before cooling to room temperature. Poly(n-vinylpyrrolidone) (PVP) with average molecular weight of 10,000 g/mol was dissolved in water to a concentration of 50 g/L, and added to the reaction solution under stirring in the ratio of 1000 g PVP / mol Au. After two hours the solution was concentrated in a rotary evaporator, precipitated with acetone, centrifuged at 4000 rpm for 5 min, and redispersed in ethanol with a concentration of 15 mM.

100 μL of 210 μM Au MNPs dispersed in anhydrous methanol were added drop-by-drop to 2 mL propylamine under stirring. UV-vis absorption spectra were taken every hour for 14 hours to investigate the behavior of the MNPs in propylamine over time. 25 μL of 50 mg/mL $Ge_{23}Sb_7S_{70}$ solution in propylamine was added to the Au MNPs in propylamine, and also characterized with UV-vis spectroscopy.

For optimization of Au MNPs in $Ge_{23}Sb_7S_{70}$ solutions, the Au MNPs were redispersed in anhydrous methanol to the concentration of 300 μM. This was done to minimize water added to the solution, as well as to ensure a very small change in Au nanoparticle concentration with each drop added to $Ge_{23}Sb_7S_{70}$ solution. A 50 mL $Ge_{23}Sb_7S_{70}$ in propylamine solution was prepared, and the Au nanoparticles were added drop-by-drop into the solution according to Table 3.3. This was done using a syringe

through the lid of the jar to prevent solvent evaporation, and the solution was stirred vigorously to prevent aggregation.

Table 3.3: Volume of 300 μM Au MNP solution added to 50 mL $Ge_{23}Sb_7S_{70}$ solution and corresponding Au MNP loadings

Volume of Au Nanoparticle Solution Added (mL)	Au Nanoparticle Loading (μM)
0	0
1	5
2	12
3	19
3.5	24
4	30
5	41

The solution was added at a rate of one drop every 10 seconds, and each drop had a volume of about 10 μL. Samples of 3 mL were taken at each concentration increment, and anhydrous methanol was added such that all samples contained the same ratios of propylamine, methanol, and dissolved glass. UV-vis spectra were taken on the solutions diluted by a factor of 10 with propylamine in a quartz cuvette with a 2 mm pathlength.

Films were deposited from different solutions (corrected for methanol concentration but not diluted by propylamine) containing 0, 7, 13, 23 and 32 μM Au MNPs. For the spin-coated solutions, the final volume fraction of methanol was 0.1, and the glass concentration was 0.045 g/mL. They were spin-coated at 3000 rpm for 10 s on microscope slides, and only "soft-baked" at 100°C on a hot plate for a few minutes. The films were analyzed with transmission UV-vis spectroscopy.

3.2.2 Doping with QDs

Multiple types of QDs were evaluated in this effort. QD materials were obtained or fabricated by various methods as discussed below. Where noted, variations in process protocols used (i.e., dots prepared with or without capping layers) are presented.

CdSe

Core/shell CdSe/ZnS QDs capped with tri-n-octyl-phosphine oxide (TOPO) were obtained from a seperate experiment done in our group in Bordeaux [7]. The purpose of using this material was that it was in hand and could serve as a starting point to familiarize processing methods needed for subsequent incorporation into a solution of ChG. The core CdSe QDs were synthesized by heating 0.20 mmol CdO and 0.80 mmol stearic acid at 170°C under argon flow and stirring until the solution turns from reddish to clear. The mixture was cooled to room temperature, and 0.5 g TOPO, 1.5 g 1-hexadecylamine (HDA) and 2.0 g 1-n-octadecene (ODE) were added. The mixture was heated to 250°C, and a solution of 2.0 mmol Se, 0.65 g TBP and 1.5 g dioctylamine was added, at which point the QDs began to grow. The temperature was set immediately to 220°C after injection, and after cooling to room temperature, the QDs were extracted using 3 cycles of a 1:1 methanol/hexane mixture. The diameter of the QDs was found to be 5.8 nm based on the position of the first excitonic absorption band. The shell synthesis was performed by loading a mixture of $4x10^{-5}$ mmol CdSe dispersed in hexane, 1.0 g oleic acid and 5 g ODE. This was placed under vacuum to remove the hexane, oxygen, and water, and then heated to 70°C, at which point an argon atmosphere was added. The

temperature was then raised to 230°C, and a solution of 0.04 M Zn (ZnO:oleic acid 1:8 in ODE), and S (S:oleic acid 1:8 in ODE) were added alternatively every 20 min, growing a half layer upon each addition. Three full layers of ZnS were added, resulting in a shell thickness of 2.1 nm, giving a final nanocrystal diameter of 7.9 nm.

The core/shell CdSe/ZnS QDs were used to dope $Ge_{23}Sb_7S_{70}$ films were made in two ways, by depositing the QDs on the film surface and incorporating them inside the film matrix. In order to deposit the QDs on the film surface, the film was coated with QD solution, and left at room temperature while the solvent evaporated. The QDs were incorporated into the film matrix by spin-coating a mixture of 0.35 μM CdSe QDs and 0.033 g/mL $Ge_{23}Sb_7S_{70}$ in 2:1 propylamine to chloroform solution. The mixture was made by adding 100 μL of 0.1 μM CdSe QDs dispersed in chloroform to 200 μL of 0.05 g/mL $Ge_{23}Sb_7S_{70}$ solution in a small vial. The solutions were mixed for approximately 5 seconds before depositing 100 μL on the substrate and spin-coating at 3600 rpm for 10 s. An undoped film was made at the same time for comparison, but was not diluted to 1/3 chloroform to match the doped film.

PbS

As bulk CdSe has a band-gap of 1.74 eV, the maximum possible emission wavelength of CdSe QDs is around 700 nm. However, target wavelengths for our effort are as close to $\lambda_{emission} \sim 3$ μm as possible, so we thus expanded our study to PbS QDs which have been shown to have emission in some hosts in the range of 1-1.6 μM due partially by its smaller bulk band-gap of 0.4 eV [8]. PbS QDs were synthesized via a

reaction of lead (II) acetate trihydrate with thioacetamide in anhydrous methanol in an argon purged Schlenk line. 0.4 g (1.23 mM) lead acetate was dissolved in 5 mL anhydrous methanol with stirring. 0.8 mL acetic acid was added, and then 40 μL (0.06 mol) 6-mercapto-1-hexanol was added dropwise. In a separate flask, 0.09 g (1.19 mM) thioacetamide was dissolved in 2 mL anhydrous methanol, and added rapidly to the lead acetate solution to nucleate PbS particles in a short range of time. The solution turned from clear to dark brown over a period of about 10 minutes, and left to react for 2 hours at room temperature under vigorous stirring. The PbS QDs were then precipitated with 15 mL acetone per mL of reaction solution and centrifuged at 3000 rpm for 10 min. The precipitate was washed by replacing the acetone twice. A spatula was used to scrape the QDs off the side of the flask if necessary. They were then redispersed in the desired solvent, chloroform or tetrachloroethylene and washed twice to remove the acetone. About 15 μL of 1-dodecanethiol per mL of reaction solution was used as a stabilizer.

The procedure was modified in an attempt to obtain PbS QDs capped with thioctic acid. The same reaction was utilized, mercaptohexanol was replaced with 0.06 mol thioctic acid. The thioctic acid was in the form of a powder, so it was dissolved in approximately 1 mL anhydrous methanol before adding to the reaction. It was found that the QDs would go into solution with sonication and heating with a water bath at about 40°C. Dodecanethiol was also added at the end of the reaction as a stabilizer, so the identity of the capping ligand is unclear at the moment, whether it is thioctic acid or dodecanethiol, or a mixture of both. As discussed previously, the goal of using a capping layer is to aid in dispersal of the QDs in subsequent solvent/glass mixtures, and thioctic

acid is an attractive ligand because it has the potential to form two Pb-S bonds with the QD, as opposed to one for mercaptohexanol. This means that thioctic acid capped PbS QDs could be more stable in amine solvents, due to a lower chance of cleaving the capping agent from the QD surface.

Concentration of the PbS QD solutions was estimated by drying a known volume of solution under vacuum for 3-4 hours and weighing the precipitate. If necessary, the solutions could be made more concentrated through the use of a rotary evaporator at 50°C and a pressure of 200 mbar.

3.3 Characterization of doped solutions and films

Absorption spectra in the UV-vis-NIR were taken with a Cary 5000 spectrophotometer. Typical settings were 0.5 – 1 s integration time and 1 nm data interval. Transmission spectra were taken in the MIR using a Nicolet 6700 FT-IR with a resolution of 8 cm^{-1} and 100 acquisitions.

Dynamic light scattering (DLS) with a 548 nm laser was used to characterize the size distribution of MNPs and QDs in solution.

For QD doped samples, photoluminescence spectra, fluorescent lifetime, and quantum yield were obtained using a Horiba Jobin-Yvon Fluorolog-3 spectrofluorimeter. In these experiments, the excitation source was either a 450 W Xenon lamp with a double monochromator, or a 532 nm 12 kHz laser. Detection of infrared luminescence was achieved using a Hamamatsu 10330-4S photomultiplier, while detection of visible luminescence was with a Hamamatsu R2658P. Lifetimes were taken via the time-

correlated single photon counting method using a 1 mHz, 460 nm pulsed nano-LED excitation source.

Absolute quantum yield values were determined by taking spectra using a PTFE Labsphere optical Spectralon integrating sphere with diameter of 100 mm, providing a reflectance of >99% over the 400-1500 nm range, and >95% within 250-2500 nm range. Six spectra are required, three fluorescence spectra where the emission wavelengths are scanned, and three spectra where the excitation source is scanned, as shown in Table 3.4. Ultimately, the goal of these spectra is to count the number of photons absorbed and emitted per second according to the definition of quantum yield in Equation 2.3. The scans of the emission provide the number of photons emitted per second, and the scans of the excitation source provides the number of photons absorbed per second. All spectra must be taken using the same instrument settings, such as slit sizes, which would change the relative intensities of fluorescence and the excitation source.

Table 3.4: Spectra taken to measure internal quantum yield

Scan Name	Description
EM1	Emission of sample directly in the excitation beam
EM2	Emission of sample rotated out of excitation beam
EM3	Emission of empty integrating sphere
EX1	Excitation with sample directly in excitation beam
EX2	Excitation with sample rotated out of excitation beam
EX3	Excitation with empty integrating sphere

Scan EM1 provides the total number of emitted photons per second measured by the detector. Scan EM2 accounts for photons which are not absorbed during the first time the excitation light interacts with the sample. Photons which are not initally absorbed reflect

off of the surface of the integrating sphere and can interact again with the sample, causing more fluorescence. EM3 provides a baseline, and the total number of photons emitted by the sample per second is given by Equation 3.1, where the units of scans EM1, EM2 and EM3 are all counts per second:

$$\frac{Emitted\ photons}{second} = EM1 - EM2 - EM3 \qquad \text{(Eq. 3.1)}$$

The number of photons absorbed by the sample is found by scanning the excitation source in the same manner as the emission source is scanned. When measuring the excitation, it is important to use a filter to reduce the intensity so the detector is not damaged. Typical filters that were used reduced the source intensity to 0.5% or 2.5% of its original level. This reduction is taken into account when making the calculations. EX3 provides the total number of incident photons, while EX1 represents the number of photons which are not absorbed by the sample, and EX2 accounts for photons which interact with the sample a second time after reflecting off the integrating sphere. The number of photons absorbed per second is then given by Equation.

$$\frac{Absorbed\ photons}{second} = EX3 - (EX1 - EX2) \qquad \text{(Eq. 3.2)}$$

The internal quantum yield is then calculated by dividing Equation 3.1 by Equation 3.2.

3.4 Summary

This chapter defines and describes the experimental techniques used to process and characterize MNPs and QDs in their as-fabricated state, in solution and in their doped film form. Bulk and undoped glass films were characterized by UV-vis-NIR spectroscopy and refractive index measured by ellipsometry. Additional characterization techniques used for doped films and solutions included dynamic light scattering, emission spectra, lifetime and quantum yield. These experimental techniques were designed in order to investigate the questions proposed in Section 1.2, as the goal of this thesis was to determine how the surface chemistry of a nanoparticle can be tuned to aid dispersion, what is the maximum concentration of nanoparticles that can be dispersed in a ChG solution and deposited film, and how the properties of the deposited film are affected by varying concentrations of nanoparticles.

3.5 References

[1] N. Carlie, "A solution-based approach to the fabrication of novel chalcogenide glass materials and structures," **2010**, PhD thesis, Clemson University.

[2] L. Petit, N. Carlie, F. Adamietz, M. Couzi, V. Rodriguez, K. Richardson, "Correlation between physical, optical and structural properties of sulfide glasses in the system Ge–Sb–S" *Mat. Chem. and Phys*, **2006**, *97(1)*, 64-70.

[3] S. Song, N. Carlie, J. Broudies, L. Petit, K. Richardson, C. Arnold, "Spin-coating of $Ge_{23}Sb_7S_{70}$ chalcogenide glass thin films" *J. Non-Cryst. Solids*, **2009**, *355*, 2272-2278.

[4] M. Waldmann, J. D. Musgraves, K. Richardson, C. B. Arnold, "Structural properties of solution processed $Ge_{23}Sb_7S_{70}$ glass materials" *J. Mater. Chem.*, **2012**.

[5] J. Wilkinson, "Characterization and optimization of solution-derived chalcogenide glass thing films" MS thesis, Clemson University **2012**.

[6] E. D. Gaspera, A. Antonello, M. Guglielmi, M. L. Post, V. Bello, G. Mattei, F. Romanato, A. Martucci, "Colloidal approach to Au-loaded TiO_2 thin films with optimized optical sensing properties" *J. Mater. Chem.*, **2011**, *21*, 4293.

[7] M. Amelia, A. Lavie-Cambot, N. D. McClenaghan, A. Credi, "A ratiometric luminescent oxygen sensor based on a chemically functionalized quantum dot" *Chem. Commun.*, **2011**, *47*, 325-327.

[8] L. Bakueva, S. Musikhin, M. Hines, T. Chang, M. Tzolov, "Size-tunable infrared (1000–1600 nm) electroluminescence from PbS quantum-dot nanocrystals in a semiconducting polymer" *Appl. Phys. Lett.*, **2003**, *82*, 2895.

CHAPTER 4

PRELIMINARY TESTING OF BULK GLASS AND UNDOPED FILMS

As previously discussed in section 3.1, the goal of this doped solution-derived ChG film optimization was to be able to fabricate compositionally homogeneous films possessing RMS roughness levels of less than 5 nm, and thickness greater than 200 nm. Low roughness is important to reduce scattering loss in a sensing device. While a 200 nm film thickness is adequate for testing QD-doped ChG films, ultimately the target thickness of the material for a mid-infrared device (to allow coupling into bus waveguides and then to a microdisk resonator that serves as the heart of the sensor) should be between 800 – 1000 nm in thickness. However, obtaining quality films of this thickness was done in parallel with this research [1], and the principles and experimental findings of that study have been applied to the current effort. Solvent removal is also crucial for the intended application, but for the purposes of testing, film properties are characterized over a range of solvent contents to investigate the environment-dependent properties of the nanomaterials.

4.1 Effect of solvent water content on glass solubility and film quality

Previous work done in our group [2] on solution-derived chalcogenide films was performed in a glove-box without moisture control. When performing tests in a glove-box held with moisture content monitored and known to be less than 1 ppm H_2O, it was observed that films made from As_2S_3 displayed inconsistent solubility, with irregular film

quality. As with efforts in the prior attempts, film quality achieved could not be readily repeated from run to run. This prompted an investigation of how water content in both the process environment and raw materials (i.e., including the solvent) affected glass solubility and film quality. It was determined that $Ge_{23}Sb_7S_{70}$ (0.05 g/mL) is soluble over a wide range of water contents, at least 0.26 to 0.40 vol% of water in the propylamine. However, As_2S_3 is soluble (0.05 g/mL) over a very narrow range of water content, from 0.26 – 0.28 vol% These tests were done by attempting to dissolve 0.5 g of glass in 10 mL of dried propylamine with varying amounts of added water. When attempting to dissolve As_2S_3 in propylamine outside of the solubility window, a yellow precipitate is formed. This precipitate is presumed to be sulfur. Solutions of As_2S_3 are transparent yellow, while solutions of $Ge_{23}Sb_7S_{70}$ are transparent brown. The effect of water content on film roughness is shown in Figure 4.1, for films made from solutions of 0.5 g glass per 10 mL propylamine. This concentration, is at or near the maximum room temperature solubility of $Ge_{23}Sb_7S_{70}$ in propylamine. Up to 1.5 g of As_2S_3 was dissolved in 10 mL propylamine, but no studies on the effect of water were made at concentrations other than 0.5 g / 10 mL.

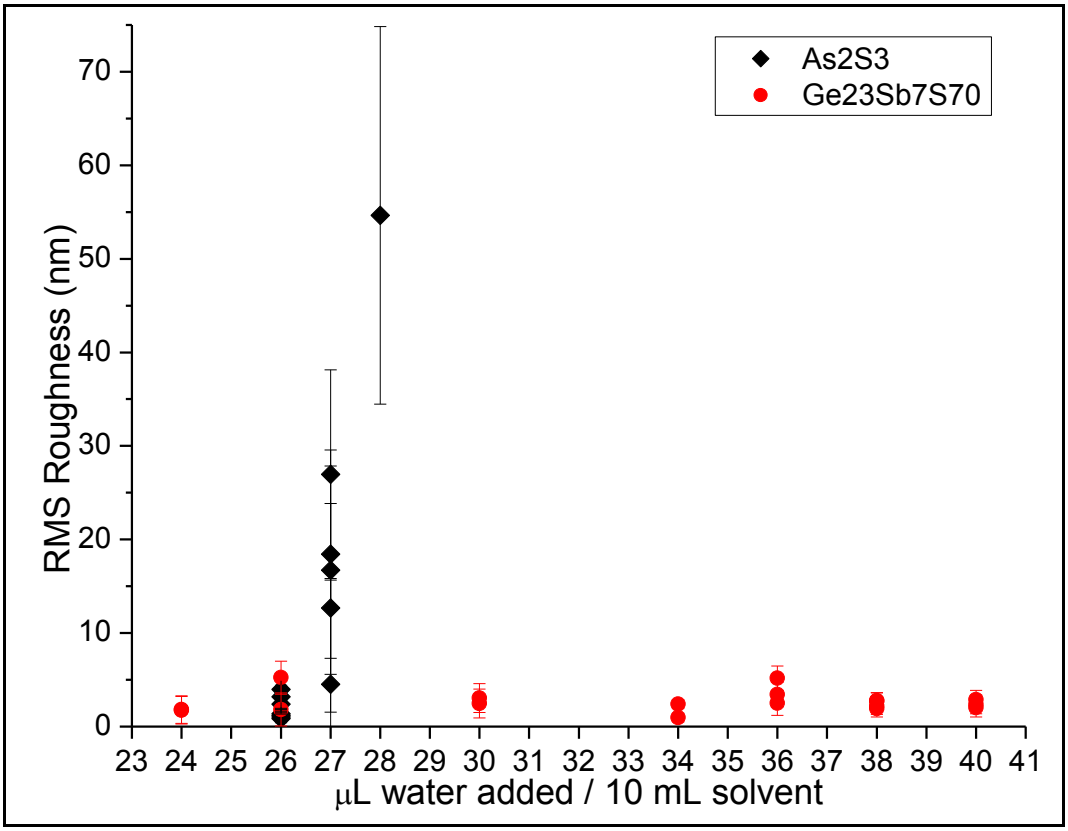

Fig. 4.1 Effect of solvent water content on film roughness

As_2S_3 film quality is very sensitive to the amount of water in the solvent, while $Ge_{23}Sb_7S_{70}$ film quality is not. This is the main reason that the $Ge_{23}Sb_7S_{70}$ was chosen as the composition to dope with nanoparticles. When the nanoparticles are added to the glass solution before spin-coating, the carrier solvent may contain water, which would be more likely to affect film quality or cause precipitation in the As_2S_3 system.

The properties of undoped solution-derived films were compared to bulk glass in order to understand the effects of film processing on the glass. The films used as reference in this comparison were produced by spin coating a 0.05 g/mL solution of $Ge_{23}Sb_7S_{70}$ in propylamine on a microscope slide at 4000 rpm for 10s. The films were

heat treated for a few minutes at 50°C and 3 hours at 105°C. The glass properties differ widely between bulk and film. This is evidenced by the differences in the visible transmission cut-off shown in Figure 4.2.

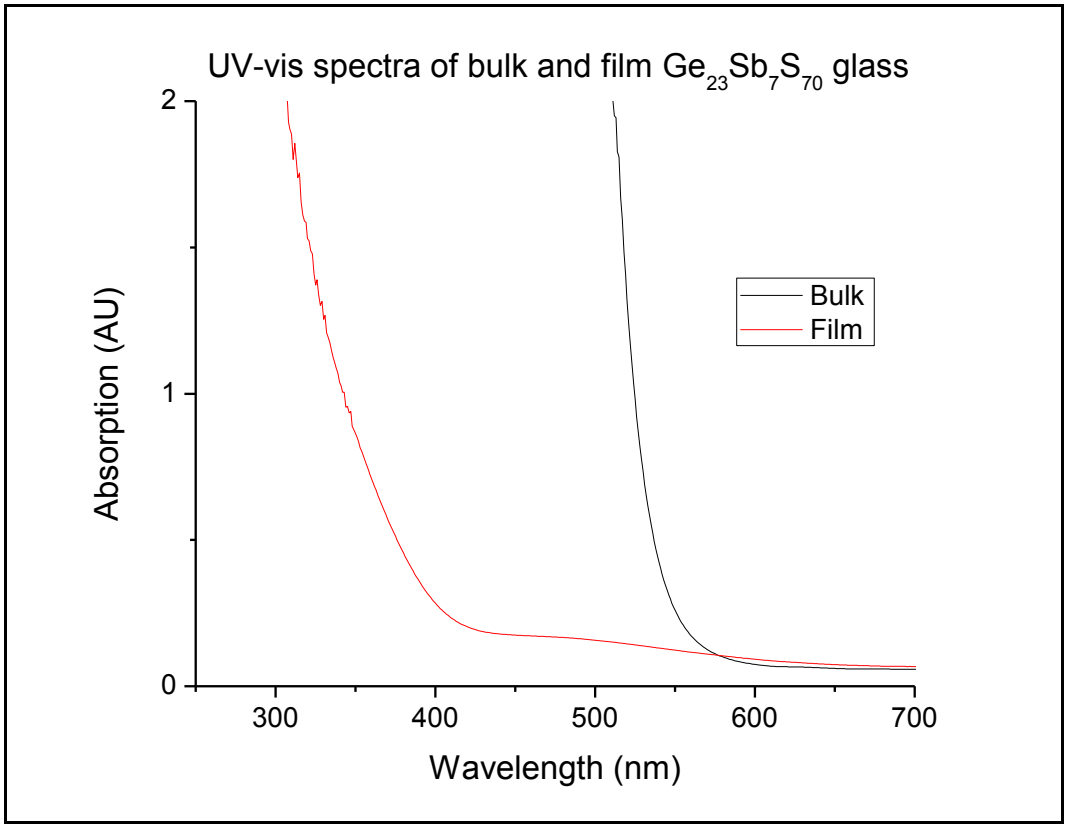

Fig. 4.2: UV-vis absorption spectra of bulk glass and solution derived glass film $Ge_{23}Sb_7S_{70}$

The figure shows that the visible cut-off of the film is strongly blue-shifted from the bulk by about 150 nm. This difference is attributed mainly to residual propylamine solvent in the film matrix, which is transparent over the entire visible spectrum, but could also be a result of compositional variances due to film processing. The difference between the properties of bulk and film glass is also evident by the difference in the refractive indices of the two specimens, shown in Figure 4.3.

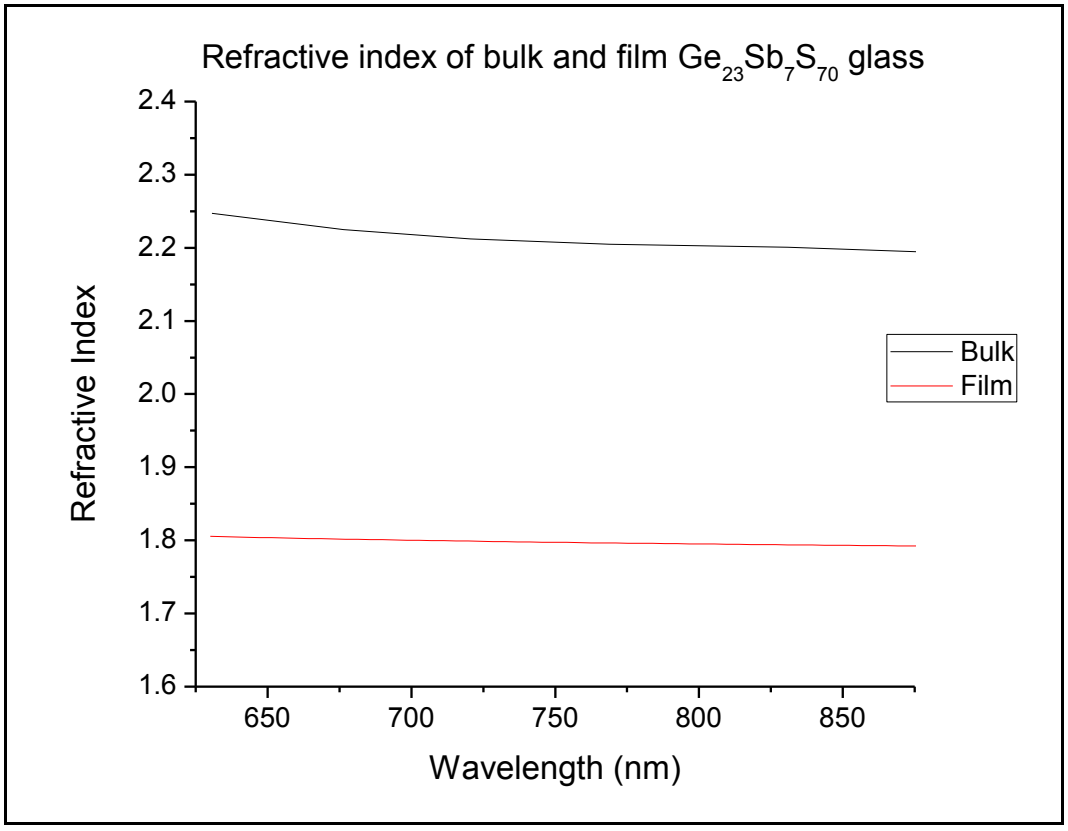

Fig. 4.3 Real component of refractive index of bulk and film $Ge_{23}Sb_7S_{70}$ glass measured by ellipsometry on microscope slide substrate

There is a large decrease in the refractive index of the film compared to bulk glass. Again, this is explained mainly by residual solvent in the matrix, but other sources of the shift include variations in composition and possible surface oxidation of the film. Surface oxidation was not mentioned as a major cause of difference of the visible cut-off of the film because it is expected, if present, to only affect a small near-surface volume fraction of the film, and does not have a strong effect on the transmission of light through the film's ~250 nm thickness. However, ellipsometry measures the index by determining the angles at which light is reflected off the surface of the sample. As a result, surface

oxidation would play a bigger role in an ellipsometry measurement than transmission UV-vis.

4.2 Summary

The initial testing and optimization of undoped films shows that the best candidate composition for nanomaterial dispersion is $Ge_{23}Sb_7S_{70}$ because it is much less sensitive to solvent water content than As_2S_3. This is important because the addition of nanomaterials can possibly bring water into the glass solution. It is reasonable to believe that $Ge_{23}Sb_7S_{70}$ solutions might also be more stable in terms of solubility and resulting film quality against other substances brought into the glass solution, such as stabilizers of the nanomaterial solution.

Based on the analysis of the as-formed solution-derived ChG films, we can assume that nanomaterials incorporated into the film matrix will 'see' an environment that contains both chalcogenide glass constituents as well as propylamine. This is important because environment can have a strong effect on the performance of the dopant nanomaterial as well as the resulting doped ChG optical behavior.

4.3 References

[1] J. Wilkinson, "Characterization and optimization of solution-derived chalcogenide glass thing films" MS thesis, Clemson University **2012**.

[2] N. Carlie, "A solution-based approach to the fabrication of novel chalcogenide glass materials and structures," **2010**, PhD thesis, Clemson University.

CHAPTER 5

DOPING OF ChG FILMS WITH GOLD METALLIC NANOPARTICLES (MNPs)

Reiterating our initial goal of doping ChG films with either MNPs or QDs, the focus of this effort aimed to investigate the principles of nanomaterial incorporation into ChG solutions. This includes what type of nanoparticle surface chemistry allows it to disperse in the highest concentrations in the glass solution before aggregation, and how the properties of the resulting film are modified. This chapter summarizes the results of efforts to incorporate gold nanoparticles in ChG, and the attributes of the resulting doped glass films. Included in this section are measurements made on the solutions of glass prior to deposition and solvent removal, as well as post-processed films. Measurements of solution and film absorption spectra are reported, and comparisons are made between the solutions and the films.

5.1 Au MNP doped glass solutions

Au MNPs of diameter 12 nm were obtained from Dr. Alex Martucci's group [1]. Transmission electron microscopy (TEM) and dynamic light scattering (DLS) were used for preliminary testing of the Au MNPs dispersed in anhydrous methanol in order to verify the size and investigate the size distribution. A TEM image is shown in Figure 5.1.

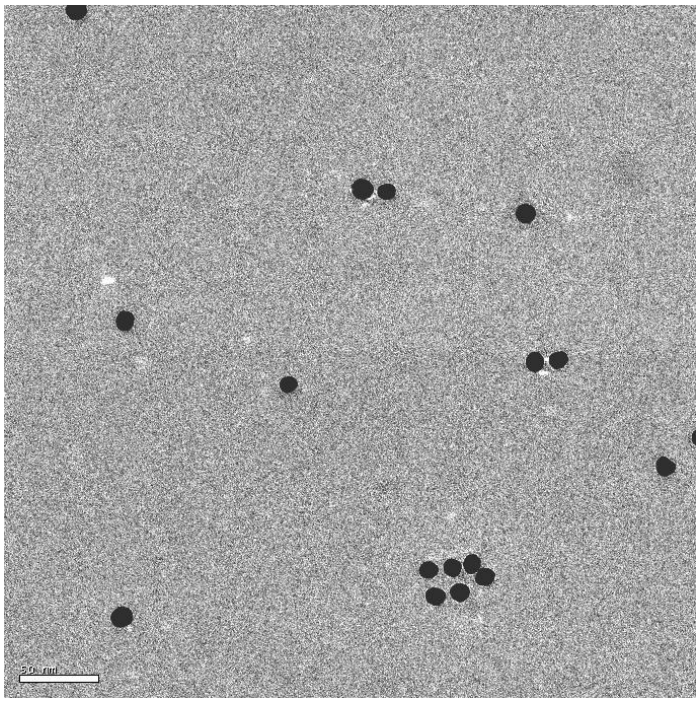

Fig. 5.1: TEM image of Au MNPs

The approximate diameter found from the size of 50 nanoparticles in 5 TEM images is 12.2 nm, with a standard deviation of 0.82 nm. This verifies the size reported by Dr. Martucci's group, and shows that the MNPs are well-monodispersed. The results of testing the size-distribution with DLS are shown in Figure 5.2.

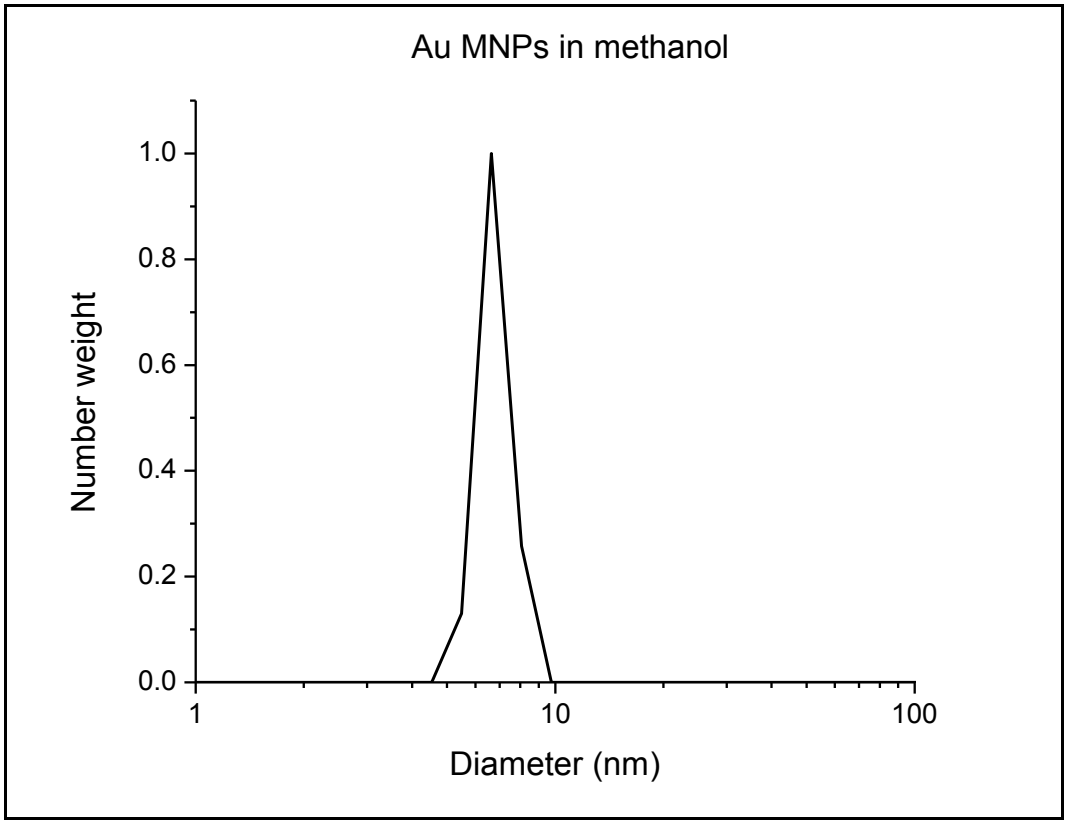

Fig. 5.2: Size distribution of Au MNPs tested using DLS

The size-distribution measured by DLS is less than expected, as the average diameter is 6.7 nm. One main source of variation is that the Au MNPs are capped with PVP having a molecular weight of 10,000 g/mol. This affects DLS measurements, which rely on the rate at which particles move through a solution of known viscosity. TEM imaging shows the Au as dark features because the contrast is due to higher mass-thickness and diffraction contrast. However, even though consistent results were not obtained between DLS and TEM, the size distribution measured by DLS is also very narrow, and further confirms the monodispersity of the MNPs.

These MNPs were used to dope $Ge_{23}Sb_7S_{70}$ solutions according to the details presented in Section 3.2.1. The results of adding the MNP solution to propylamine are shown in Figure 5.3. The sample was stirred constantly, and spectra were taken periodically. The concentration of 19 μM Au MNPs in propylamine was chosen based on experiments with optimization of MNP concentration in glass solution, the results of which are presented later.

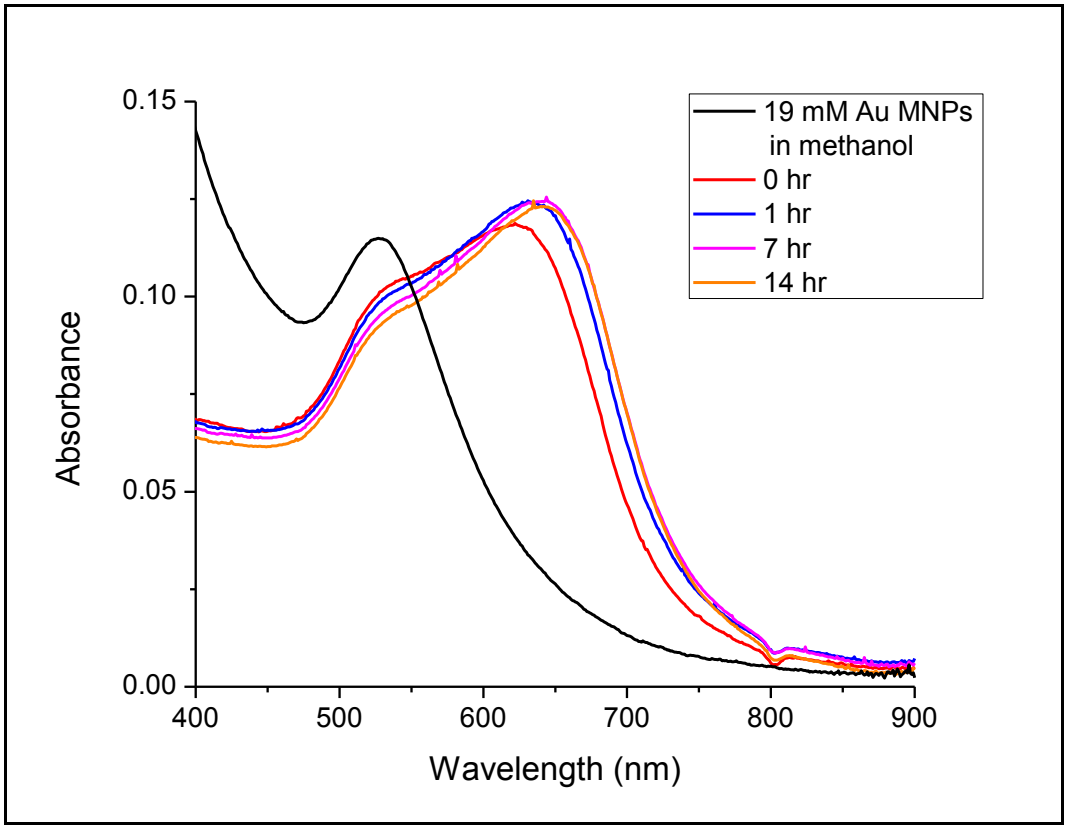

Fig. 5.3: Time-evolution of absorption spectra of 19 μM Au MNPs in propylamine in a cuvette with a pathlength of 1 cm

These spectra indicate how the Au MNPs react when in propylamine, and give an approximation of how they will behave in glass solution, which is valuable because $Ge_{23}Sb_7S_{70}$ has absorption bands in the same range as the Au MNPs. Some initial

aggregation is observed when the MNPs are added to the propylamine. This is evidenced by the formation of a second band centered at approximately 640 nm, which is attributed to the presence of larger particles. The spectrum continues to change over time, with an observed increase in the intensity of the band at 640 nm. However, after the first hour, the spectra only change slightly, indicating a very low rate of aggregate formation.

A small amount of glass solution was added to the Au MNPs in propylamine to investigate if the presence of dissolved glass has an effect on the stability of the Au MNPs in solution. The results are shown in Figure 5.4.

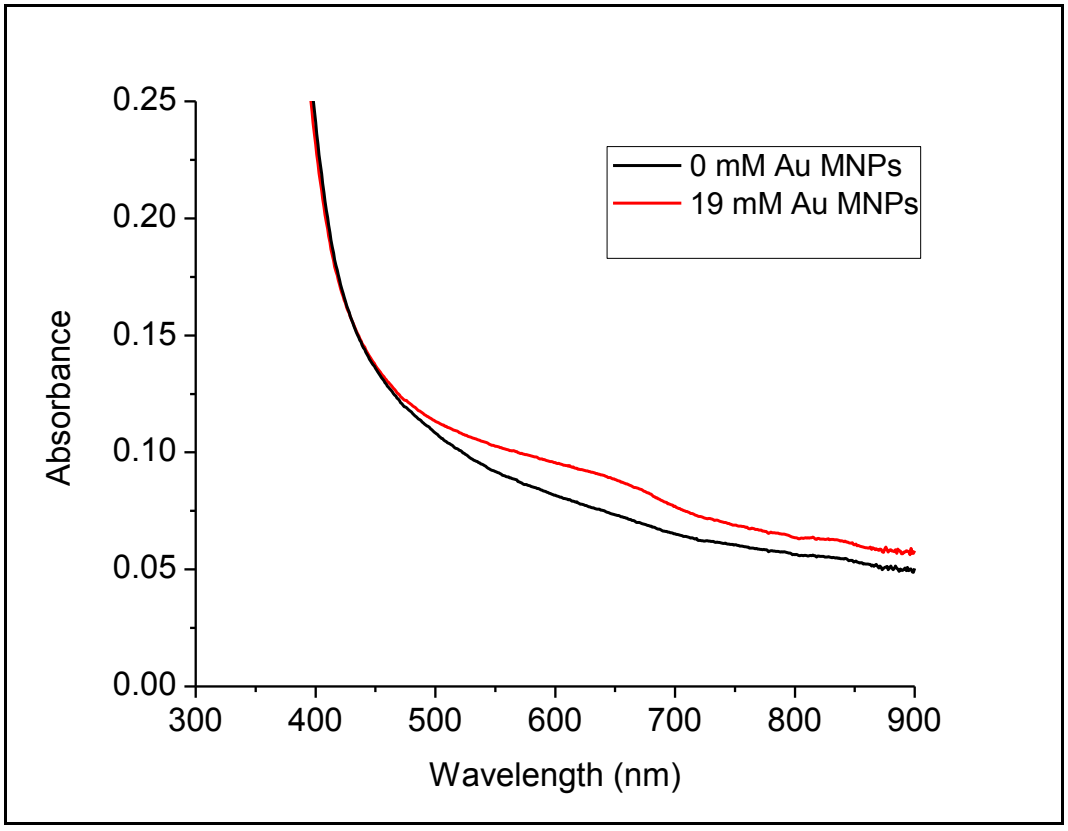

Fig. 5.4: Absorption spectra of Au MNP doped solutions of 3 mg/mL $Ge_{23}Sb_7S_{70}$ glass solution in propylamine in a cuvette with pathlength of 2 mm

The Au SPR band is observable in the glass solution, and its position is not shifted relative to that of the Au MNPs in pure propylamine. This indicates that there is some stability of Au MNPs in ChG solution. Although some aggregation is observed in Figure 5.3 due to the presence of propylamine, the possibility to modify the properties of solution-derived ChG films through the incorporation of MNPs has been demonstrated in Figure 5.4. However, a film deposited from such a solution with only 3 mg/mL ChG is would be extremely thin compared to films deposited from 0.05 g/mL (50 mg/mL) ChG, the typical glass concentration studied in this thesis, and would not meet the target attributes detailed in Table 3.2. Therefore, it is necessary to optimize the concentration of Au MNPs in a $Ge_{23}Sb_7S_{70}$ solution which does satisfy these requirements, and would come much closer to meeting the ultimate properties required for the planar chemical sensor presented in Table 3.1.

The results of this testing is shown in Figure 5.5. As methanol is the carrier solvent for the Au MNPs, more methanol is added to the glass solution as more Au MNPs are added. Therefore, the initial sample solutions have varying amounts of methanol. Methanol was thus added to the solutions such that they all contained the same amount of propylamine, methanol and glass. Additionally, solutions were diluted by a factor of 10 with propylamine to better see the absorption bands present. However, since the purpose of this test was to determine a maximum concentrations level of Au MNPs in the highly loaded glass solution, the concentrations presented are that of the Au MNPs before dilution by propylamine, and do not reflect the actual Au MNP concentration of the solution measured.

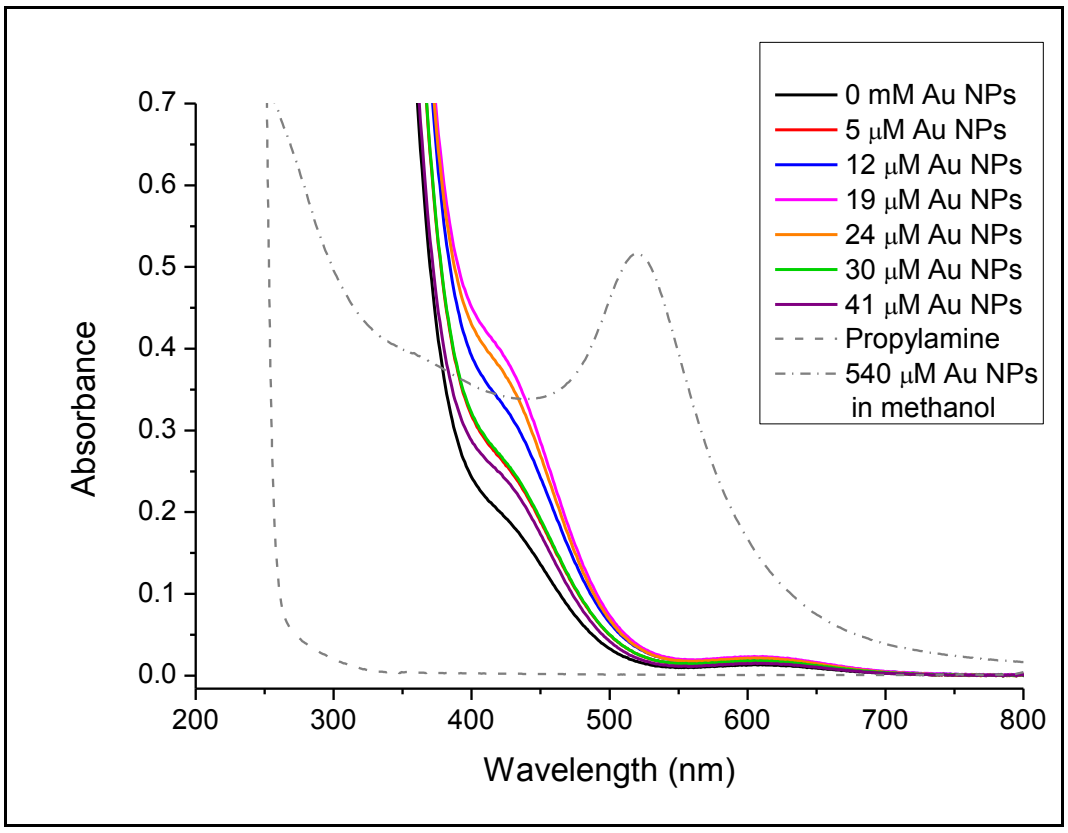

Fig. 5.5: Absorbance of Au MNP doped $Ge_{23}Sb_7S_{70}$ solution, Au MNPs in methanol, and propylamine. Glass solutions were diluted by a factor of 10 with propylamine, and a cuvette with a 2 mm pathlength was used.

Shown in Figure 5.5 is the influence of Au MNP concentration on the UV edge of the solution. For reference, the absorption spectra of propylamine and is added to show that it is transparent over the range of interest, as well as the spectrum of Au MNPs dispersed in pure methanol. It is clear that the addition of Au MNPs to the solution affects the absorption spectra, especially between 375 and 700 nm, as evidenced by the evolution of the absorption spectra from the black solid curve (undoped) to the pink curve (21 μM). The trend is most evident in the range of 400 to 500 nm, where there is a

combination of absorption from the glass solution and Au MNPs. For concentrations increasing up to 19 μM, there is a linear increase of absorbance, shown in Figure 5.6.

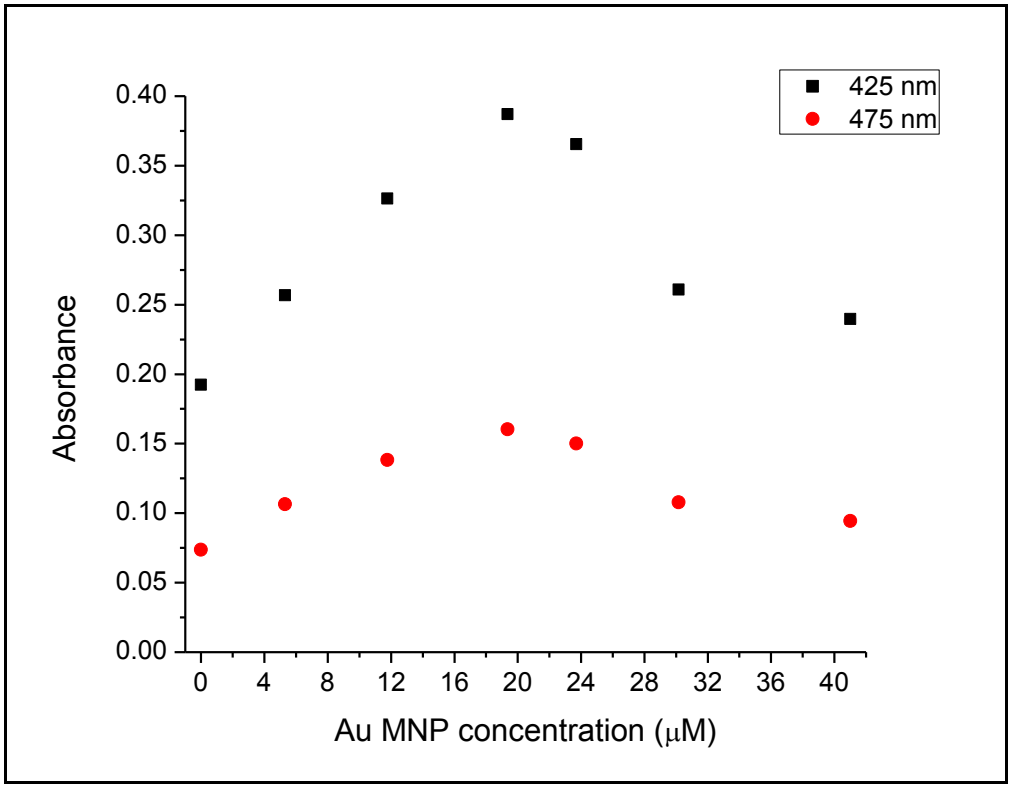

Figure 5.6: Absorbance values of varying concentrations of Au MNPs in $Ge_{23}Sb_7S_{70}$ solution. Error on these measurements are within the size of the data point.

Figure 5.7 shows an expansion of the spectra in the 500 to 700 nm range.

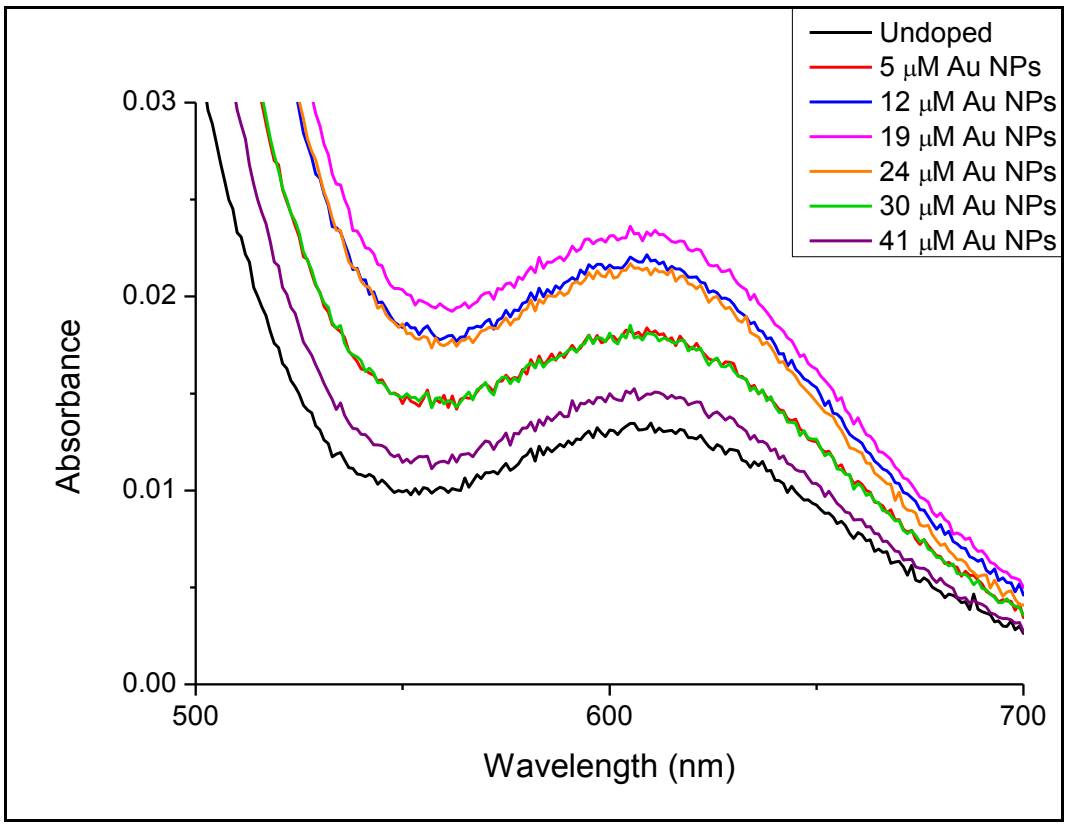

Fig. 5.7: Absorbance of Au MNP doped $Ge_{23}Sb_7S_{70}$ solutions expanded in the range of 500-700 nm (path length = 2mm)

Figures 5.5, 5.6 and 5.7 all show that absorption begins to decrease for Au MNP loadings over 19 μM. However, it was expected that the absorption would reach an equilibrium value, due to the maximum concentration of Au MNPs in the solution, and remain constant for higher loadings of MNPs. Instead, the trend observed indicates that for Au MNP loadings above the maximum concentration, more and more MNPs begin to aggregate and precipitate from the solution.

Figure 5.7 shows that the same trend in absorbance vs. Au MNP concentration seen in the range of 400 to 500 nm is also seen in the range of 500 to 700 nm. With increasing Au concentration, the absorption increases in intensity for loadings up to 19

μM, and decreases for loadings greater than 24 μM. By identifying the concentration of maximum absorption as the maximum concentration of Au MNPs, we determine that the maximum concentration for these MNPs in $Ge_{23}Sb_7S_{70}$ solution lies between 19 μM and 24 μM. Note that there is no additional red-shift of the spectra for the 24 μM loading, which would be expected in solutions where the Au NPs were starting to aggregate and remained suspended in the solution. For this reason, it is believed that when aggregation occurs above 19 μM, the aggregates simply drop out of the solution. This assumption is made based on the fact that no visible evidence of MNP precipitation was observed, and the absorption spectrum of 24 μM Au NPs appears nearly identical to that of 12 μM Au MNPs. This indicates that even though the solution was loaded with higher amounts of Au MNPs, the effects of doping are actually reduced.

The position of the surface plasmon resonance (SPR) band is unclear from the spectra in Figure 5.5 and 5.7 because it appears that they all have approximately the same shape, just varying amounts of absorbance.

5.2 Au MNP doped glass films

Films were deposited from different solutions containing 0 to 23 μM Au MNPs onto microscope slide substrates. Films were processed using the deposition and heat treatment protocol described in Section 3.2.1. Because the film surface is not perfect, it is expected that some scattering of the light incident on the MNP-containing films may occur. Varying film thickness is another source of error in transmission UV-vis, and this parameter is noted along with the spectra in Figure 5.5.

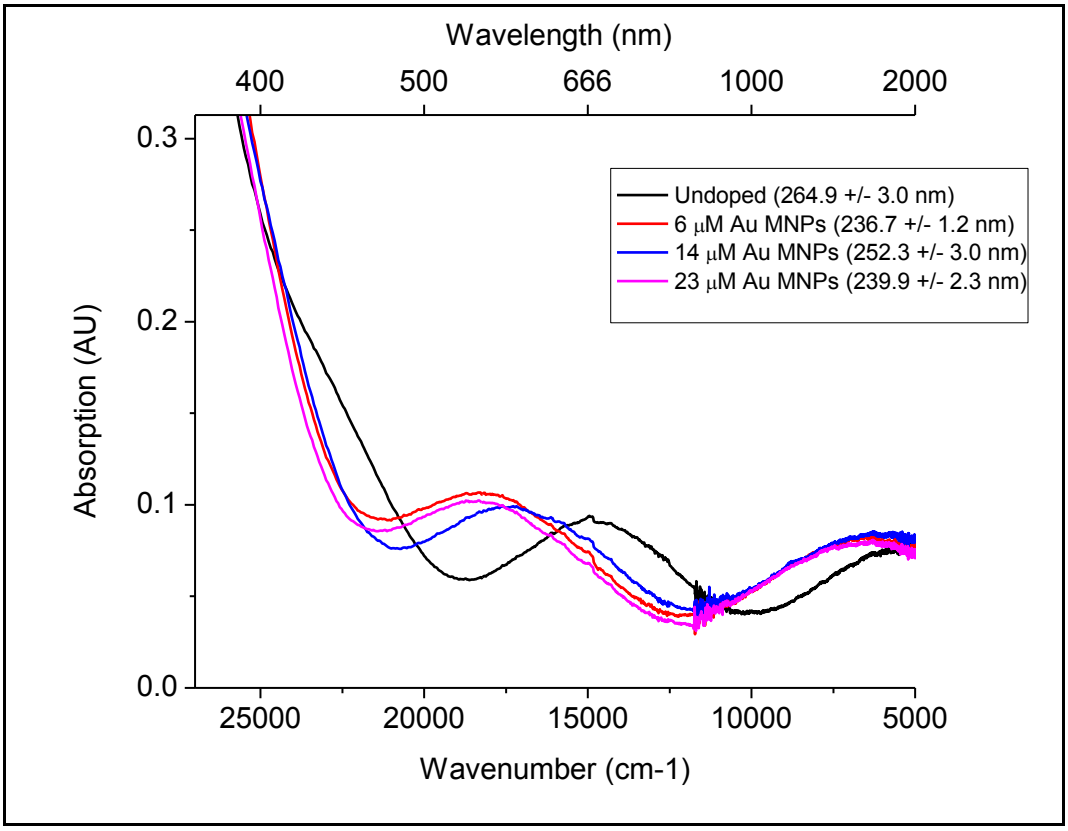

Fig. 5.8: Absorption spectra of Au MNP doped $Ge_{23}Sb_7S_{70}$ films

Figure 5.8 shows the UV-vis-NIR absorption spectra of Au MNP doped films. Because there are interference fringes due to multiple reflections from the various interfaces in the two-layer system, the spectra are plotted in wavenumber so that the period of the fringes does not change. The fringes in the spectra of the doped films differ in their position and intensity from that of the undoped film, but the difference cannot be attributed to the presence of Au. There are many other factors that play a role, such as thickness and index variation due to normal fluctuations in the processing conditions. The presence of the characteristic SPR band of the Au MNPs is not observed. This is most likely because the concentration of Au MNPs is too low to be detected using UV-vis-NIR

spectroscopy, and because there is some glass absorption masking the presence of the MNPs.

From working with Au MNPs in $Ge_{23}Sb_7S_{70}$ solutions, it was also determined that the Au MNP doped solutions are typically stable for 3-4 days when stored in a nitrogen-purged glovebox. After 3-4 days, either a red precipitate is observed, or there is no difference in the absorption spectra of the solutions upon retesting. The red precipitate is indicative of glass precipitation, while nearly identical absorption spectra means that the Au MNPs have dropped out of solution, although this Au precipitation is too small to be observed with the naked eye. The experiment of slowly adding Au MNPs to glass solution was repeated three times, each time refining the Au MNP loadings. The trends observed in the absorption spectra of the solutions were consistent with the results presented previously in this chapter. Futhermore, spectra obtained from the same solutions tested multiple times within 3 days of doping was also consistent. Although no precipitation could be seen in solutions older than 3 days, all UV-vis spectra of 5 day old solutions were essentially the same, regardless of NP loading levels. Originally, solutions were diluted with methanol, but it was discovered that dilution by a factor of 10 caused the glass to precipitate, so propylamine was used instead.

5.3 Summary

The results of the experiments performed on Au MNP doped $Ge_{23}Sb_7S_{70}$ solutions and films show first and foremost that it is possible to modify the properties of each system by the addition of Au MNPs. Evidenced by the maximum absorbance of

solutions, the maximum concentration of Au MNPs was found to lie between 19 and 24 μM. Although the presence of the SPR band was not observed in the deposited films, it is likely that higher concentrations can be made possible by different organic capping agents on the Au MNP surface. The testing methods developed in this work can be applied to such MNPs, as the potential for enhanced magneto-optic properties and applications in sensing through the SPR band of MNPs is demonstrated through the results of testing done with solutions.

5.4 References

[1] E. D. Gaspera, A. Antonello, M. Guglielmi, M. L. Post, V. Bello, G. Mattei, F. Romanato, A. Martucci, "Colloidal approach to Au-loaded TiO_2 thin films with optimized optical sensing properties" *J. Mater. Chem.*, **2011**, *21*, 4293.

CHAPTER 6

DOPING OF CHALCOGENIDE GLASS (ChG) FILMS WITH CADMIUM SELENIDE QUANTUM DOTS

As stated in the goals of the project discussed in section 3.2.2, the purpose of doping films with visibly-emitting CdSe QDs was essentially a proof-of-concept with the most well-studied variety of QDs. Ultimately, we are more interested in infrared luminescence, as the target wavelength for our mid-IR ChG sensor system is ~3-3.5 μm. Therefore, initial testing of behavior of the CdSe QDs in various environments was done while selecting and learning a process for the synthesis of infrared-emitting PbS QDs. For this reason, the study on CdSe is not as complete as the study on PbS. The objectives of testing the CdSe QDs were as follows:

- Demonstrate visible luminescence from QDs dispersed in $Ge_{23}Sb_7S_{70}$ film matrix and investigate the behavior of QDs in various environments, as characterized by quantum yield and luminescence measurements
- Learn these characterization techniques and develop a testing protocol for PbS QDs
- Gain an understanding of the QD concentration required to observe luminescence and how QDs capped with TOPO behave in $Ge_{23}Sb_7S_{70}$ solutions

6.1 Size of CdSe QDs

The concentration of the stock solution of CdSe QDs was estimated using a method described in [1]. With this method, average diameter and molar extinction coefficient is determined by taking luminescence and/or absorption UV-vis spectra, and experimental fitting equations can be used to estimate concentration. The position of the first excitonic absorption peak is the wavelength corresponding to maximum emission, and according to Equation 6.1, the average diameter, D, of the CdSe QDs is given by:

$$D = (1.6122\ x\ 10^{-9})\lambda^4 - (2.6575\ x\ 10^{-6})\lambda^3 + (1.6242\ x\ 10^{-3})\lambda^2 - (0.4277)\lambda + 41.57 \quad \text{(Eq. 6.1)}$$

Using D, the molar extinction coefficient, ε, of CdSe is given by Equation 6.2:

$$\varepsilon = 5857(D)^{2.65} \qquad \text{(Eq. 6.2)}$$

From ε, the concentration of the QDs is estimated by Equation 6.3, where A is the absorbance at the first excitonic absorption wavelength, C is the molar concentration (mol/L), and L is the pathlength of the cuvette in cm.

$$A = \varepsilon CL \qquad \text{(Eq. 6.3)}$$

The luminescence spectrum, shown later in Figure 6.3, shows that the luminescence band of the CdSe is centered at 618 nm. Using 618 nm as the position of the first excitonic absorption peak, the average diameter of the QDs was estimated to be 5.5 nm. The absorbance of the QDs at 618 nm was measured to be 5.65 x 10^{-3}, resulting in a stock concentration of 0.1 μM.

The size distribution of the CdSe QDs was also investigated using DLS, with the results presented in Figure 6.1.

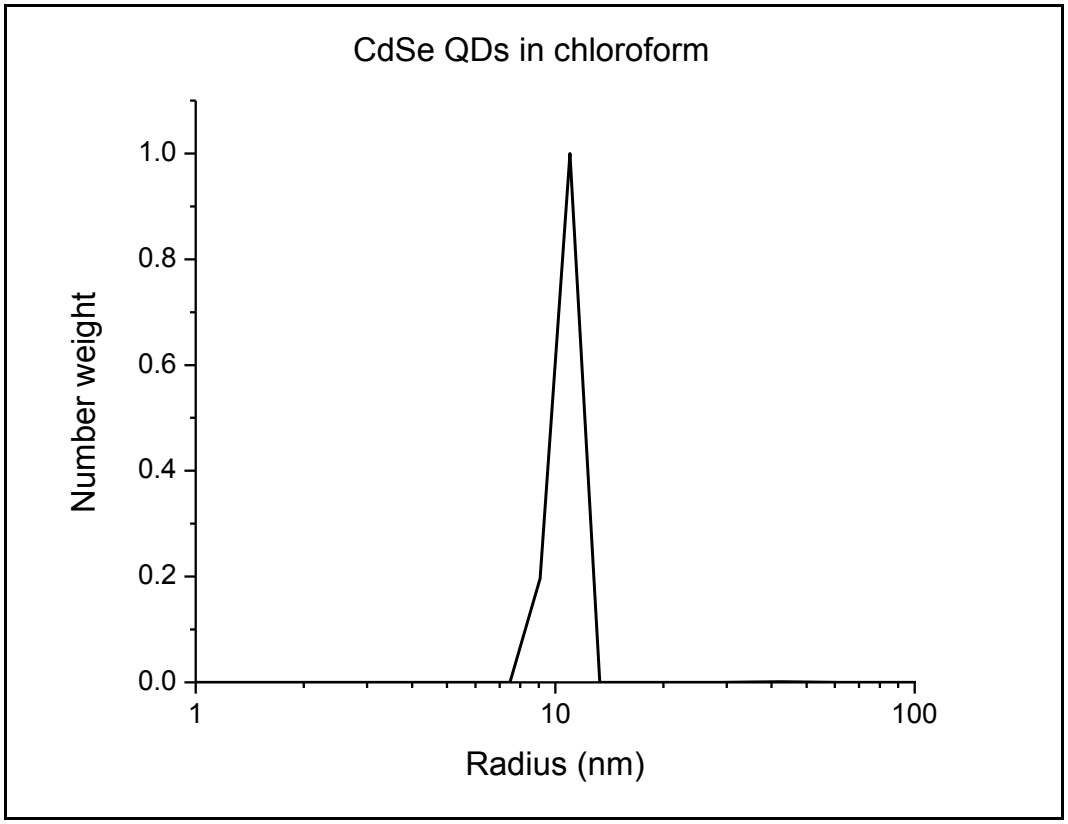

Fig. 6.1: Size-distribution of CdSe QDs measured by DLS

The size distribution of the CdSe QDs is centered at 10 nm diameter, which is consistent with the results obtained using the position of the first excitonic absorption peak reported by the group who synthesized the QDs. Including the ZnS shell, the total diameter of the core/shell structure was reported to be 7.9 nm, and the TOPO ligands on the surface of the shell add roughly 1 nm to the radius of the structure, resulting in a total diameter of about 10 nm, which is in very good agreement with the results measured by DLS.

6.2 Behavior of CdSe QDs in the presence of propylamine

First, because the properties of a nanoparticle are strongly environment-dependent, the CdSe QDs were titrated with propylamine to investigate how propylamine affected their properties. Figure 6.2 shows the UV-vis spectra of CdSe QDs in pure chloroform, and titrated with varying amounts of propylamine.

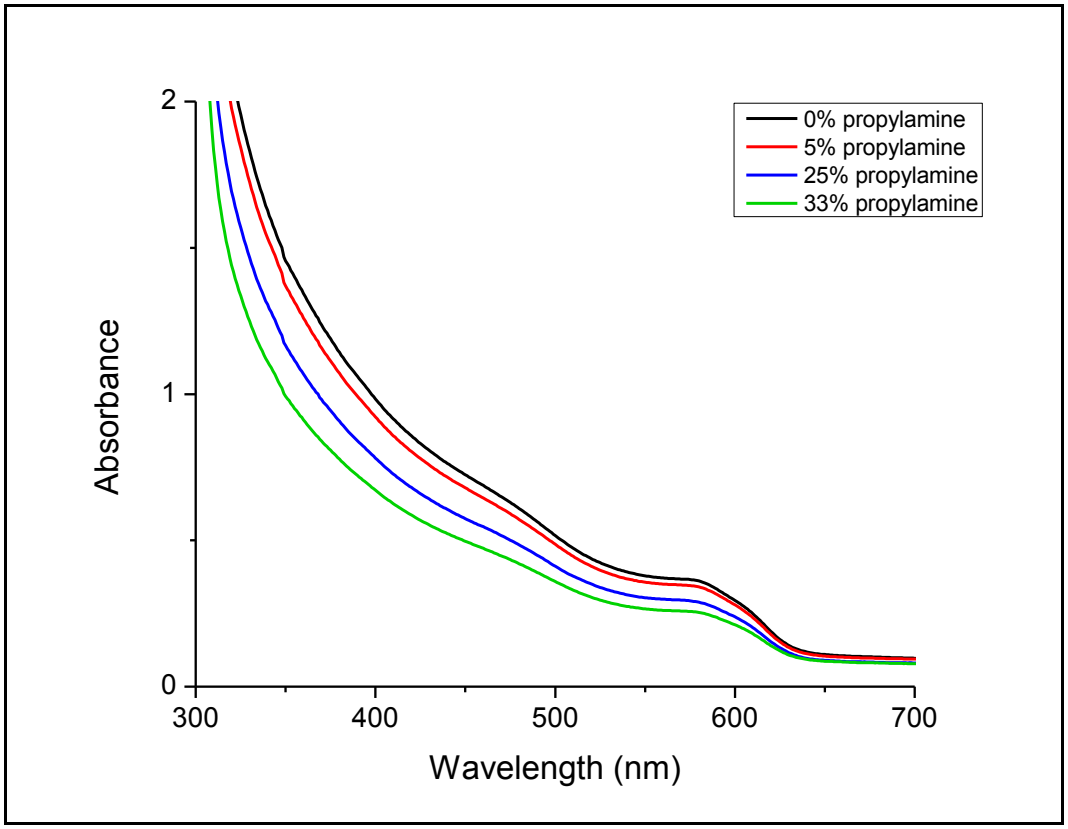

Fig. 6.2: UV-vis spectra of CdSe QDs titrated with propylamine from pure chloroform (path length = 2 mm)

Figure 6.2 shows the effect of propylamine addition on the absorption spectra of CdSe QDs dispersed in pure chloroform. With increasing volume fraction of propylamine, there are no shifts in the absorption spectra of the QDs, only decreases in absorption, presumably due to dilution. Aggregation is one of the main challenges when

introducing QDs into a new environment, which could be indicated by a red-shift of the absorption spectrum. However, UV-vis spectra alone do not indicate that QDs are not interacting with the solvent, or that no aggregation has occurred. For example, as seen in the Au MNP doped glass solutions, only decreases in intensity were observed because aggregates had dropped out of solution and did not contribute to the absorption spectrum. In the case of CdSe, it is unlikely that aggregates formed and dropped out of solution in the time scale of each spectrum, which was approximately 10 min. Therefore, the lack of shifts in the absorption spectra indicate that no aggregation has occurred. Further investigation of QD properties is done by measuring the photoluminescence spectra of the QDs, shown in Figure 6.3.

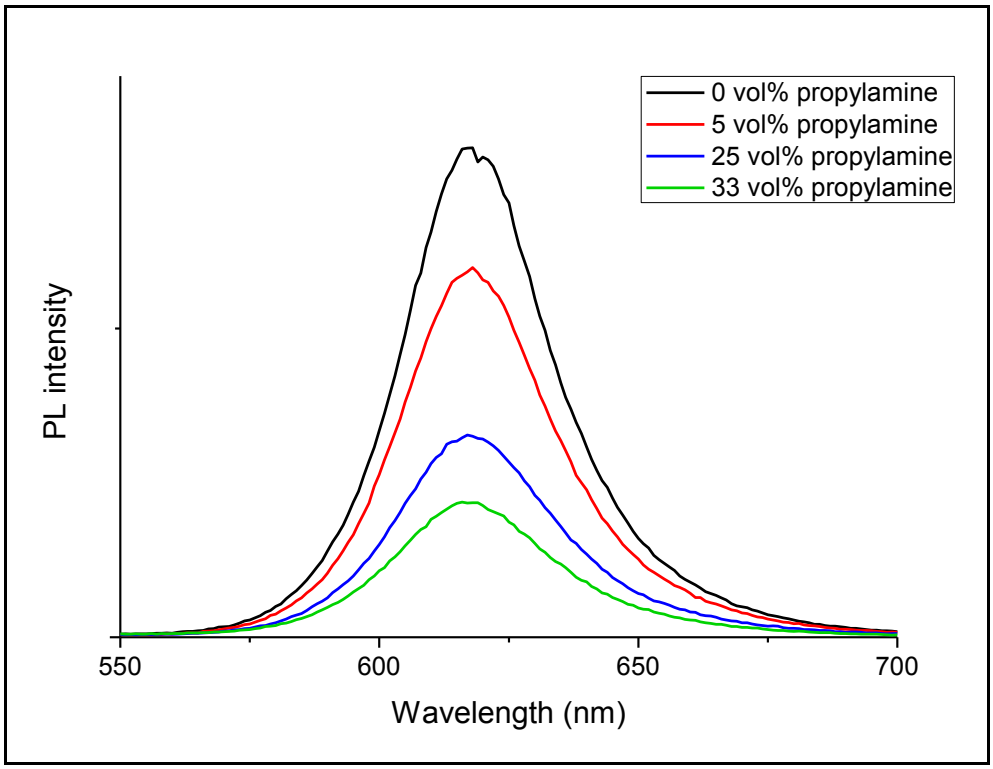

Fig. 6.3: Photoluminescence spectra of CdSe QDs dispersed in chloroform and titrated with varying amounts of propylamine. Samples were placed in a 10 mm square quartz cuvette. Excitation wavelength: 500 nm.

The PL spectra were taken using the same experimental parameters, such as excitation wavelength and slit sizes, which control the amount of light going to the sample and to the detector. Some reduction in luminescence intensity is expected due to dilution of the QDs upon titration. However, the titration of the QD solution to only 5 vol% propylamine reduces the PL intensity by 25%, with similar results as the solution is titrated further. Therefore, these spectra indicate luminescence quenching caused by the propylamine, such as by photoelectron transfer (PET). Amines are well-known to act as donors due to the easily oxidized lone-pair, which can quench excited luminophores.

6.3 CdSe QDs and their optical behavior in solution, on ChG surface and in ChG films

CdSe QDs deposited on the surface of the film, and inside the film matrix, were also tested with UV-vis and photoluminescence. Figure 6.4 shows the UV-vis spectra of CdSe QD-doped films.

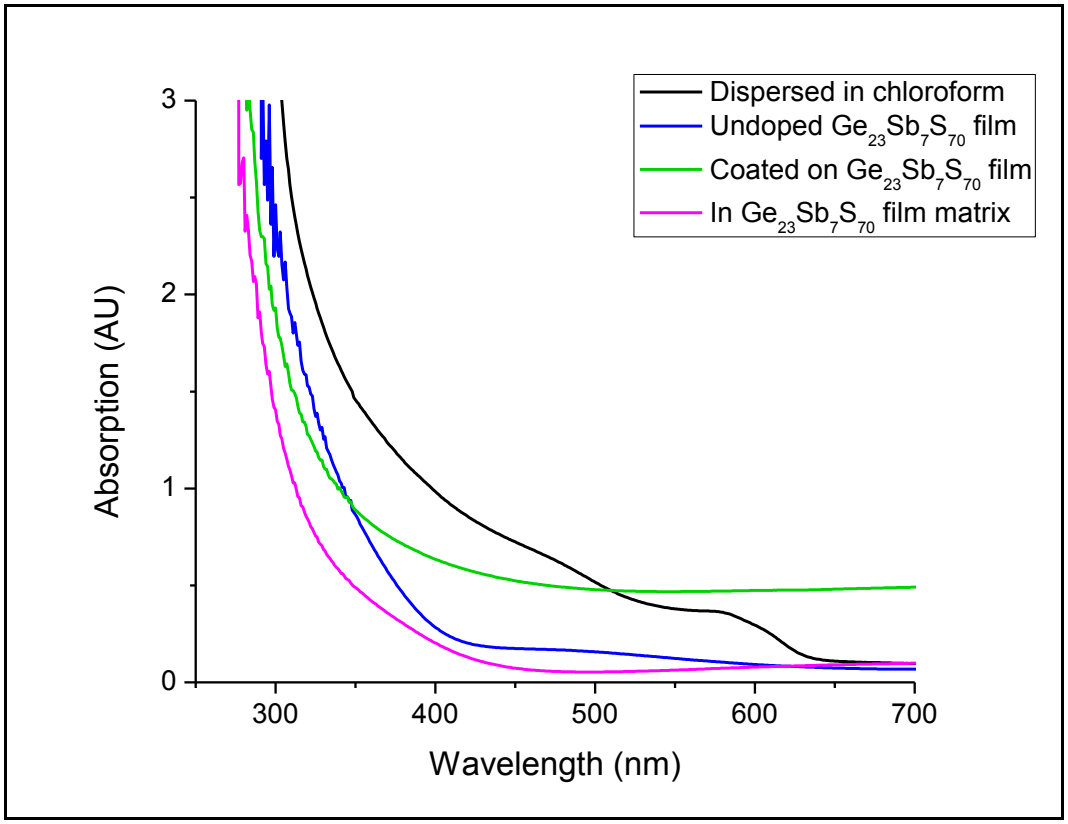

Fig. 6.4: UV-vis spectra of CdSe QDs in solution, on film surface, in film matrix, and undoped film

Most notable from these spectra are the lack of characteristic QD absorption bands in the doped films. This indicates that the concentrations of QDs on the film surface and in the film matrix are too low to detect by UV-vis spectroscopy. Obtaining adequate doping level for strong luminescence is a major challenge in the development of QD-doped solution-derived chalcogenide films. This is because QDs are typically only stable in solution up to 5 vol%, so a large volume of QD solution must be added to the chalcogenide solution. This reduces the thickness of the film because it dilutes the glass solution. However, the doped films were still found to be luminescent, as shown in Figure 6.5.

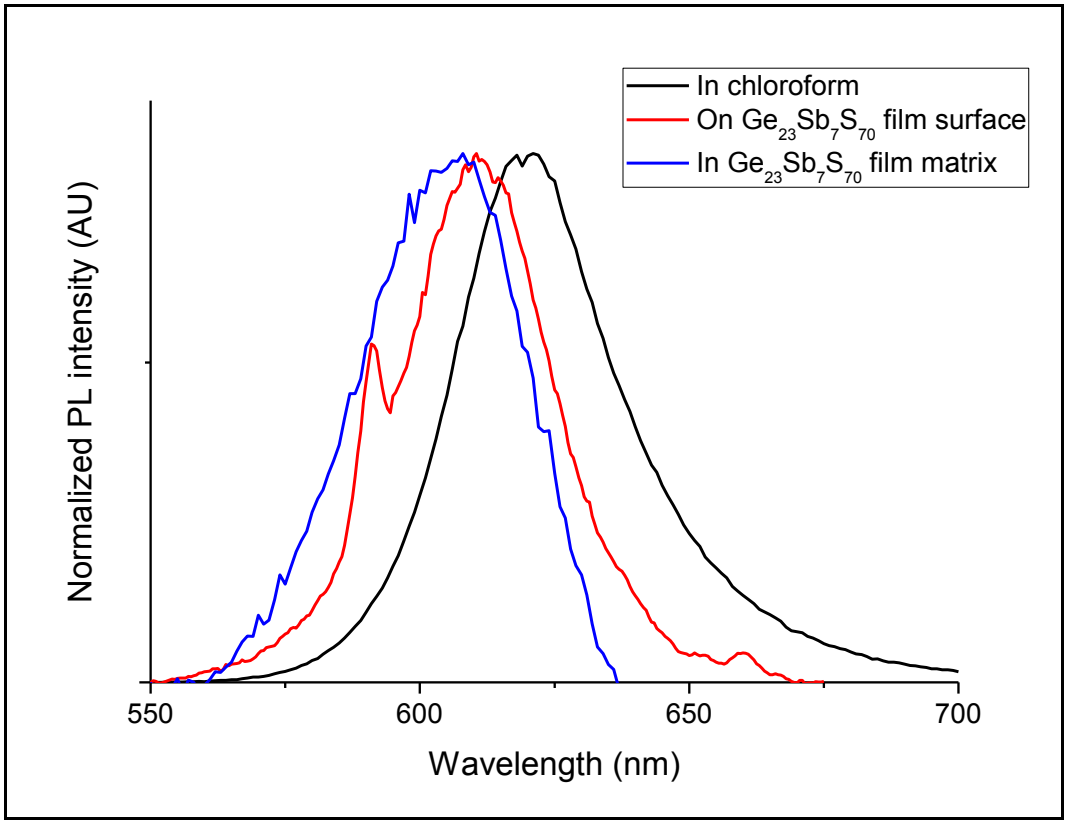

Fig. 6.5: Photoluminescence spectra of t ~ 200 nm ChG films doped with CdSe QDs on the surface and in the matrix normalized by their maxima. Excitation wavelength: 500 nm. The feature at 590 nm on the film surface spectra is a reflection artifact of the instrument.

These spectra show that while the doped films are luminescent, the peak luminescence wavelength for both are shifted slightly from the QDs dispersed in chloroform. The luminescence of the QDs in solution is centered at 618 nm, while that of the QDs on the film surface is 610 nm, and that of the QDs in the film matrix is 605 nm. This is due to interactions with the glass, not the propylamine solvent, because the luminescence spectra of the QDs in solution, titrated with propylamine, were not shifted. The feature at 590 nm on the luminescence curve of QDs on the film surface is a reflection artifact. Reflections are common when measuring luminescence of solid

samples, and are a function of sample geometry and excitation wavelength. The feature was confirmed to be a reflection by varying the excitation wavelength and noting that its position moved. Similarly, the luminescence was confirmed to be real by varying the excitation wavelength and noting that there was no shift.

6.4 Quantifying luminescent quantum yield and lifetime

The spectra in Figure 6.4 are normalized by their maxima for viewing purposes, and say nothing about the quantity of luminescence from each sample. The quantity of luminescence is characterized by the internal quantum yield, which is a ratio of emitted photons to absorbed photons. As mentioned in Chapter 3, internal quantum yield can be measured by taking the six spectra in Table 3.2. The spectra used to calculate the quantum yield of the CdSe QDs on the surface of a $Ge_{23}Sb_7S_{70}$ film are shown as an example. Figure 6.6 shows the scans of the luminescence, EM1, EM2, and EM3, and Figure 6.7 shows the scans of the excitation source, EX1, EX2 and EX3.

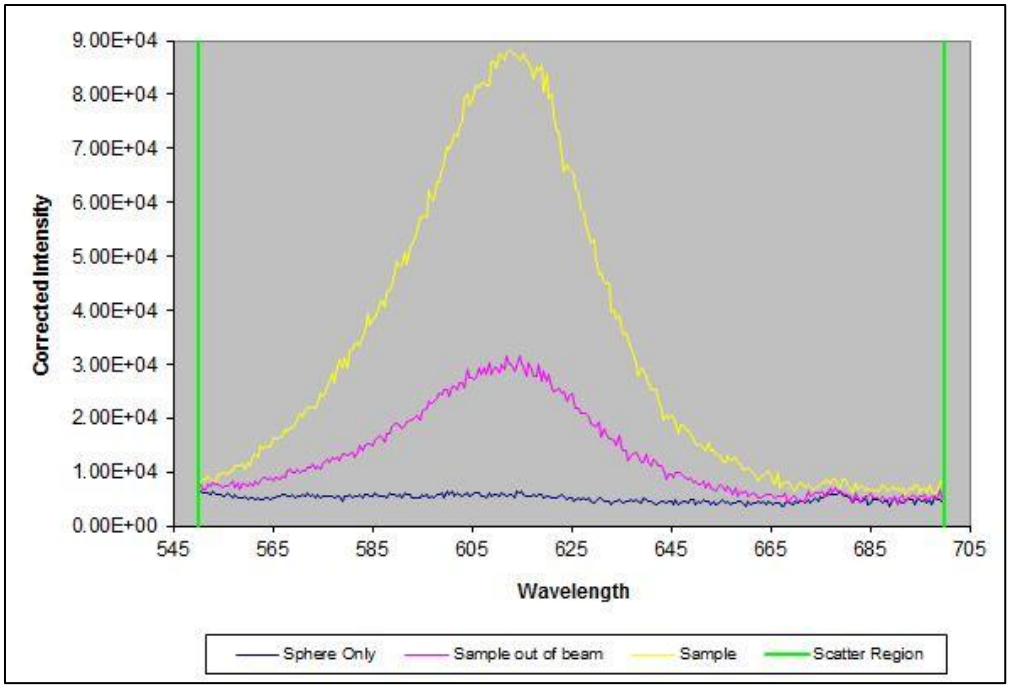

Fig. 6.6: Scans of fluorescence of CdSe QDs used to calculate quantum yield

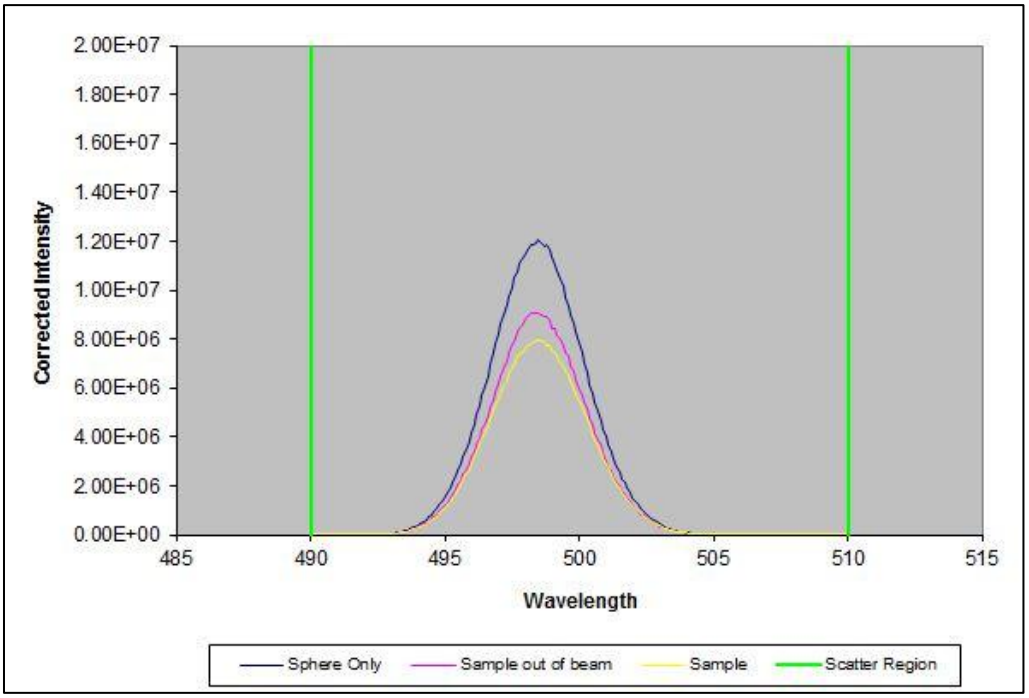

Fig. 6.7: Scans of excitation used to calculate quantum yield of CdSe QDs on $Ge_{23}Sb_7S_{70}$ film surface

Quantum yields calculated from the data illustrated in Figure 6.5 and 6.6 are shown in Table 6.1.

Table 6.1: Calculated absolute quantum yields of CdSe QDs in various environments

	Dispersed in chloroform	In 33 vol% propylamine / 67 vol% chloroform	On $Ge_{23}Sb_7S_{70}$ film surface	In $Ge_{23}Sb_7S_{70}$ film matrix
Quantum Yield	21.9%	9.0%	26.6%	Not luminescent enough to obtain data

These measurements further confirm that the luminescence from the QDs is partially quenched by propylamine. Roughly the same quantum yield was measured between QDs dispersed in chloroform and deposited on the film surface. The quantum yield of the QDs dispersed in the film matrix was not able to be measured because the luminescence signal was too low. This was likely caused by a combination of quenched luminescence and low concentration of QDs in the film. It is also possible that luminescence from QDs in the film matrix is contained inside the film due to total internal reflection, reducing the signal such that quantum yield could not be determined. If this phenomenon does occur, the calculated value of the quantum yield would not be valid. To further investigate the performance of the QDs in the various environments, luminescence lifetimes were taken, shown in Figure 6.8.

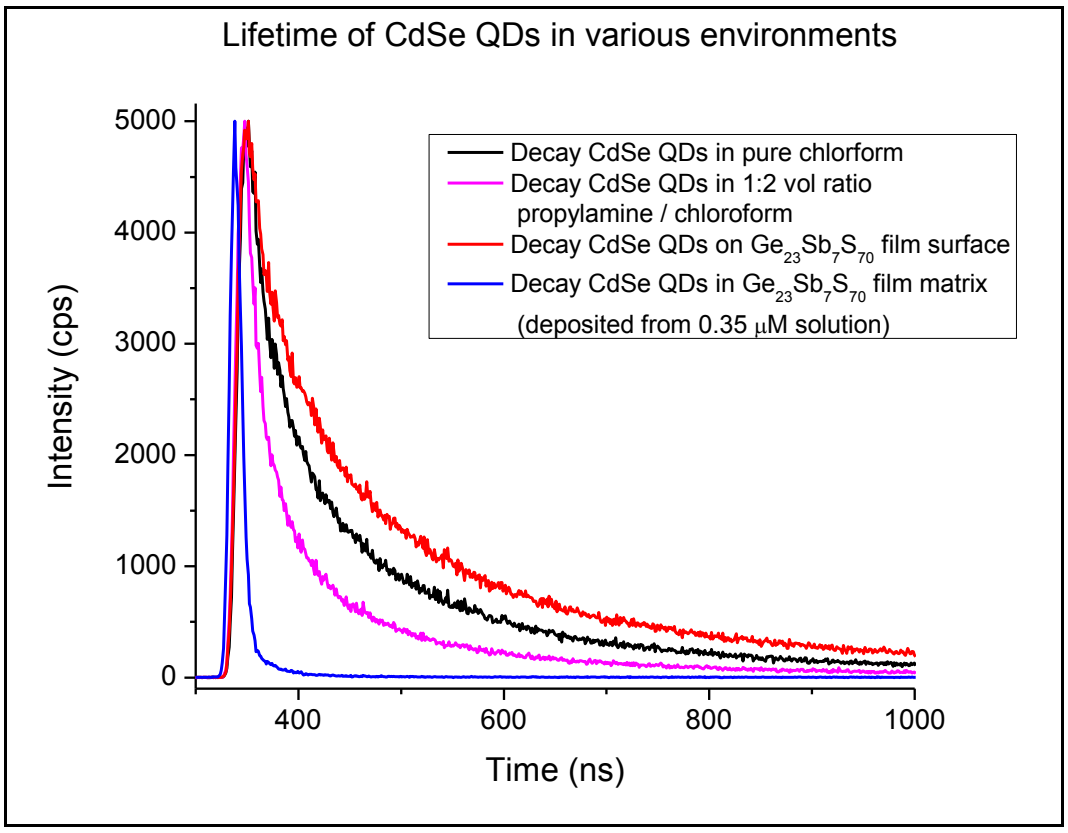

Fig. 6.8: Photoluminescence lifetimes of CdSe QDs in different environments using a pulsed 460 nm source

Lifetimes are a representation of competition between different processes happening in the material. When an electron is excited, there are many paths it can take to reduce its energy back to ground state. Of course, in a QD, emission of a photon is the desired outcome, but there are non-radiative de-excitation pathways such as photoinduced electron transfer and thermal absorption to the glass lattice that can impact lifetime. Longer lifetimes mean that there is less driving force for non-radiative de-excitation, and quantum yield increases with increasing lifetime. The lengths of the arrows in Figure 6.7 represent relative lifetimes between the CdSe QDs, and this data is shown in Table 6.2.

Table 6.2: Fluorescence lifetimes for CdSe QDs in various environments

CdSe QD Environment	Fluorescence Lifetime (ns)
Pure chloroform	25
1:2 propylamine/chloroform	16
On $Ge_{23}Sb_7S_{70}$ film surface	30
In $Ge_{23}Sb_7S_{70}$ film matrix	0.2

The lifetime of the QDs in 1:2 propylamine/chloroform is reduced from those dispersed in pure chloroform. This indicates fluorescence quenching caused by the propylamine, and the mechanism is likely transfer of the excited electron from CdSe to the amine group. However, the most noteworthy result is that the lifetime of the QDs on in the film matrix is more than two orders of magnitude less than the QDs in pure chloroform. The mere presence of glass also cannot explain this result because the lifetime of QDs on the film surface is longer than that of the QDs in pure chloroform. Residual propylamine in the film matrix likely plays a small role, but this cannot be the principle factor because the lifetime of QDs in the presence of 33 vol% propylamine is only reduced slightly from that of the QDs in pure chloroform. Therefore, there must be some change in the QDs due to the solution-based film processing. Aggregation is one possible explanation. When the mixture of glass solution and QDs is spin-coated, solvent begins to evaporate, and the concentration of QDs increases, which causes a higher thermodynamic driving force for aggregation. This is countered by the mixture increasing in viscosity, providing a kinetic barrier to aggregation, but it is very likely that some aggregation is occurring. This has not been investigated experimentally, but transmission electron microscopy would likely help to provide a quantitative estimate of the dispersion of QDs in the film matrix. Damage to the QDs caused by propylamine is also possible,

such as by cleaving of the TOPO capping agent and dissolution of the ZnS shell (propylamine was chosen as the glass solvent due to its ability to dissolve sulfides). However, the duration of QDs in the presence of propylamine during the titration of QD solution is much longer than when depositing the films, as the QD solution was mixed with the glass solution for approximately 5 seconds before spin-coating. During the titration with 33 vol%, lifetime was only reduced from 25 to 16 ns, but the QDs were in the presence of 67 vol% propylamine during the fabrication of doped films, so it is difficult to make a comparison. More future work is necessary to make a conclusive, quantitative explanation for such a strong reduction in lifetime of CdSe QDs in the glass film matrix.

6.5 Summary

The results of the testing with CdSe QDs in various environments such as in the presence of propylamine, on the $Ge_{23}Sb_7S_{70}$ film surface, and in film matrix show first and foremost that the behavior of the QDs is strongly dependent on the surroundings. Propylamine clearly quenches luminescence, as both quantum yield and lifetime were found to decrease when titrating QDs dispersed in pure chloroform with propylamine. Furthermore, the luminescence band of the QDs blue-shifts in the presence of $Ge_{23}Sb_7S_{70}$. This is evidenced by a shift in the maximum emission wavelength from 618 nm in solution, to 610 nm on the film surface, to 605 nm in the film matrix.

Visible luminescence has been successfully demonstrated from QDs incorporated into a solution-derived chalcogenide glass film matrix. Although visible luminescence is

not the ultimate goal of the project, the goals of learning the characterization techniques, developing a testing protocol, and investigating the behavior of QDs in solution-derived film processing were accomplished. The principles learned in this study can be applied to QDs which emit IR light in order to accomplish the ultimate goals of the project.

6.5 References

[1] W.W. Yu, L. Qu, W. Guo, X. Peng, "Experimental determination of the extinction coefficient of CdTe, CdSe, and CdS nanocrystals" *Chem. Mater.*, **2003**, *15*, 2854-2860.

CHAPTER 7

DOPING WITH LEAD SULFIDE QUANTUM DOTS

Bulk PbS has a smaller band-gap than CdSe (0.40 eV vs. 1.73 eV), so PbS QDs can emit longer wavelengths of light than CdSe QDs. While our ultimate goal is luminescence above 3 μM, PbS QDs have not been shown to emit above 2000 nm. However, they have been studied in more detail than other QDs which can emit in the desired range, such as PbTe [1], and provide a very attractive system to study in order to learn the principles of NIR emission from QDs dispersed in a solution-derived chalcogenide film matrix. In accordance with the goals of this thesis, we seek to investigate what concentrations of PbS QDs are required to observe luminescence, how the optical and luminescent properties of the film depend on QD concentration, and how the ability of the QD to disperse in the film matrix depends on the surface chemistry of the QD.

7.1 PbS QDs in solution and the effect of capping agents

PbS QDs were first tested in solution. Figure 7.1 shows the UV-vis-NIR spectrum of PbS QDs capped with mercaptohexanol and thioctic acid.

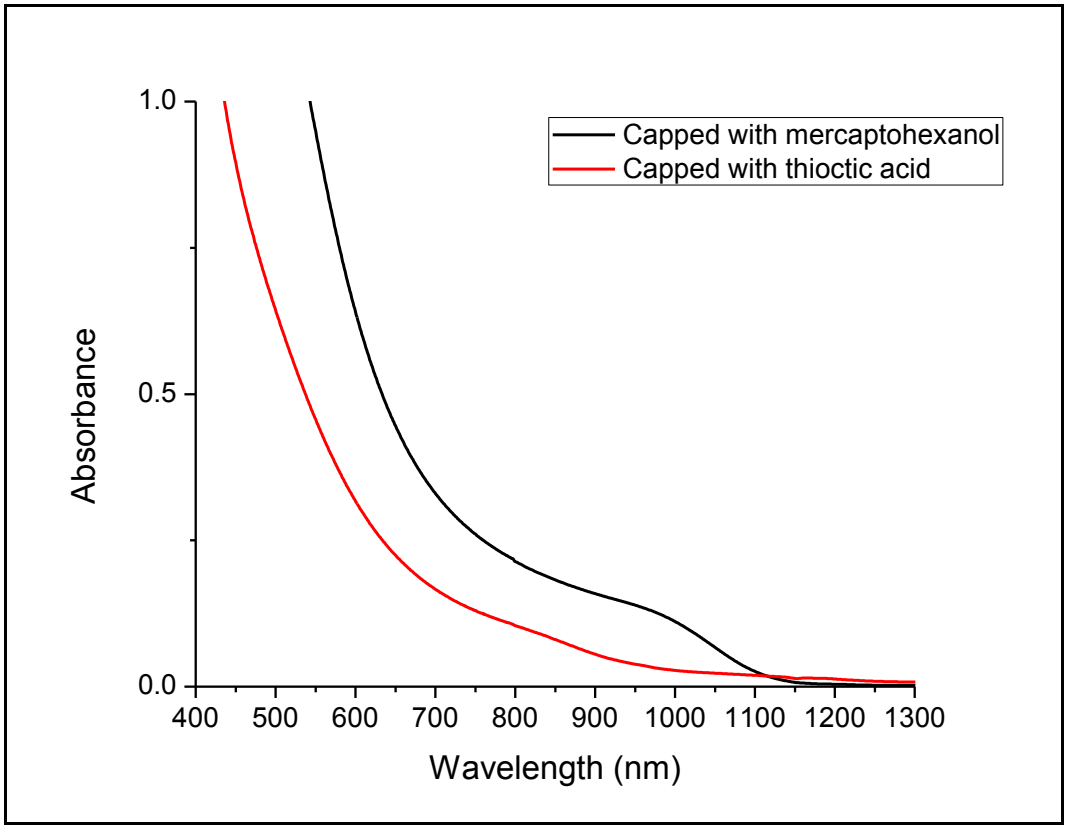

Fig. 7.1: Absorption spectra of PbS QDs (70 μM) synthesized with different capping agents and otherwise identical reaction parameters

These spectra show that when changing the capping agent from mercaptohexanol to thioctic acid, identical reaction parameters, such as ratio of lead acetate to thioacetamide and length of reaction, smaller QDs are obtained when using thioctic acid. This is apparent because due to the quantum confinement effect, absorption blue-shifts with decreasing particle size. QD size is extremely important because it also dictates the peak emission wavelength, which can be observed in Figure 7.2.

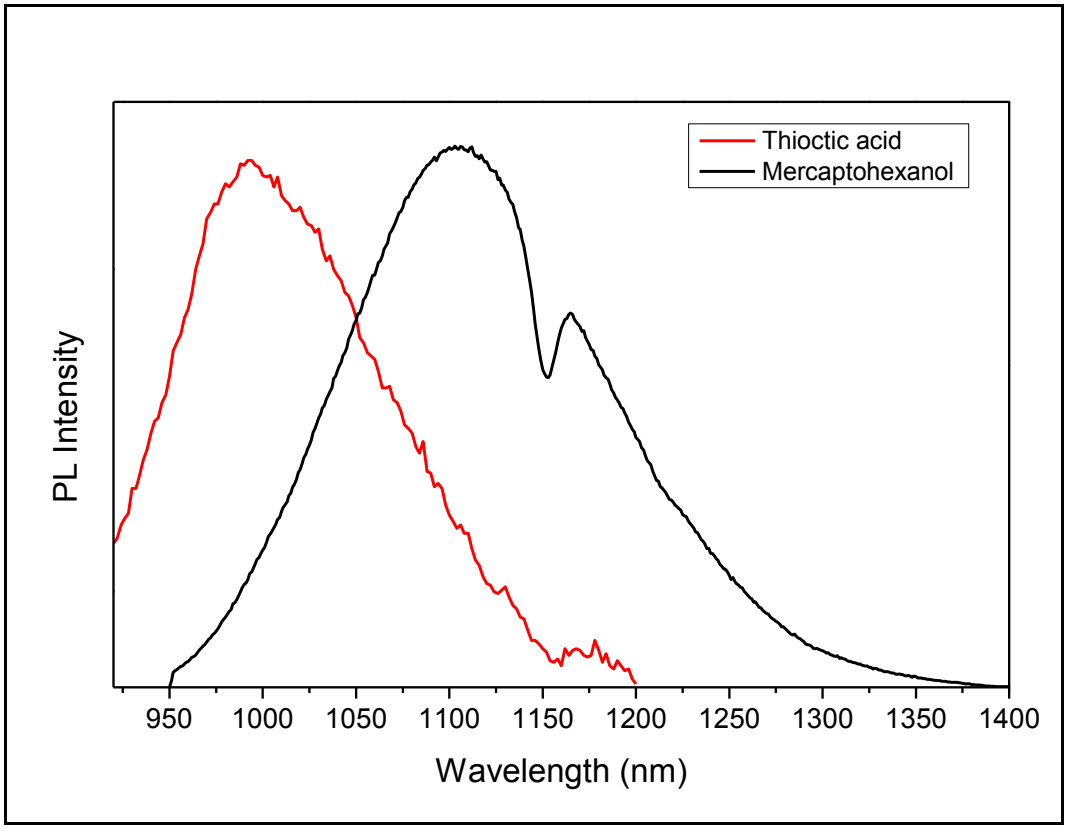

Fig. 7.2: Photoluminescence spectra of PbS QDs synthesized with different capping agents: thioctic acid (425 nm excitation source) and mercaptohexanol (532 nm excitation source)

First, the feature at 1150 nm most evident in the QDs capped with mercaptohexanol is due to a chloroform absorption peak. This is shown in Figure 7.3, where the absorption spectrum of chloroform is overlaid on the luminescence spectrum.

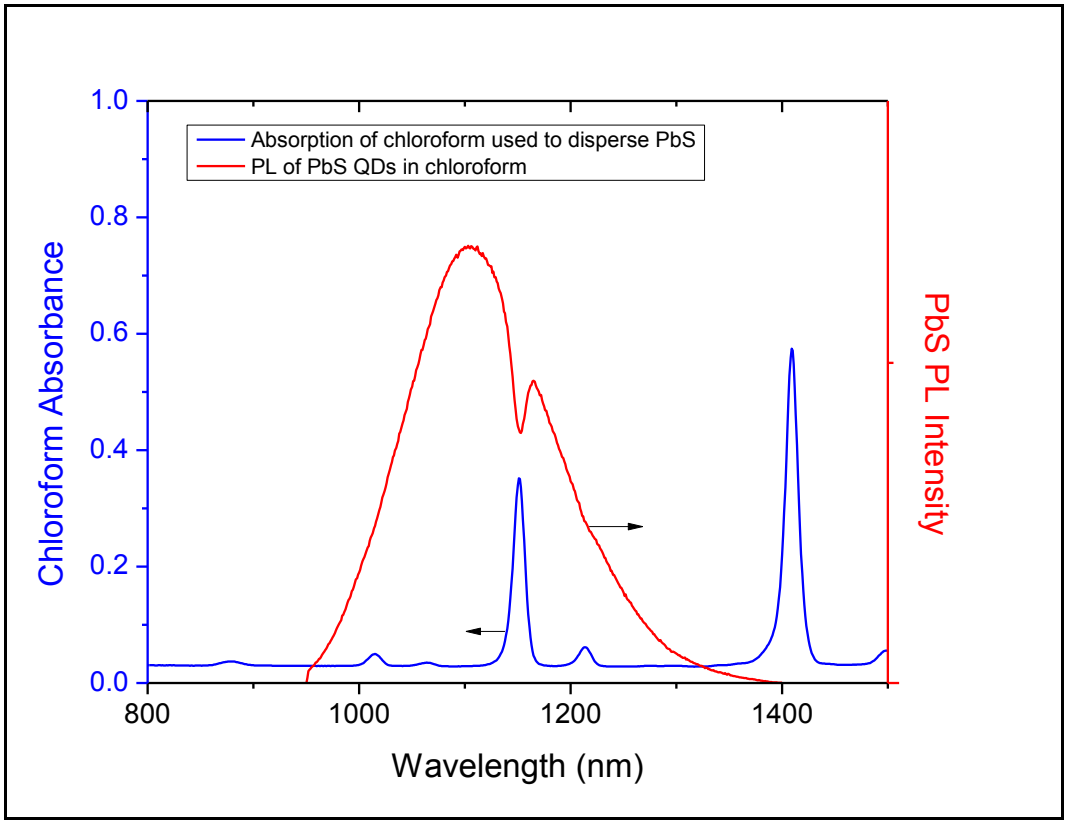

Fig. 7.3: Luminescence of PbS QDs capped with mercaptohexanol and dispersed in chloroform, and absorption spectrum of chloroform. Excitation source: 532 nm.

To solve this problem, the QDs must be dispersed in a solvent having no absorptions in the luminescence band of the QDs, as the absorption of chloroform affects quantum yield measurements. For this reason, it was determined that tetrachloroethylene (TCE) should be used to disperse the QDs when taking luminescence spectra. However, chloroform is ideal for studies of QDs in glass films due to its lower boiling point (61°C vs 121°C). If a mixture of TCE and $Ge_{23}Sb_7S_{70}$ solution in propylamine is spin-coated, the glass tends to precipitate irregularly as the propylamine evaporates quicker than TCE. This is because $Ge_{23}Sb_7S_{70}$ is insoluble in TCE, and results in films with very poor surface quality. Although the glass is also insoluble in chloroform, it is attractive as a

carrier solvent for QDs because it evaporates at nearly the same rate as propylamine (boiling point 48°C), and film quality is unaffected. Unfortunately, residual chloroform was seen to remain in the film after heat treatment, and possibly quenches some luminescence by reabsorption of the emitted photon.

For the QDs synthesized with mercaptohexanol as a capping agent, the peak emission wavelength is 1100 nm, and with thioctic acid, it is 990 nm. This means that the average band-gap of the QDs capped with mercaptohexanol is 1.12 eV, and 1.25 eV for those capped with thioctic acid. Particle size of the QDs capped with mercaptohexanol and thioctic acid was calculated to be 3.70 nm and 3.25 nm, respectively, using Equation 7.1, where E_0 is the band-gap in eV and d is the diameter is nm [2]:

$$E_0 = 0.41 + \frac{1}{0.0252d^2 + 0.283d} \qquad \text{(Eq. 7.1)}$$

7.2 Behavior of PbS QDs in the presence of propylamine

PbS QDs capped with mercaptohexanol were first tested in solution to investigate the effects of titration by propylamine. The QDs were dispersed from pure chloroform to 75 vol% propylamine, the results of which are shown in Figure 7.4.

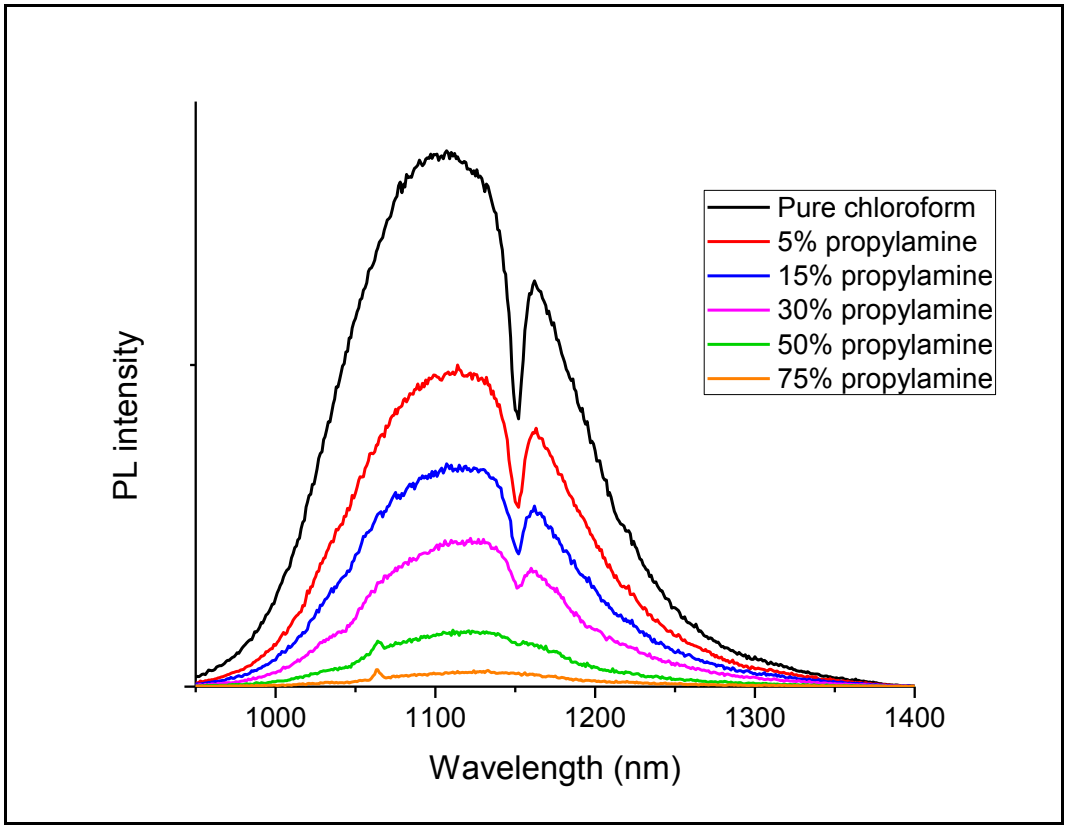

Fig. 7.4: Effect of propylamine titration on the photoluminescence spectrum of PbS QDs capped with mercaptohexanol using 532 nm excitation source

There is severe quenching caused by the propylamine, which is most evidenced by the reduction of peak photoluminescence intensity by about 40%, upon the addition of only 5 vol% propylamine. The spectra were all taken with the same instrument settings, such as slit sizes, so they can be directly compared.

7.3 Comparison between PbS QDs with different capping agents

Both varieties of QDs, mercaptohexanol capped and thioctic acid capped, were coated on microscope slides substrates and $Ge_{23}Sb_7S_{70}$ films. The difference between the

behavior of the QDs with different capping agents is remarkable, and is shown in Figure 7.5.

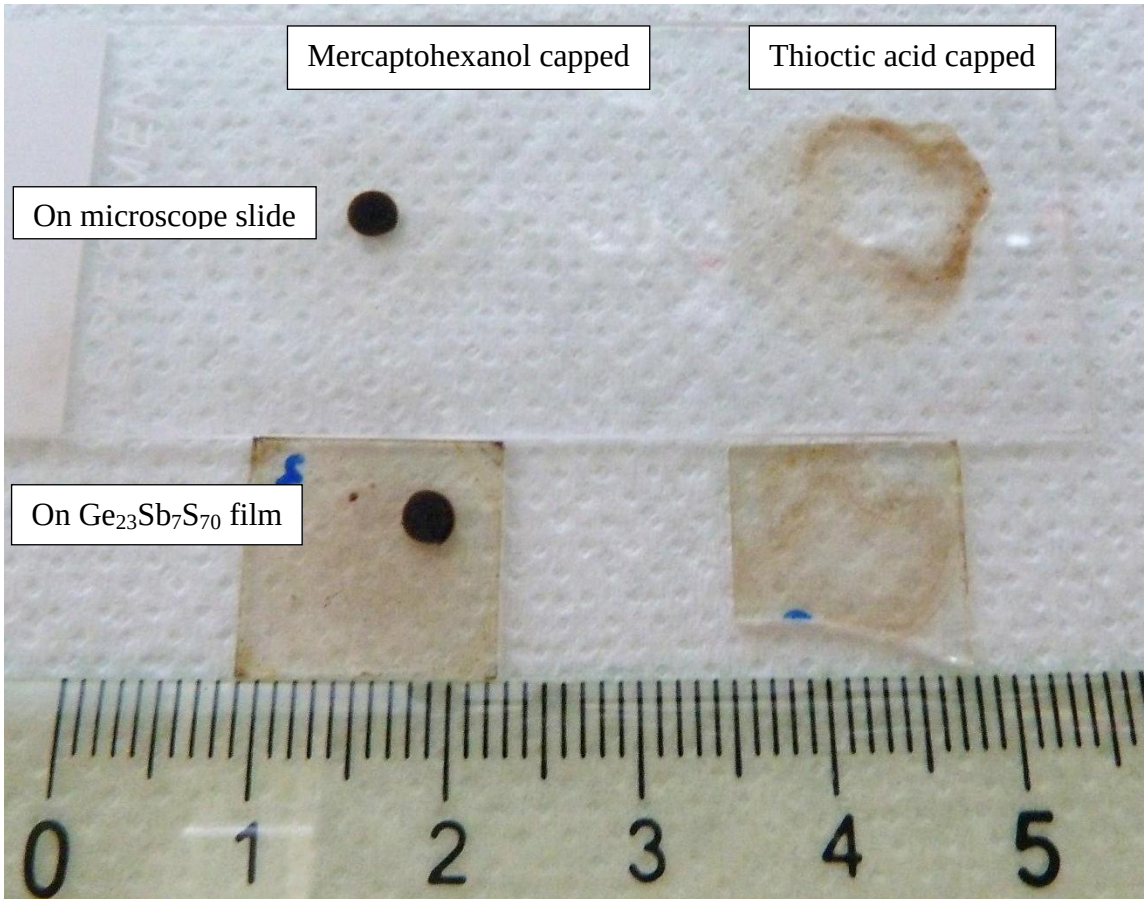

Fig. 7.5: Mercaptohexanol capped and thioctic acid capped PbS QDs deposited on the surface of a microscope slide and $Ge_{23}Sb_7S_{70}$ films

In all cases, 20 μL of PbS QDs of concentration 70 μM were dripped on the surface and left to dry. The QDs capped with mercaptohexanol tend to collect in one area, while those capped with thioctic acid are more spread out. Furthermore, for the QDs coated on the surface of $Ge_{23}Sb_7S_{70}$ films, no photoluminescence was observed from the QDs capped with mercaptohexanol, while there was luminescence from the thioctic acid capped QDs,

shown in Figure 7.6. This is presumably because the QDs capped with mercaptohexanol are too aggregated, and the test implies that PbS QDs are more prone to aggregation when using mercaptohexanol as opposed to thioctic acid. Attempts were also made to prevent the aggregation of the mercaptohexanol capped QDs by spin-coating them on the surface at 1600 rpm (the lowest speed available). The film appeared to be slightly darker, as if PbS QDs were in fact on the surface, but still no photoluminescence was observed.

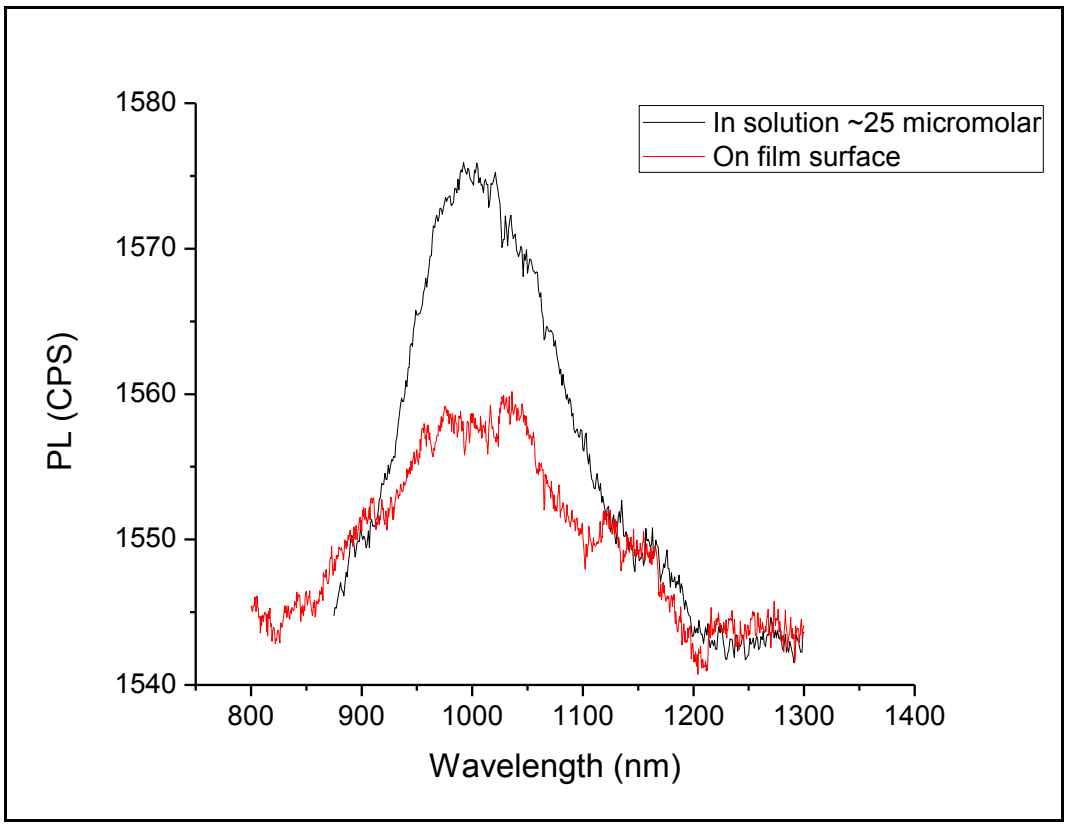

Fig. 7.6: Photoluminescence spectra of PbS QDs capped with mercaptohexanol in solution and coated on the surface of a $Ge_{23}Sb_7S_{70}$ film

Because only luminescence from PbS QDs capped with thioctic acid was observed when deposited on the film surface, the QDs capped with thioctic acid are the focus of studies performed on QDs within the $Ge_{23}Sb_7S_{70}$ film matrix.

7.4 Optimization of size of PbS QDs capped with thioctic acid

The kinetics of the PbS synthesis using thioctic acid were studied, and it was found that larger QDs could be synthesized by extending the reaction time from 2h00 to 2h15. The absorption and emission spectra are shown in Figure 7.7.

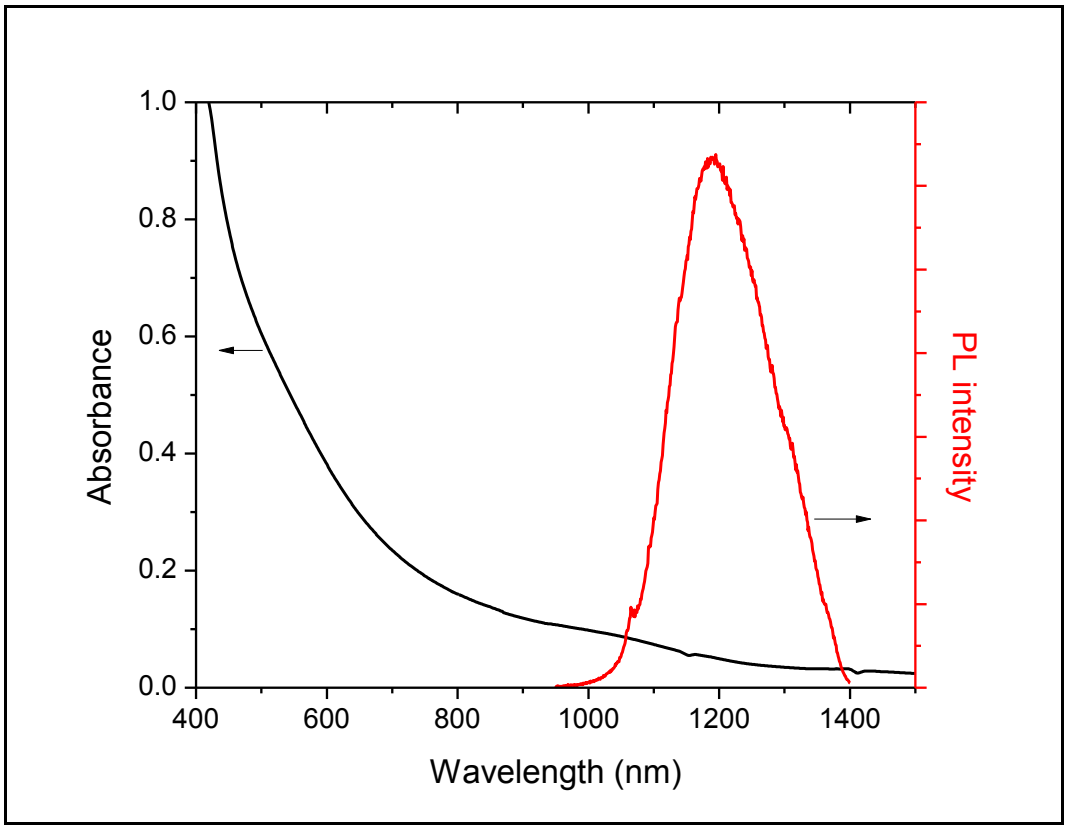

Fig. 7.7: Absorption and photoluminescence spectra of TCE dispersed PbS QDs capped with thioctic acid synthesized with a reaction duration of 2h15.

The emission of these QDs is centered at 1250 nm. According to Equation 7.1, this corresponds to an average diameter of 4.4 nm. DLS was used to confirm this size and investigate the size distribution.

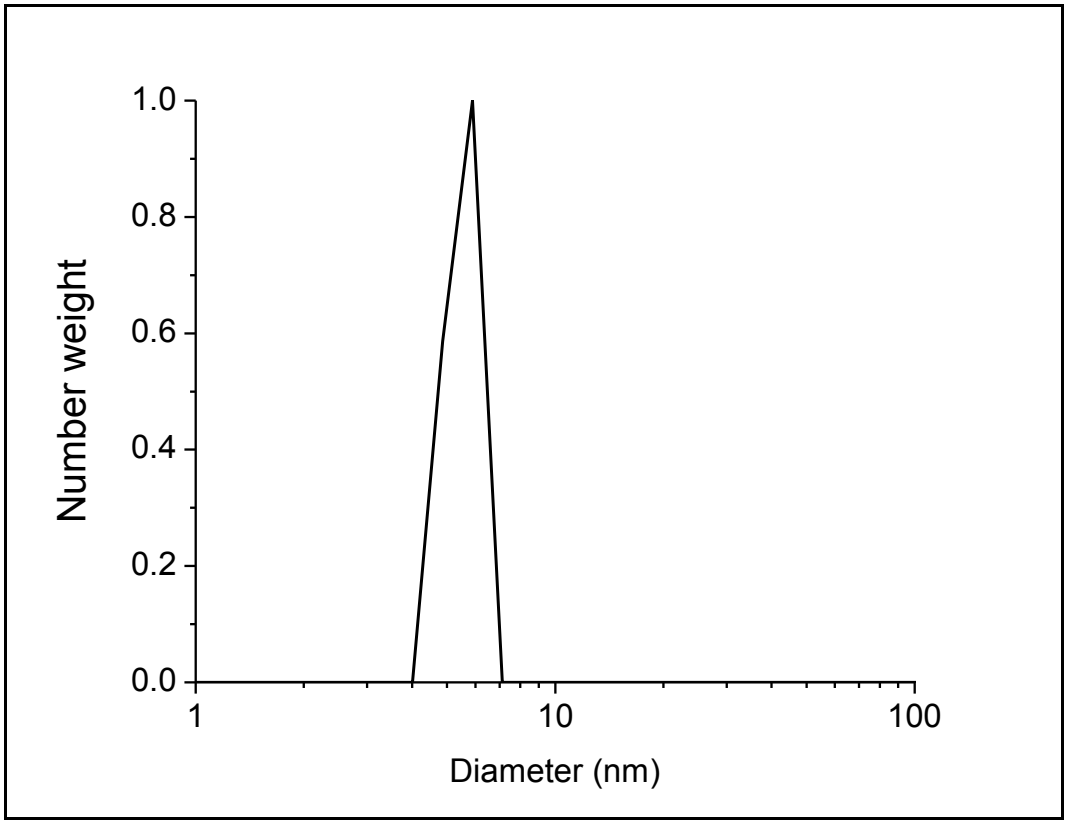

Fig. 7.8: Size distribution of PbS QDs capped with thioctic acid measured by DLS

The size distribution measured by DLS is consistent with that estimated by the luminescence spectrum, as the average diameter is about 5.8 nm. Thioctic acid on the surface of the QD adds roughly 1.5 nm to the diameter, resulting in a total diameter of ~5.9 nm, which is very close to the results of DLS. The size range was found to vary between 4 and 7 nm, or 2.5 and 5.5 nm when subtracting the thioctic acid. 2.5 nm is out of the fitting range of Equation 7.1, but the expected luminescence wavelength for 5.5 nm is 1475 nm, which appears to be consistent with the recorded luminescence spectrum. However, it should be noted that the range of the detector is 950 – 1400 nm, so it is possible that the upper tail of the luminescence band is not fully observable.

7.5 PbS QD-doped ChG films

To dope film matrices with PbS QDs, it was first attempted to perform the same experiment done with Au MNPs. PbS QDs capped with mercaptohexanol were added slowly to 30 mL vigorously stirred $Ge_{23}Sb_7S_{70}$ solution. Conservative loadings of 0 – 12 μM were used, but precipitation of PbS was observed in the mixture within 30 minutes, and samples removed from the mixture also showed precipitation within a similar amount of time. From this test, it was clear that solutions were not stable long enough for such an optimization. A similar test was repeated with thioctic acid capped QDs on a smaller scale, and it was clear that the doped solutions were also not stable for longer than 30 minutes. Therefore, the method used to fabricate PbS QD doped films was as follows: PbS QDs dispersed in chloroform were added rapidly to the glass solution in a 1:2 QD to glass solution ration by volume, and stirred for approximately 5 seconds. The mixture was then deposited on the substrate and spin-coated. Microscope slides and Si wafers were both used as substrates so that absorption spectra could be recorded from the UV to the MIR.

The QDs used to dope the films were those synthesized with a reaction duration of 2h15 and capped with thioctic acid according to the experimental details in Section 3.2. Three different concentrations of QD doped solutions were prepared by diluting the stock QD solution prior to mixing with the glass solution. Various heat treatments were tested, according to Table 7.1.

Table 7.1: Heat treatments used for PbS doped $Ge_{23}Sb_7S_{70}$ films

Heat Treatment Number	Description
HT0	5 min on hotplate
HT1	30 min at 100°C
HT2	30 min at 100°C
HT3	20 min at 162°C
HT4	20 min at 180°C
HT5	20 min at 198°C

The photoluminescence spectrum of a doped film deposited from a solution containing 17 μM PbS QDs after HT0 is shown in Figure 7.9 along with the spectrum of the QDs in solution.

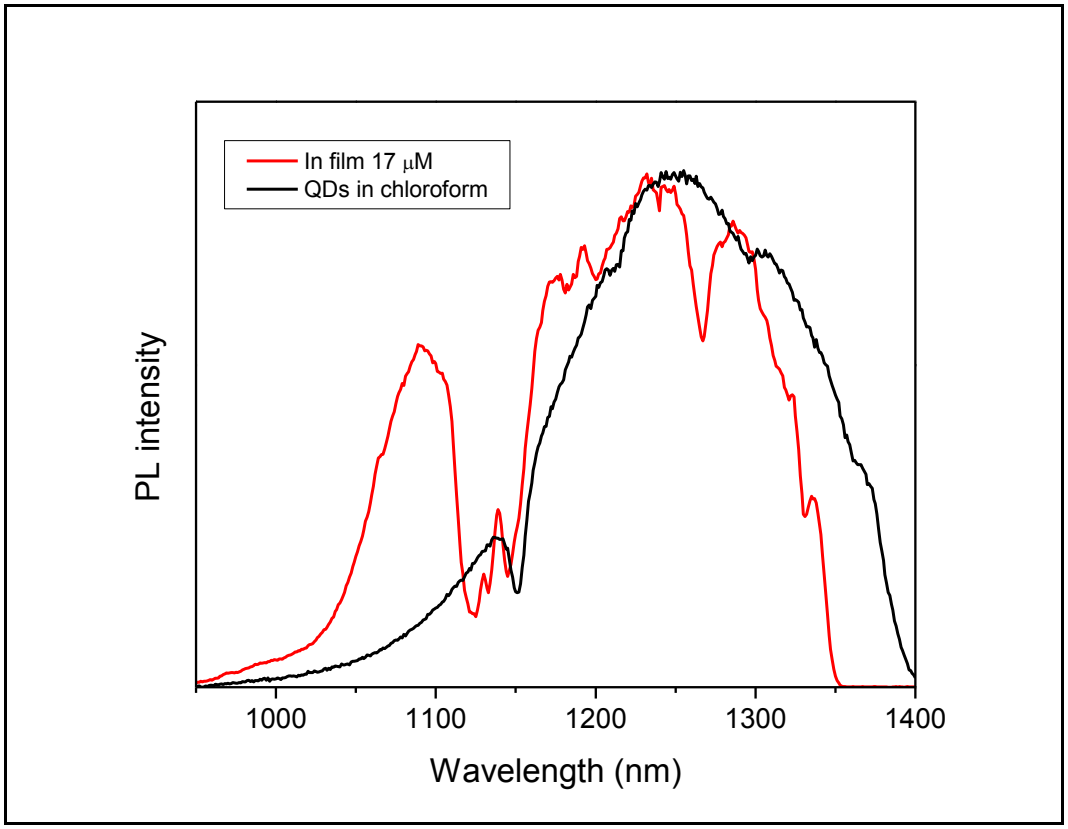

Fig. 7.9: Photoluminescence spectra of $Ge_{23}Sb_7S_{70}$ films doped with thioctic acid capped PbS QDs. Excitation: 532 nm.

Figure 7.9 shows that the shape of the luminescence spectrum is significantly different than that of the QDs in solution. First, the peak wavelength of the luminescence has blue-shifted from 1250 nm in solution to 1230 nm in the film. This is consistent with the results of the testing with CdSe QDs, whose luminescence also blue-shifts in the presence of $Ge_{23}Sb_7S_{70}$. The spectrum of the QDs in the film also has many sharp features, particularly at 1125, 1145, and 1265 nm. The origin of these features is unknown at the time. The features at 1125 and 1150 are perhaps due to residual chloroform in the film matrix, as pure chloroform has a strong absorption band at 1150 nm. It is possible that the bonds made by residual chloroform with the glass matrix are responsible, but they are not seen in the UV-vis-NIR absorption spectrum, which is shown in Figure 7.10.

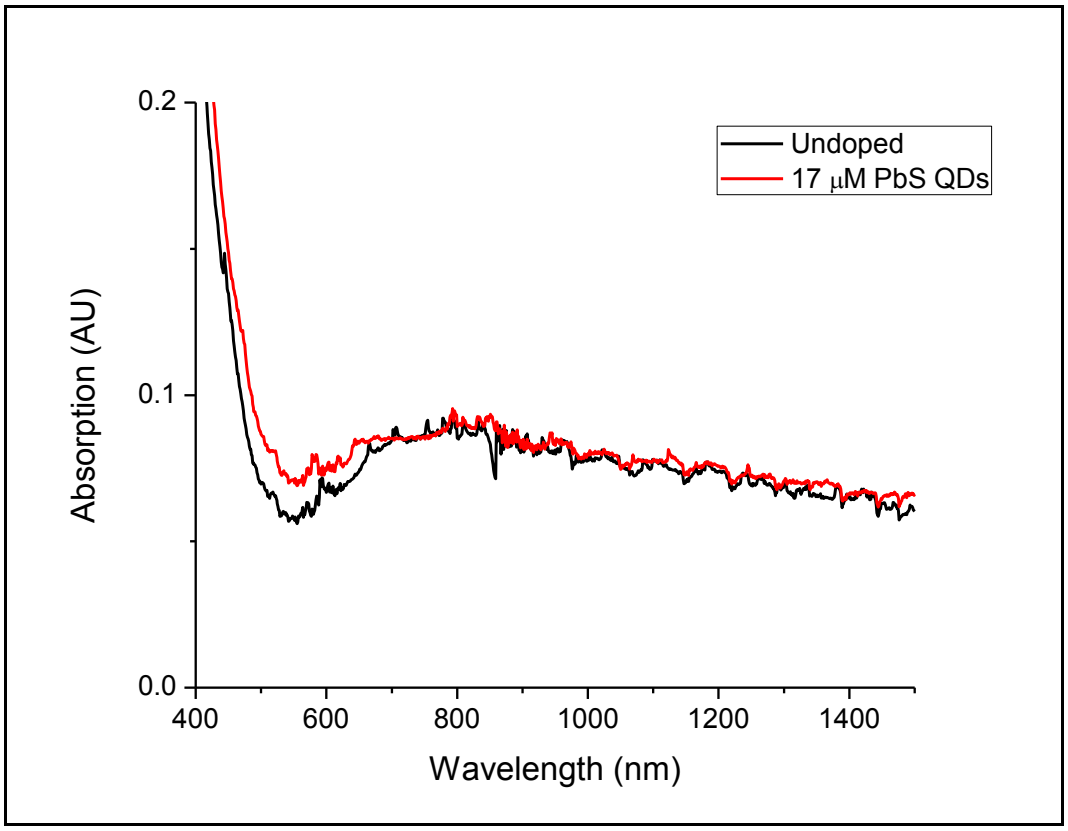

Fig. 7.10: Absorption spectra of undoped and PbS QD doped $Ge_{23}Sb_7S_{70}$ films on microscope slides.

This figure shows that the absorption of the QDs is apparent, as the doped film has higher absorption than the undoped film below 700 nm, where the QDs absorb strongly. However, there do not appear to be any absorption bands in the NIR, specifically at 1125, 1145 and 1265 nm, where reductions in the luminescence intensity are seen.

To study the effects of heat treatments on shape and intensity of the luminescence spectrum, varying heat treatments were used according to the work done in parallel to this thesis [2]. These heat treatments optimize the time and temperature such that the size of the absorption peak due to propylamine in the MIR is minimized. Figure 7.11 shows the luminescence spectra of the film deposited from a 17 μM. These spectra were all taken with the same instrument settings in an attempt to obtain relative quantum yields.

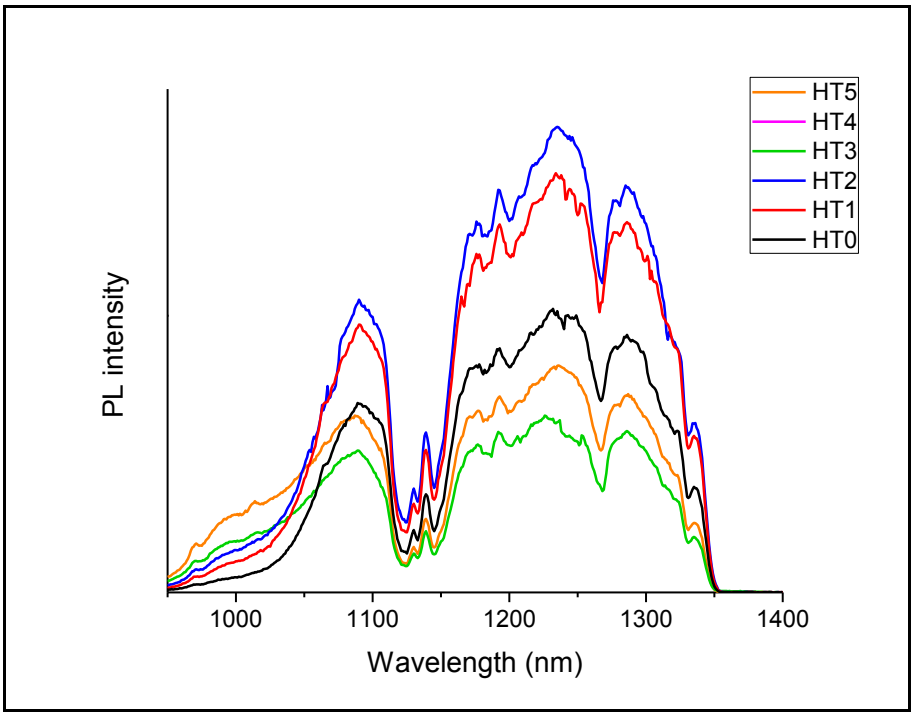

Fig. 7.11: PL spectra of $Ge_{23}Sb_7S_{70}$ film deposited from solution containing 17 μM PbS QDs capped with thioctic acid for various heat treatments. Excitation wavelength: 532 nm.

The spectra in Figure 7.11 show that the luminescence intensity increases for heat treatments from HT0 to HT2, then strongly decreases for HT3. The increase in intensity is due to the removal of residual propylamine from the film matrix, while the decrease is presumably due to a reduction in surface quality causing scattering of the luminescence. Damage to the QDs at the higher temperature heat treatments is also a possible explanation, such as by the diffusion of Pb or S atoms away from the QD. However, this is not likely because the same basic shape is seen for all of the spectra, and no blue-shift is seen that would indicate a reduction in the size of the QDs.

It was intended that relative quantum yields could be calculated and compared by integrating each luminescence spectrum of the films for varying heat treatments. Absolute quantum yields using an integrating sphere cannot be determined with our current equipment, as the range of the NIR detector is 950 – 1400 nm, and scans of the excitation cannot be taken. Additionally, lifetime was also not able to be measured because the luminescence signal was too weak when using the pulsed LED, which is much less intense than the 532 nm laser used for the emission spectra. Nevertheless, there is strong indication that quantum yield increases with the removal of solvent.

In order to quantify the amount of solvent removal from the films, FTIR transmission spectra were taken in the MIR. Figure 7.12 shows the evolution of the FTIR spectra for a PbS doped film with the various heat treatments used.

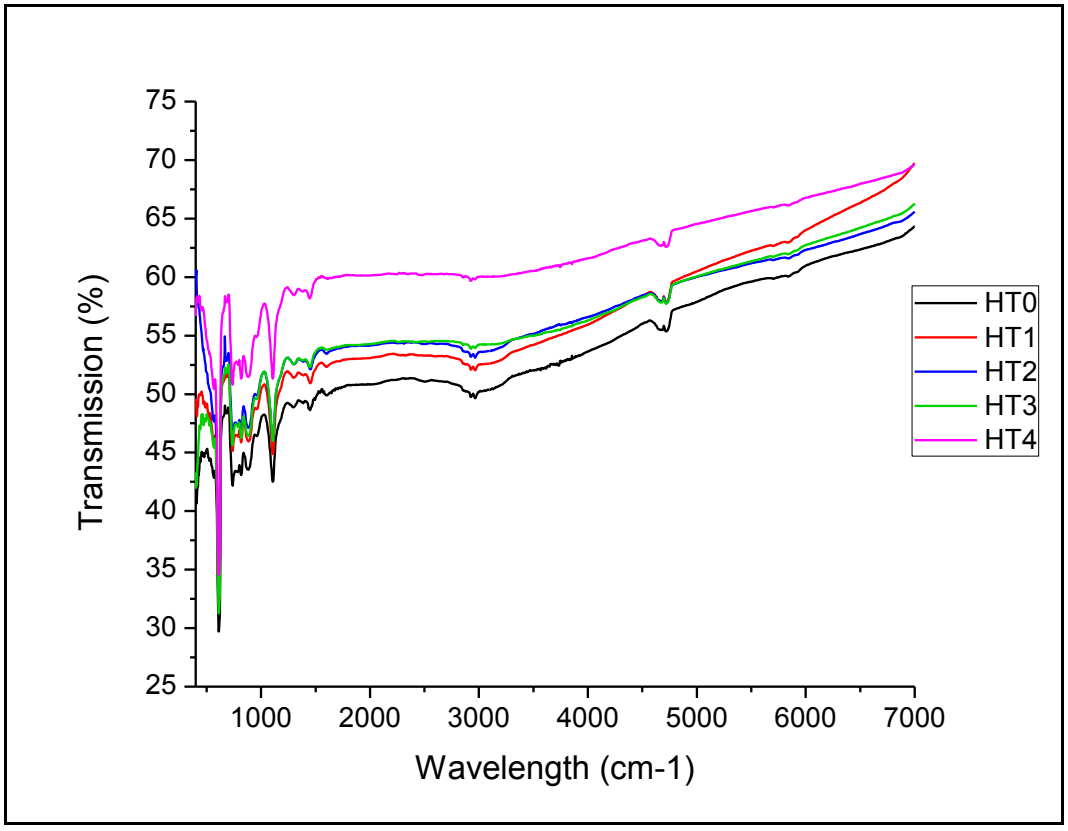

Fig. 7.12: FTIR spectra of $Ge_{23}Sb_7S_{70}$ film deposited from solution containing 17 µM PbS QDs capped with thioctic acid for various heat treatments.

The absorption bands at 3000 cm^{-1} are due to residual propylamine in the film matrix. The spectra show that the propylamine absorption bands decrease significantly with the heat treatments. To quantify the relative amount of solvent removed, the sizes of the absorption bands were measured as demonstrated in Figure 7.13. A baseline is drawn, and the distance from the baseline to the peak of the absorption band is measured in percent transmission.

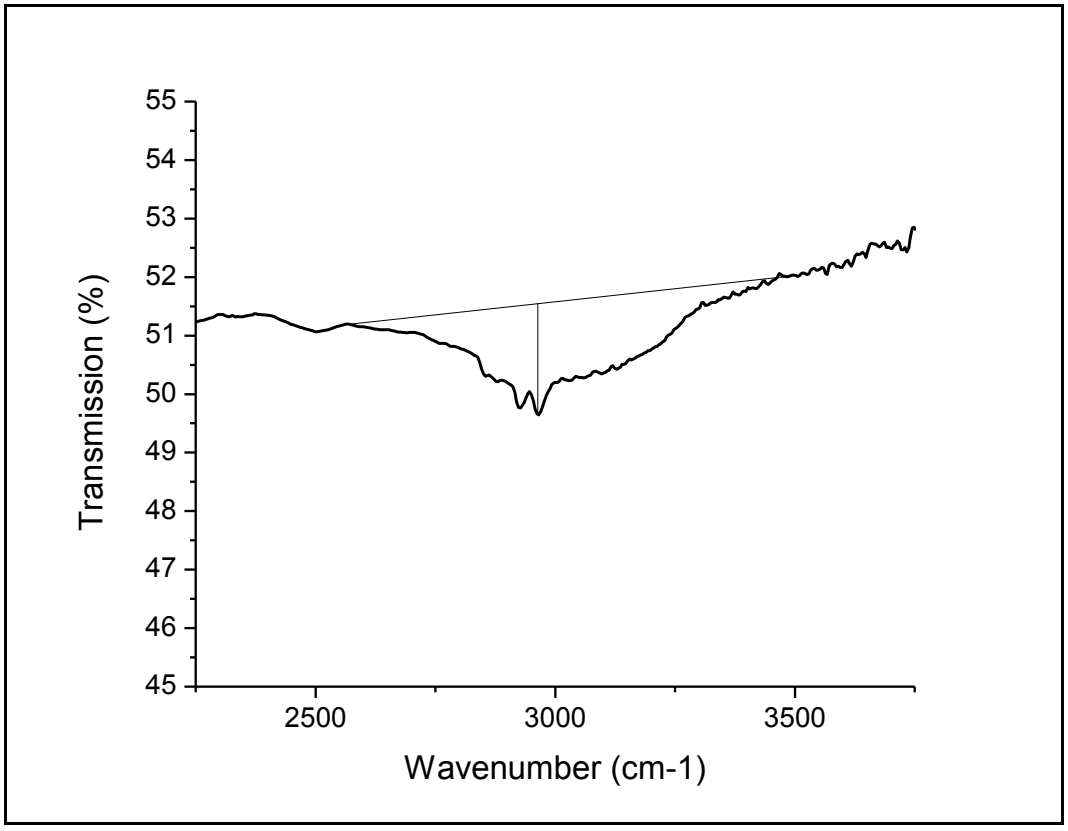

Fig. 7.13: Schematic of method used to measure size of propylamine absorption bands

This method was used in order to plot the relative size of the propylamine absorption band vs. the heat treatments of each film, shown in Figure 7.14.

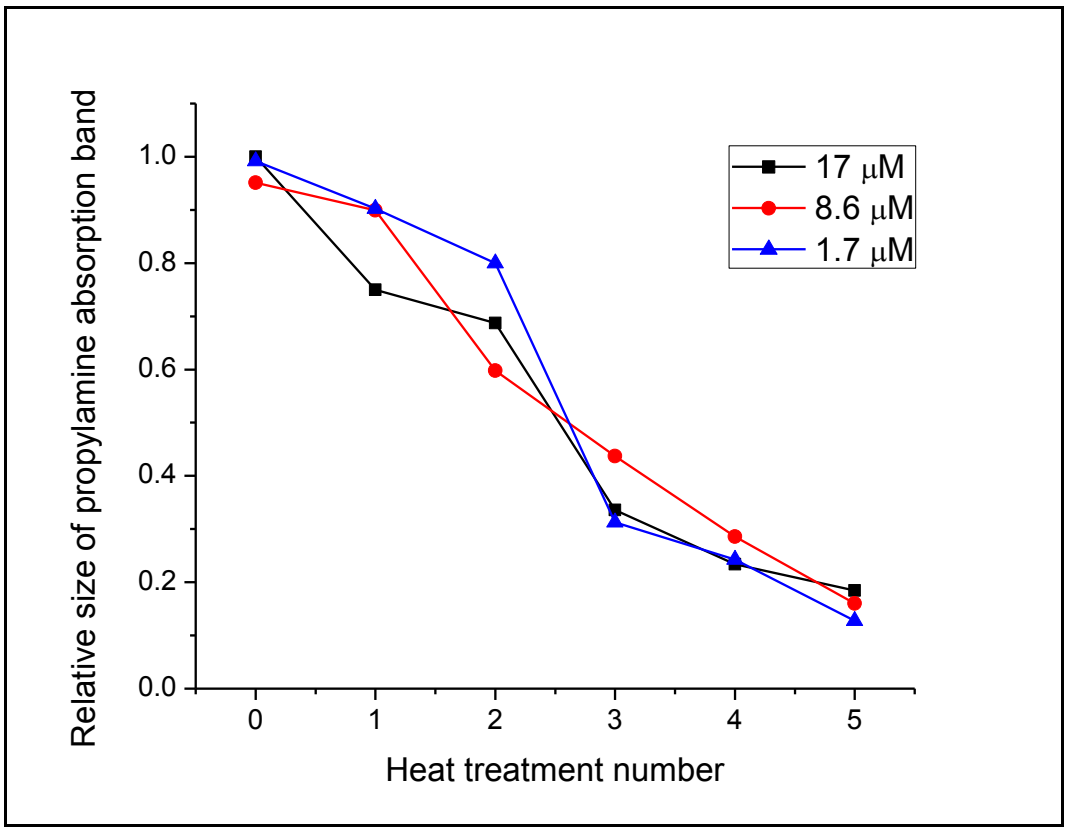

Fig. 7.14: Size of propylamine absorption band in PbS doped $Ge_{23}Sb_7S_{70}$ various heat treatments

Figure 7.14 shows that decrease in size of the propylamine absorption band is approximately linear over the heat treatments used. It is therefore expected that the luminescence intensities of the doped films will increase steadily with each heat treatment, and remain approximately constant at some point. Relative photoluminescence intensities are then plotted vs. heat treatment number, shown in Figure 7.15. The integrations of the emission spectra are normalized by the spectrum having the highest intensity, which was the film deposited from a doped glass solution containing 17 μM PbS after HT4.

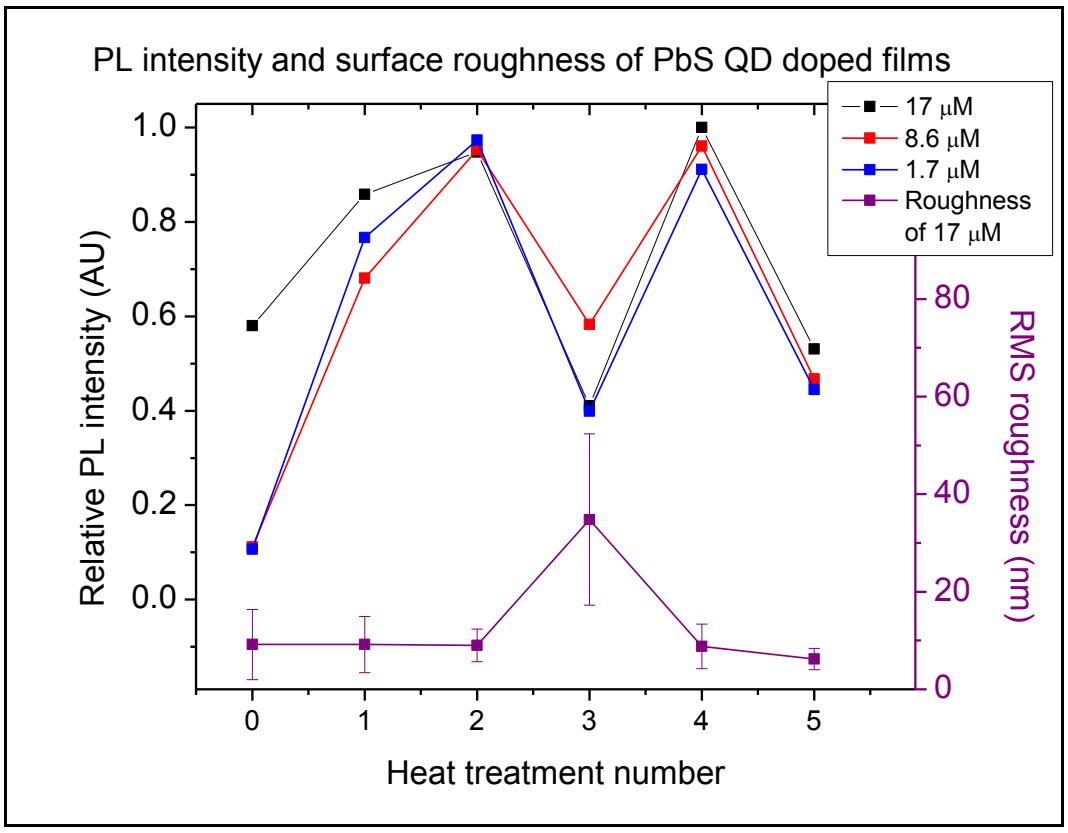

Fig. 7.15: Plot of photoluminescence intensity of $Ge_{23}Sb_7S_{70}$ films deposited from solutions containing varying concentrations of PbS QDs for various heat treatments

Figure 7.15 compares the luminescence intensities for PbS doped films of varying concentrations. It was expected that the intensity would continue to increase until no more solvent could be removed from the film, so long as the QDs are not damaged by the heat treatment. However, the reduced intensity for all films after HT3 is correlated to the RMS roughness of the film surface, and it is believed that the increased roughness scatters the luminescence, accounting for the apparent decrease. For HT5, which was 20 min at 200°C, it is suspected that the QDs may have been damaged by the high temperature, resulting in defects that lead an increased probability of non-radiative de-excitation and lower quantum yields.

It is very interesting that each film reaches approximately the same luminescence intensity at HT2, regardless of PbS QD concentration. This is an indication that there is the same concentration of active, luminescent QDs in each film. Therefore, it is likely that aggregation is occurring, especially for 17 and 8.6 μM loading levels of QDs. However, without truly quantitative measurements like quantum yield and lifetime, which are independent of the QD concentration, definitive conclusions cannot yet be made.

7.6 Summary

Luminescence in the NIR has been demonstrated in solution-derived $Ge_{23}Sb_7S_{70}$ films using PbS QDs. Like the results found in the study on CdSe QDs, propylamine was found to strongly quench luminescence, and it was shown that optimized heat treatments to remove as much residual propylamine from the film matrix is essential to maximize luminescence intensity. It was also found that the shape of the luminescence band for QDs in the film matrix differs greatly from that of the QDs in solution. The reasons for the sharp features in the spectra are unclear at the moment, but the most likely explanation is that they are due to bonds caused by residual solvent in the film matrix. Additionally, a blue-shift from 1250 nm to 1230 nm in the peak emission wavelength from QDs in solution to QDs in the film matrix was observed, similar to the blue-shift observed in the study on CdSe QDs.

Finally, these experiments show the importance of quantitative characterizations of luminescence, such as quantum yield and lifetime, when investigating the behavior of

QDs in various environments. Proposed solutions include a detector with a larger range in the NIR and higher intensity pulsed LEDs.

7.7 References

[1] W. Heiss, H. Groiss, E. Kaufmann, G. Hesser, M. Boberl, G. Springholz, F. Schaffler, K. Koike, H. Harada, M. Yano, "Centrosymmetric PbTe/CdTe quantum dots coherently embedded by epitaxial precipitation" *Applied Physics Letters*, **2006**, *88*, 192109.

[2] I. Moreels, K. Lambert, D. Smeets, D. De Muynck, T. Nollet, J. C. Martins, F. Vanhaecke, A. Vantomme, C. Delerue, G. Allan, Z. Hens, "Size-dependent optical properties of colloidal PbS quantum dots" *A. C. Nano,* **2009**, *3*, 3023-3030.

[3] J. Wilkinson, "Optimization and characterization of solution-derived chalcogenide glass thin films" MS thesis, Clemson University **2012**.

CHAPTER 8

CONCLUSIONS

Nanomaterials have been shown to exhibit extraordinary optical properties, and are very attractive in the fabrication of new materials possessing properties unattainable by any single material. MNPs exhibit a characteristic SPR absorption band, while QDs demonstrate luminescence. These properties are size-dependent, so they can be tuned to a particular application, and are also sensitive to the surrounding environment. However, dispersion in an appropriate host matrix is necessary to make use of these properties. Chalcogenide glasses are one such matrix of interest due to their well-known optical properties such as transparency to infrared light and high refractive index. They are therefore ideal candidates in the fabrication of MIR optical chemical sensors which would benefit from the incorporation of nanomaterials such as MNPs and QDs. One proposed sensor design that we are working on requires the fabrication of films, and a solution-derived approach offers the advantage of being easily loaded with nanomaterials.

The goal of this thesis was therefore to investigate the incorporation of MNPs and QDs in solution-derived chalcogenide glass films. Several issues were addressed, as both spin-coating of chalcogenides and the properties and dispersion of nanoparticles can be very sensitive to a number of processing parameters. In the case of spin-coating, research in our group has found that solubility of the glass in a solvent and resulting film quality are both sensitive to the amount of water in the solvent. Furthermore, the resulting properties of the film are affected by residual solvent in the film matrix, and the addition

of nanoparticles most often introduces a second solvent into the solution besides the solvent used to dissolve the glass. These attributes are important considerations if dopants such as MNP or QDs are to be added to the film.

The properties of a nanomaterial and ability to disperse are often strongly dependent on the environment within the host matrix. Due to the high surface area to volume ratio of a nanoparticle, the surface must be "capped" with an organic ligand that allows it to disperse in the desired environment, as well as enhance the inherent stability. Synthesizing nanomaterials with an appropriate capping agent is one of the most important aspects of successfully dispersing nanomaterials in a matrix of interest.

Because of these issues, the addition of a nanoparticle solution to a chalcogenide glass solution therefore raises many questions regarding the optical properties and characteristics of the resulting spin-coated film. Thus, the main questions addressed in this thesis were the following:

1. How can the surface of the nanoparticle be modified with different capping agents so that it can disperse well in the glass film?
2. What is the maximum loading level of the nanoparticles in the glass solution?
3. How, and in what concentration, does the addition of nanoparticles affect the properties, such as absorption bands and luminescence of the film?

Experimental techniques were developed to investigate these questions by the incorporation of Au MNPs and CdSe and PbS QDs in solution-derived $Ge_{23}Sb_7S_{70}$ films.

The nanoparticles were tested in solution as a baseline by techniques such as UV-vis-NIR spectroscopy, dynamic light scattering and photoluminescence, and their properties were monitored in the presence of the amine solvent and at different steps in solution-derived film processing, such as in the glass solution and in the film matrix throughout various heat treatments.

Results of the testing with Au MNPs showed that their concentration in the glass solution could be optimized by the slow addition of MNPs and characterization by UV-vis absorption spectra. Therefore, we have answered the question of what is the maximum concentration of PVP capped Au MNPs that can be dispersed in a chalcogenide glass solution, although the presence of the SPR band could not be identified in the deposited films. Furthermore, the experimental procedure can be applied to investigate any type of MNP with various types of capping agents. Although PVP was not compared to other organic ligands in order to answer the question of how can the surface of the MNP be modified to disperse in higher quantities, a comparison can be made using the principles learned in this thesis. Attempts were made to understand how the properties of the doped film changes with varying concentration of Au MNPs, but the differences between the various MNP loading levels is within the error caused by film thickness and surface roughness variation.

Results of the testing with CdSe and PbS QDs showed first and foremost that residual propylamine in the film matrix can strongly quench both visible and NIR luminescence. This demonstrates the importance of optimized heat treatments in order to remove as much solvent as possible from the film. In the case of CdSe, this was

characterized quantitatively by lifetime and quantum yield measurements. For PbS, these measurements are more difficult in the NIR, but it is possible with the right equipment. Future work should examine the lifetime and quantum yield of PbS doped films in order to obtain better characterization of the QD properties in various environments. However, propylamine quenching of PbS luminescence was characterized qualitatively by comparing the luminescence intensities of PbS QDs in a solution titrated with propylamine, and for doped films with varying heat treatments. It was also found that both the CdSe and PbS luminescence spectra changed from being dispersed in solution (chloroform), on the film surface, and incorporated into the film matrix. Both spectra were slightly blue-shifted, which is believed to be an effect of the glass. In the case of PbS, many sharp features in the luminescence band were observed, which appear to be reabsorption of luminescence. Chloroform absorption and interaction with the film matrix may be partially responsible, but it was found that even heat treatments up to 270°C (T_g – 40°C) for 1 hour do not reduce the size of the features.

PbS doped $Ge_{23}Sb_7S_{70}$ solutions are not stable for long enough periods of time to optimize their concentration in solution. Therefore, only the effect of PbS loading level in the deposited film was investigated, and it was found that all three concentrations (1.7, 8.6 and 17 μM) reached approximately the same luminescence intensity. This suggests that there is aggregation of QDs occurring at some stage during the film processing, and that there is an optimal concentration of QDs for maximum luminescence intensity. Although only a qualitative assessment of the optimal loading level was performed, a quantitative assessment of the optimal loading level can be determined by implementing

experimental procedures such as lifetime and quantum yield. These tests were not possible with the equipment currently available, but would allow a definitive answer to the question of how the properties of the deposited film are affected by varying concentrations of QDs.

PbS QDs with two types of capping agents were tested, mercaptohexanol and thioctic acid. It was found that their behavior differs when depositing the QDs on the surface of a $Ge_{23}Sb_7S_{70}$ film, and that QDs with mercaptohexanol were more prone to forming large aggregate(s), and were therefore not pursued further. Within the constraints of our experimental study, only the thioctic acid capped PbS QDs have been studied extensively in the film matrix, so the answer to the question of how can the surface of the QD be modified so that it can disperse better in the film matrix remains incomplete. While through the current experimental study we have begun to understand the chemistry of grafting different organic ligands to the surface of the QD, which enables the modification of QD behavior in the glass solution/film, there is much more left to discover if we want to incorporate them in a fully consolidated glass film.

There is a lot of motivation to modify the properties of solution-derived chalcogenide glass films through the incorporation of nanomaterials. In doing so, these unique properties are strongly dependent on the surrounding environment, whether it is an effect of the glass itself, or residual solvent in the film matrix. Understanding how these properties vary in a changing film environment, and correspondingly how the film properties are affected by the incorporated nanomaterials is crucial to the development of exciting next-generation optical devices such as optical sensors. However, the

applications are numerous, and the principles learned in this thesis can be extended to many other IR-transparent glass systems.

CHAPTER 9

FUTURE WORK

In addition to remaining unanswered questions, the work done in this thesis has raised many questions and plans for future work. Remaining questions include the effect of Au MNP doping on the Verdet coefficient of the glass solutions and deposited films. Similar procedures will be used to fabricate doped solutions and films, and Verdet coefficient measurements will be measured first at 632 nm in Dr. Kornev's lab at Clemson University. These experiments will provide a better demonstration of the attractive optical properties provided by the incorporation of MNPs in chalcogenide glasses than the observation of the SPR band.

More experiments are needed to understand the behavior of IR-emitting QDs. Modification of the surface chemistry is one area of interest, as many procedures have been demonstrated in the literature on CdS that can likely be extended to PbS. For example, like thioctic acid, dihydrolipoic acid offers the potential to form two Pb-S bonds on the surface of the QD when grafting the ligand, as opposed to just one from mercaptohexanol. This may allow the capping agent to bond more strongly to the surface, and result in QDs which are more stable against aggregation in amine solvents.

The cause of the sharp features seen in the luminescence spectrum of PbS in the film matrix is unknown. This question may be able to be answered by dispersing the QDs in a different solvent before dispersing in the glass solution. Additionally, we have had success redispersing PbS QD in powder form back into chloroform by sonication and

heat. It may be possible to disperse the powder in propylamine or glass solution long enough to deposit a film, eliminating the need for a QD carrier solvent.

As mentioned in the thesis, more quantitative methods are necessary to truly understand the behavior of the QDs in the film matrix during heat treatments. If quantum yield and lifetime can be measured accurately in the NIR, the effect of the changing film matrix on the properties of the QDs can be better understood, and the PbS loading can be optimized. We are also interested in these characterization techniques because the target luminescence band for the chemical sensing application is 3.0 – 3.5 μm. Eventually, doping with a QD which can emit in this range, such as PbTe, will be investigated with many of the same experiments performed on PbS.

High-resolution transmission electron microscopy (TEM) can be used to investigate how the QDs disperse in the film matrix. Are there large aggregates, or are they dispersed homogeneously? This test would help to optimize loading level, as well as give insight into the actual concentration of QDs in the film matrix. Additionally, TEM would also be beneficial in understanding how Au MNPs disperse in the film matrix.

Ultimately, there are many materials which are interesting for doping by nanomaterials, including bulk chalcogenide glass. Several groups have demonstrated QD precipitation techniques in bulk and film materials containing, for example, Pb and S ions. Although typically high temperatures are required, this technique is attractive because QD size can be controlled easily by the duration and temperature of the heat treatment, and high concentrations of QDs are possible with low risk of aggregation.